MICROFLUIDIC PREPARATION OF LIQUID CRYSTALLINE ELASTOMER ACTUATORS

TRISTAN HESSBERGER

geboren in
Bad Soden-Salmünster

Dissertation
zur Erlangung des Grades
"Doktor der Naturwissenschaften"
im Promotionsfach Chemie

am Fachbereich Chemie, Pharmazie und Geowissenschaften
der Johannes Gutenberg-Universität Mainz

Mainz, 2018

The thesis was supervised by [redacted] at the Johannes Gutenberg-Universität Mainz from March 2015 to June 2018.

1st Referee: [redacted]
2nd Referee:

Oral examination: 21.06.2018

Für Miriam

ABSTRACT

The unique thermomechanical properties of liquid crystalline elastomers (LCEs) allow the reversible shape change of these materials towards an external stimulus, which provides suitable material properties for actuator applications and artificial muscles. The microfluidic processing of LCEs enables an effective shear force induced alignment of the liquid crystalline molecules (mesogens) in ordered director fields and features the preparation of variously shaped LCE microparticles.

In the present work, capillary based microfluidic devices are optimized for the fabrication of advanced LCE actuators. For the first time, actuating LCE Janus particles are synthesized in various shapes via microfluidics and their stimuli-responsive properties are studied at the nematic-isotropic phase transition via polarized optical microscopy (POM) and wide angle X-ray scattering (WAXS). Furthermore, dual temperature-responsive Janus particles are presented, which contain a lower critical solution temperature (LCST) hydrogel part beside a hydrophobic actuating LCE part to allow the independent shape change of each part at different temperature ranges and solvent environments. The amphiphilic character of these Janus colloids is utilized in a specially developed multi-step molding process for the self-assembly of rod-like Janus particles in well aligned monolayers at water/oil interfaces. By this approach, actuator functionalized surface devices of different shapes are obtained, which show collective and locally addressed actuation of the LCE covered surface during the phase transition.

In addition, a main-chain liquid crystalline monomer system is adopted for the microfluidic synthesis of strongly elongating LCE particles via thiol-ene click chemistry. The study of the nematic-isotropic LCE phase behavior concerning the amount of a liquid crystalline crosslinker reveals tunable and completely reversible actuation properties of corresponding main-chain LCE particles. Furthermore, the different microfluidic preparation methods of variously shaped homogeneous, core-shell and Janus LCE particles are reviewed with special regard to the microfluidic device construction and processability of liquid crystalline monomers.

In this work, the addressed advances in the field of LCE actuator research open new possibilities for the development of future LCE applications, such as temperature-responsive composite materials or actuator functionalized surfaces with variable adhesive and wetting properties.

ZUSAMMENFASSUNG

Die einzigartigen thermomechanischen Eigenschaften von flüssigkristallinen Elastomeren (LCEs) ermöglichen eine reversible Formänderung dieser Materialien durch einen externen Stimulus und liefern geeignete Eigenschaften für deren Verwendung als Aktuatoren und künstliche Muskeln. Die mikrofluidische Verarbeitung von LCEs erlaubt die effektive Ausrichtung der flüssigkristallinen Moleküle (Mesogene) in geordneten Direktorfeldern durch auftretende Scherkräfte und ermöglicht die Herstellung von LCE-Mikropartikeln mit verschiedensten Formen.

Die vorliegende Arbeit zeigt die Optimierung kapillarbasierter mikrofluidischer Reaktoren zur Herstellung weiterentwickelter LCE-Aktuatoren. Die mikrofluidische Synthese unterschiedlich geformter LCE Janus Partikel wird zum ersten Mal erfolgreich demonstriert und die Untersuchung deren Stimuli-responsivem Verhalten gegenüber nematisch-isotroper Phasenübergänge mithilfe von Polarisationsmikroskopie und Weitwinkel Röntgenstreuung durchgeführt. Darüber hinaus werden doppelt Stimuli-responsive Janus Partikel hergestellt, welche neben dem hydrophoben aktuerienden LCE ein thermoresponsives Hydrogel mit kritischer Lösungstemperatur aufweisen und die unabhängige Formveränderung beider Materialien in verschiedenen Temperaturbereichen und Lösungsmittelumgebungen erlauben. Der amphiphile Charakter dieser Janus Kolloide wird außerdem in einem mehrstufigen Formverfahren genutzt, um die Selbstassemblierung stäbchenförmiger Janus Partikel in Form von dicht gepackten Einzelschichten an Wasser/Öl Grenzflächen zu erzeugen. Mithilfe dieses Verfahrens werden unterschiedlich geformte Hydrogele präpariert, deren Oberfläche mit LCE Aktuatoren beschichtet sind und sowohl kollektive als auch lokal adressierte Aktuationen durch Phasenübergänge der LCEs zeigen.

In einer weiteren Studie wird die Integration eines flüssigkristallinen Hauptkettenmonomers in die mikrofluidische Synthese stark elongierender LCE-Partikel vorgestellt, wobei Thiol-Alken Klickchemie zur radikalischen Polymerisation genutzt wird. Die Untersuchung des nematisch-isotropen Phasenverhaltens dieser LCEs in Abhängigkeit des Anteils eines flüssigkristallinen Vernetzers ermöglicht die manuelle Regulierung der vollständig reversibel ablaufenden Formänderung der Hauptketten LCE-Partikel. Darüber hinaus werden alle relevanten mikrofluidischen Präparationsmethoden zur Herstellung unterschiedlich geformter homogener, Kern-Schale und Janus LCE-Partikel diskutiert und vor allem die Konstruktion der mikroflu-

idischen Reaktoren, sowie die Verarbeitung von flüssigkristallinen Monomeren detailliert erläutert.

Die in dieser Dissertation erarbeiteten Fortschritte im Forschungsbereich flüssigkristalliner Aktuatoren eröffnen neue Möglichkeiten für die Entwicklung zukünftig nutzbarer LCE-basierter Anwendungen, wie beispielsweise Temperatur-responsive Kompositmaterialien oder Aktuator-funktionalisierte Oberflächen mit variablen Haft- und Benetzungseigenschaften.

PUBLICATIONS

The following list contains all publications, which have been written or contributed to during this PhD thesis. The first author publications [1–4] are included as chapters 5 to 8 in the present thesis.

[1] T. Hessberger, L. Braun, R. Zentel, *Advanced Functional Materials* **2018**, 1800629 (Early View).

[2] T. Hessberger, L. B. Braun, C. A. Serra, R. Zentel, *Journal of Visualized Experiments* **2018**, *135*, e57715.

[3] T. Hessberger, L. B. Braun, F. Henrich, C. Müller, F. Gießelmann, C. Serra, R. Zentel, *Journal of Materials Chemistry C* **2016**, *4*, 8778–8786.

[4] T. Hessberger, L. Braun, R. Zentel, *Polymers* **2016**, *8*, 410.

[5] L. B. Braun, T. G. Linder, T. Hessberger, R. Zentel, *Polymers* **2016**, *8*, 435.

[6] L. B. Braun, T. Hessberger, R. Zentel, *Journal of Materials Chemistry C* **2016**, *4*, 8670–8678.

[7] L. B. Braun, T. Hessberger, C. A. Serra, R. Zentel, *Macromolecular Reaction Engineering* **2016**, *10*, 611–617.

CONTENTS

Part I

INTRODUCTION

1 LIQUID CRYSTALS

The discovery of the liquid crystalline phase is attributed to the botanist Friedrich Reinitzer and his studies about the molecular weight of cholesterol in the late 19th century. In the year 1888, Reinitzer analyzed the melting point of cholesteryl benzoate. Thereby, he unexpectedly observed two different melting points. At first, his sample of cholesteryl benzoate turned into a turbid fluid at 146.6 °C and he already noticed the optical anisotropy of the substance in terms of colorful reflections. By further heating, the turbid fluid turned into a transparent liquid at 180.6 °C, which he declared as the second melting point.[8] Unknowingly, Reinitzer had discovered the cholesteric liquid crystalline phase. Afterwards, Otto Lehmann formed the term *liquid crystal* to describe the discovered order in liquid phases. In this context, a new area of reserach was created, which has fascinated many scientists in the fields of chemistry and physics till this day.[9,10]

1.1 FUNDAMENTALS

Liquid crystals represent a special kind of matter, which exhibits the physio-chemical properties of an isotropic liquid in combination with a certain degree of the molecular order of anisotropic crystals. As liquid crystals can neither be classified into the liquid state nor the crystalline phase, the term *mesophase* was introduced to describe the liquid crystalline phase as a state of matter in between.[11] The highly anisotropically shaped molecules of liquid crystals are called *mesogens*. The high tendency of mesogens towards self-organization and supramolecular assembly brings partial order to the mobility of liquid crystals.[12,13] In general, liquid crystals are subclassified into two main kinds of mesophases: thermotropic and lyotropic liquid crystals. The appearance of lyotropic mesophases is associated with a

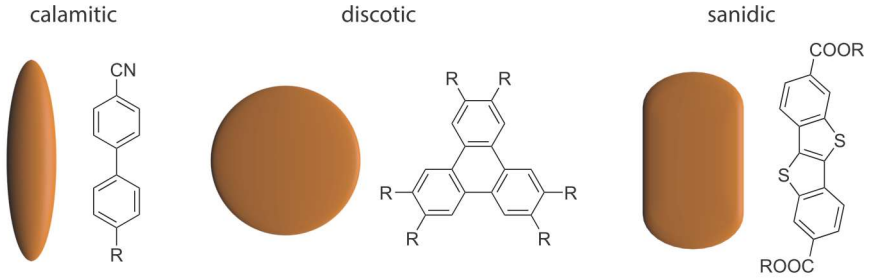

Figure 1.1 Illustration of different mesogen shapes and corresponding examples of the rigid aromatic cores of liquid crystalline compounds.

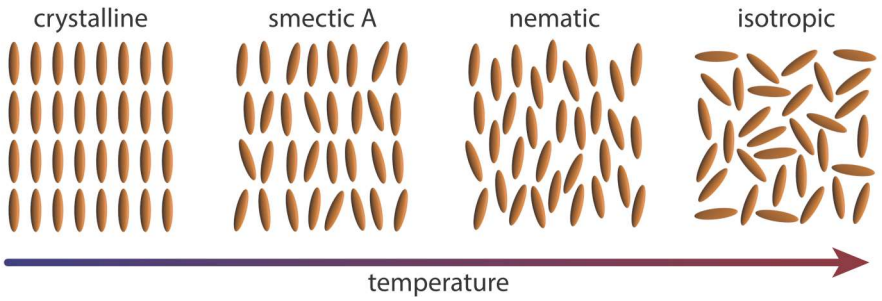

Figure 1.2 Schematic illustration of the temperature dependent appearance of different mesophases in an exemplified thermotropic liquid crystal. (a) crystalline phase: 3D positional long range order, (b) smectic A phase: one dimensional long range positional and orientational order, (c) nematic phase: only long range orientational order, (d) isotropic phase: no long range orders.

multi-component system, which contains at least one sort of mesogenic units and a solvent to provide the necessary mobility of the system. In this case, both the concentration and the temperature define the lyotropic phase behavior.

Thermotropic Liquid Crystals

In contrast, thermotropic liquid crystals are single-component systems, which exclusively contain the mesogens and show their phase behavior temperature dependent.[14] The anisotropic shape of the mesogens generates an orientational order, whereas the fluidity of the mesophase is provided by the thermal motion of the mesogens. In that matter, the structural order originates from the rigid mesogen core, which usually consists of a variable number of phenyl or biphenyl units. However, the mesogens' mobility is assured by flexible alkyl or alkoxy chains, which are linked to the outside of the aromatic core and prevent crystallization. The most frequently occurring mesogen types in thermotropic liquid crystals are calamitic (rod-like), discotic (disc-like) and sanidic (board-like) shapes, which are illustrated in Figure 1.1.[15–19]

Different liquid crystalline phases can occur sequentially in various temperature ranges, thus offering different degrees of orientational and positional order.[20,21] Commonly studied thermotropic mesophases of calamitic mesogens are the nematic phase (N) and the smectic A phase (SmA). Both phases show a long range orientational order, in which the mesogens' long axis is largely aligned along the director $\vec{n}$. This is a non-dimensional unit vector and points the direction of the spatial and temporal average of the mesogen alignment. In addition to the orientational order, the SmA phase exhibits a long range positional order, which results in lamellar arrangements of the mesogens and a layered structuring. However, the mesogens of a SmA phase do not show a positional order within the layers, which leads to a one dimensional positional order and a higher degree of order than the nematic phase. Thus, the nematic phase of an exemplary liquid crys-

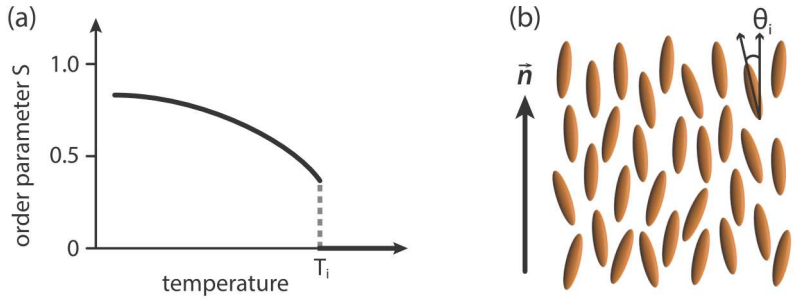

Figure 1.3 (a) Typical decrease of the order parameter S of a nematic liquid crystal in dependence of the temperature. T_i is the clearing temperature, which describes the temperature at the nematic-isotropic phase transition. (b) Schematic illustration of the angle θ_i in relation to the director $\vec{n}$ in the nematic phase.

tal arises at higher temperatures than a smectic phase (see Figure 1.2). Furthermore, other liquid crystalline phases with higher degrees of order (e.g. the smectic C phase) could arise at lower temperatures. By falling below the crystallization temperature (T_{cr}), the mesogens are arranged in a three-dimensional long range positional order at which their centers of mass fill the defined lattice sites of the crystalline state. On the other side, exceeding the clearing temperature T_i leads from the weakly ordered nematic phase to the isotropic state, in which the mesogens loose long range orders of any kind.

Liquid Crystalline Order Parameter

The degree of orientational order for nematic or smectic phases is quantified by the scalar order parameter S, which arises from the mean deviation of the mesogens' alignment from the director $\vec{n}$ (Equation 1.1). The angle θ_i represents the tilt of a single mesogen's main axis from the director $\vec{n}$ within a defined domain of mesogens, which is illustrated in Figure 1.3b. For the isotropic state, in which the mesogens' main axes are distributed randomly in all spatial directions, the order parameter corresponds to $S = 0$. On the contrary, the mesogens of the ideal crystalline state are perfectly aligned along the director $\vec{n}$, which results in an order parameter of $S = 1$. Typical values of S for nematic phases are between 0.3 and 0.8 and the schematic decrease of S as a function of temperature is illustrated in Figure 1.3a. The experimental determination of the order parameter is commonly performed by magnetic resonance spectroscopy, polarized Raman scattering or X-ray scattering measurements.[22]

$$S = \frac{1}{2}\left\langle 3\cos^2\theta_i - 1 \right\rangle \tag{1.1}$$

POM

The most widely used method for the characterization of liquid crystalline phases arises from the optical birefringence of liquid crystals. Polarized optical microscopy (POM) uses two stacked polarization filters, whose polarization directions are oriented perpendicular to each other (Figure 1.4 illustrates the setup of a polarizing micro-

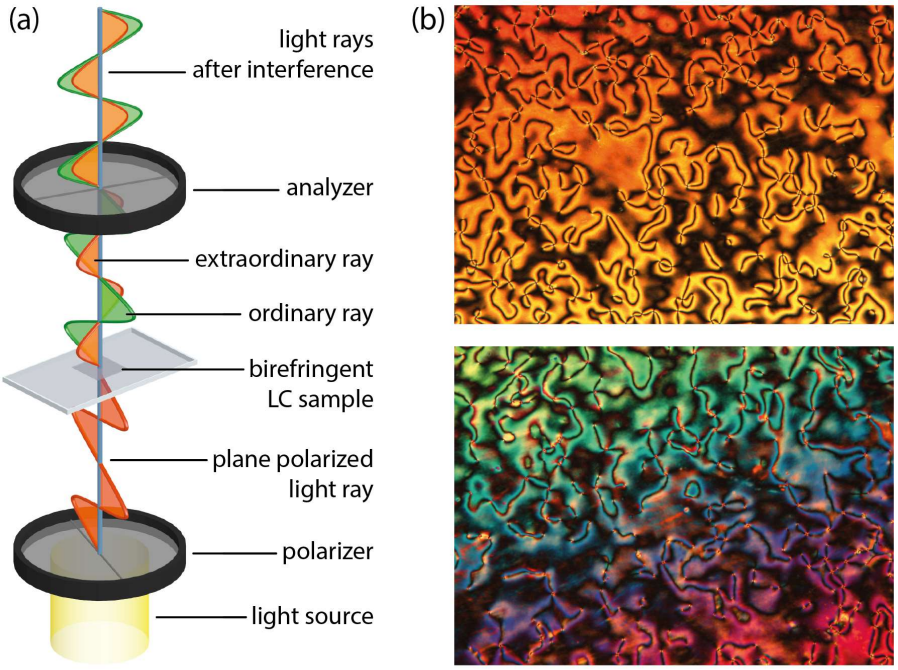

Figure 1.4 (a) Schematic illustration of the optical path of a polarized optical microscope. (b) POM images of Schlieren textures, which occurred during the thermal analysis of the nematic mesogen 2-methyl-1,4-phenylene-bis(4-(3-(allyloxy)propoxy)benzoate.

scope). In between the so called *polarizer* and *analyzer*, birefringent materials such as liquid crystals can be characterized. Since only light can pass through the analyzer, which changes its polarization direction inside the sample, various liquid crystalline phases can be identified by their characteristic textures.[23] The optical birefringence of liquid crystals originates from the anisotropic shape of the mesogens, which generates two different refractive indices in dependence of the molecular axes. Thus, the propagation velocity of light is different along the main axis of the mesogen which is defined by the extraordinary refractive index n_e, compared to the propagation velocity perpendicular to the main axis, characterized by the ordinary refractive index n_o. The consequential phase shift of uniformly polarized light inside a liquid crystalline sample leads to the colorful textures, which are influenced by the temperature and the film thickness of the sample, as well. Since the orientation of the director $\vec{n}$ dictates the visible texture of a liquid crystal, bright and dark areas as well as defect structures enable the interpretation of corresponding director fields and mesogen orientations.

Properties and Applications

Beside the anisotropic optical properties of liquid crystals, the magnetic, electric and elastic properties show anisotropic behavior with respect to the director $\vec{n}$, too. Thus, liquid crystalline phases are sensitive to various external forces, such as electric or magnetic fields, mechanical forces and surface anchoring. This gives rise to utilize

these effects for the systematic modification of the liquid crystalline director $\vec{n}$. The most famous application of liquid crystals is the usage of mainly nematic phases for the fabrication of liquid crystalline displays (LCDs).[24–27] In this case, the high sensitivity of nematic liquid crystals for the molecular orientation in an electric field is used to switch the director between two crossed polarizers. The self-alignment of liquid crystalline mesogens along the director facilitates the collective orientation in an electric field and consequentially enables the manipulation of light, which can not be realized by the usual dipole interactions of non-mesogenic molecules or the electro-optic Kerr effect. Thus, the polarization direction of the nematic layer between the polarizers is controlled by the applied electric field and the transmittance of light can be switched by variation of the voltages applied to the electrodes. The application of LCDs reaches from simple 7-segment displays for the illustration of numbers in digital clocks to high definition displays with a large number of small pixels in LCD-televisions. The same basic technology is used in all of these displays.

1.2 LIQUID CRYSTALLINE POLYMERS

The promising capability of combining the concept of liquid crystalline ordering with the elastic properties of polymers had already been forecast by Pierre de Gennes in the year 1969.[28] The incorporation of mesogenic units into polymer chains leads to mechanically stable liquid crystalline polymers, which provide the basis for thermotropic or lyotropic mesophases. If the mesogens are linked to the polymer chain, their ability of self organization transfers a certain degree of anisotropy to the conformation of the polymer chain. Compared to the almost spherical shape of a random coil polymer conformation in the isotropic state, the polymer's radius of gyration changes reversibly in the liquid crystalline state with respect to the director $\vec{n}$. The geometry of an anisotropic deformation as well as the magnitude of the polymer chain's shape change relies on the liquid crystalline phase behavior (e.g. nematic or smectic), the coupling of the mesogens to the polymer chain and the chemical structure of the polymer backbone.[29–32] In general, two different architectures of liquid crystalline polymers are specified: main-chain and side-chain polymers. Figure 1.5 illustrates the different types of mesogen linkage to the polymer chain.

Main-Chain LC Polymers

In main-chain liquid crystalline polymers, the mesogenic units are incorporated directly into the polymer backbone and thus, the coupling of the mesogens with the polymer chain is very strong. In the case of calamitic mesogens in a nematic main-chain polymer, the director $\vec{n}$ is aligned parallelly to the propagation of the polymer chain, which leads to a highly anisotropic deformation of the polymer con-

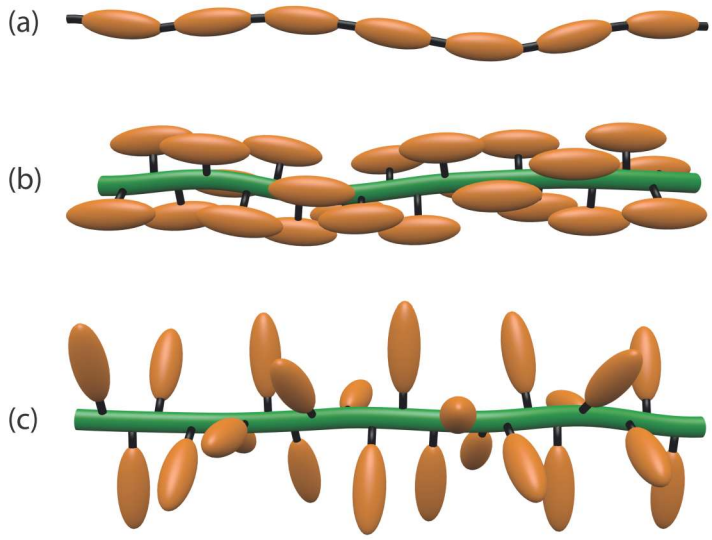

Figure 1.5 Different architectures of liquid crystalline polymers: (a) main chain polymer, (b) side-on side-chain polymer and (c) end-on side-chain polymer.

formation in the liquid crystalline state. Consequentially, the radius of gyration parallelly to the director $R_{\parallel}$ is increased, whereas the radius of gyration perpendicular to the director $R_{\perp}$ is reduced, which leads to a prolate conformation of the polymer chain (see Figure 1.6). Beside the mesogens, the spacer units in between play an important role on the anisotropy of the coil conformation and the phase behavior, as well. Very short and inflexible spacers lead to so called *rigid-rod* polymers, which feature a stiff and highly elongated polymer conformation and the assembly into lyotropic mesophases. These polymers mostly offer high Young's moduli and melting points beyond the decomposition temperature, which is why they are frequently used for the fabrication of fire-resistant and highly mechanically stable fibers via spinning processes.[33] On the contrary, long alkyl chains in between the mesogenic units weaken the influence of the mesogens on the polymer conformation and bring more flexibility to the polymer chain. This results in lower phase transition temperatures and consequential occurrence of nematic or smectic thermotropic liquid crystalline phases, in which the polymer conformation exhibits a less anisotropically shaped prolate conformation.

The synthesis of main chain liquid crystalline polymers is typically carried out in polycondensation reactions, which however implicate several drawbacks, such as the difficult control over the molecular weight and long reaction times. However, thiol-ene click chemistry allows the radical initiated chain growth polymerization of main-chain liquid crystalline polymers and enables an efficient control over the molecular weight at shorter reaction times.[34–37]

Side-Chain LC polymers

Side-chain liquid crystalline polymers are subclassified according

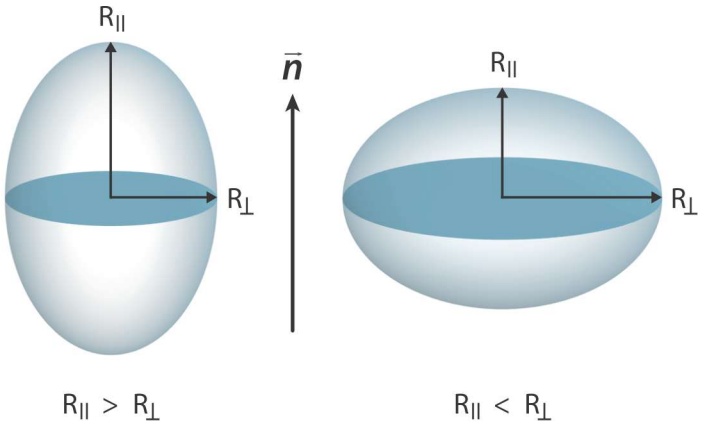

Figure 1.6 Illustration of different chain conformations for liquid crystalline polymers. The prolate chain conformation (left) shows an elongation along the director $\vec{n}$ and a contracted radius of gyration $R_\perp$. The oblate shaped conformation (right) displays an enlargement perpendicular to the director $\vec{n}$ and a contraction of the radius of gyration $R_\parallel$.

to the *side-on* or *end-on* linkage of the mesogenic units with regard to the polymer backbone. Both types are commonly synthesized either by radical chain growth polymerization of polymerizable mesogens (*e.g.* acrylate or methacrylate group containing mesogens), or by polymer analogous conversion of precursor polymer chains (e.g. polysiloxane-based polymers) with reactive mesogens via click chemistry.[38–40]

Side-on bonded liquid crystalline side-chain polymers usually form thermotropic mesophases, in which the director of the mesogens is mostly aligned along the polymer chain. The radius of gyration along the director $R_\parallel$ is consequentially larger than $R_\perp$, which results in a prolate shaped polymer conformation. However, the transfer of the anisotropy to the polymer chain is weaker compared to the main-chain polymers and furthermore depends on the spacer length between the mesogens and the polymer backbone.[41]

Side-chain polymers with end-on connected mesogenic units resemble a comb-like structure and show the weakest anisotropy of the polymer conformation in thermotropic liquid crystalline phases. As the mesogens are aligned perpendicular to the propagation direction of the polymer backbone, the coupling through the binding spacer works against the mesogens' assembly along the director $\vec{n}$. Depending on which effects predominate, the end-on liquid crystalline polymer chain can assume a prolate ($R_\parallel > R_\perp$) or an oblate ($R_\parallel < R_\perp$) shape.

The chain anisotropy of liquid crystalline polymers has a high impact on the expected shape changes of liquid crystalline elastomers (LCEs), which are discussed in the following section. For this reason, the right selection of the polymer type is crucial and the high

anisotropic shape change of side-on side-chain polymers and especially main-chain polymers favor these types for their use in LCE actuators.

1.3 LIQUID CRYSTALLINE ELASTOMERS

During the nematic-isotropic phase transition of a liquid crystalline polymer, the order parameter decreases and the polymer conformation changes from an anisotropic to a spherical shape, at which the predefined director orientation is lost. To reversibly regain the director orientation of a polymeric sample after the phase transition, crosslinking of the liquid crystalline polymer chains is necessary. In liquid crystalline elastomers, the polymer chains are slightly crosslinked to obtain a three dimensional network structure, in which the distance between crosslinking points is long enough to maintain mesogen movement and alignability. For this reason, LCEs combine the entropy elastic properties of rubbery polymeric networks with the liquid crystalline ability of self-organization and anisotropic polymer deformation.[42–45]

General Considerations

Above the glass transition temperature, reversible stretching of LCE samples is possible and large strains of the material can be realized due to elastic moduli in the range of Mega Pascal. In the isotropic state, the network structure prohibits free flow and limits the translation of the random coil polymer chains to each other. During the phase transition from the isotropic to the nematic phase, the director of the mesogens and the original anisotropic shape of the polymer chains is restored. Higher crosslinking densities lead to liquid crystalline networks (LCNs), in which the liquid crystalline order is kept permanently frozen even at high temperatures, as the mesogen mobility is highly restricted by the close-meshed network. These so called *thermosets* commonly hold hard, glassy material properties in terms of high elastic moduli in the range of several Giga Pascal. In this case, phase transitions are no longer observed as the densely crosslinked material lacks the necessary mobility.[46,47]

Thermomechanical Properties

However, the slight crosslinking density in LCEs allows their unique thermomechanical response, which had already been predicted by Pierre de Gennes 1975: A reversible macroscopic shape change of LCE samples at the nematic-isotropic phase transition.[48] The prerequisite for a shape-changing effect in LCEs is the uniform alignment of the director over the whole sample to receive a liquid crystalline monodomain or at least a well defined preferred orientation of the directors in a polydomain sample.

In the nematic state of an oriented LCE sample, the anisotropic deformations of the polymer coils cause a strain along the director through the whole sample, which leads to a deformed macroscopic shape of the sample due to the material's elasticity. During the

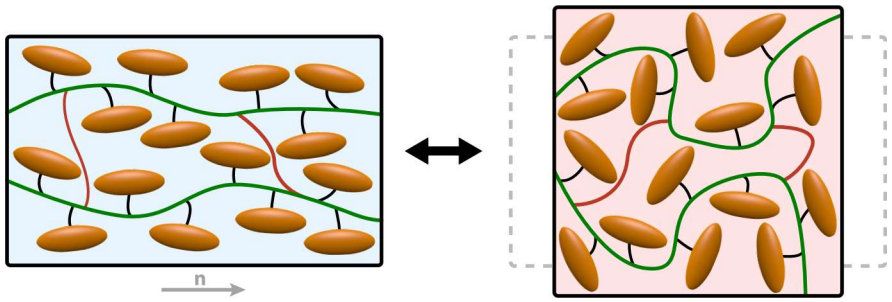

Figure 1.7 Reversible shape change of an uniformly aligned LCE sample during the nematic-isotropic phase transition. In the nematic state (left), the mesogens are aligned horizontally along the director $\vec{n}$, which forces the network to assume an anisotropic shape. At the transition to the isotropic state (right), the network structure relaxes due to the mesogen's loss of orientational order, which causes a contraction of the LCE sample along $\vec{n}$ and an expansion perpendicular to $\vec{n}$

nematic-isotropic phase transition, the average tilt of the mesogens orientation towards the director increases and the entropy driven random coil conformation of the polymer chains is recovered. For this reason, a collective decrease of the polymers' radii of gyration $R_{\parallel}$ along the director transfers a contraction to the whole macroscopic LCE sample in the same direction. As the density of the sample remains constant, an expansion of the sample perpendicular to the director comes along with the increase of the polymer coil radius of gyration $R_{\perp}$. By restoring the nematic phase of the LCE, the original shape of the sample is assumed again, as the crosslinking points of the network regain their original coordinates and restore the nematic order and the polymer chain anisotropy, as well. Figure 1.7 illustrates the reversible shape change of an aligned LCE sample during the phase transition.

Stimuli Responsiveness

In comparison to other shape changing materials, LCEs feature larger shape changes than piezo-elements, but smaller forces are generated during the phase transition. Furthermore, no mass transport is necessary as known from hydrogel shape changes by solvent swelling. The slight crosslinking density of LCEs enables strong swelling by organic solvents, at which the liquid crystalline order and the anisotropic polymer shape vanishes and the isotropic phase transition is triggered. However, trespassing the clearing temperature of LCE samples by an external temperature control represents the most commonly used method to provide the phase transition and the consequential shape change. Various techniques have been developed to either change the LCE's environmental temperature or heat the sample via integrated heaters, such as heating wires (for electric heating), carbon black (for conductive heating), magnetic iron oxide nanoparticles (for inductive heating) or single walled carbon nanotubes (to enable heating via visible light or IR-irradiation).[49–52]

Beside temperature control and solvent swelling, pH- and chemo-responses are well-known to induce a phase transition and therefore the shape change of LCEs. Furthermore, the incorporation of azobenzene compounds into nematic liquid crystalline phases enables the light induced switch between the nematic and the isotropic state. In this case, the photoisomerizable azo-group can be switched by visible or UV-light between the *cis*- and the *trans*-form. To this effect, the azo-molecule resembles either a calamitic shape in the *trans*-isomer or a bent shape in the *cis*-form, which disturbs the nematic order of the calamitic shaped mesogens. For this reason, an isothermal conversion of azo-mesogens from *trans* to *cis* close to the clearing temperature causes a shape change of the LCE as the phase transition temperature is decreased by the disturbance of the nematic phase order.[38,53]

Shape Changes at Phase Transitions

The magnitude of LCE shape changes primarily depends on the nature of mesogenic units and their kind of linkage within the LCE architecture. Furthermore, the quality of the director alignment over the whole LCE sample plays an important role (techniques for the alignment of LCE samples will be discussed in Section 1.4).The symmetry of the mesogens and their ability of intermolecular assembly and self alignment into ordered phases influences the magnitude of the polymer chains anisotropic deformation in the liquid crystalline state. Accordingly, the ratio of the radii of gyration $R_{\parallel}$ to $R_{\perp}$ of a polymer conformation dictates the extent of shape change for LCE samples with respect to the director $\vec{n}$. As described in Section 1.2, the main chain architecture of liquid crystalline polymers shows the strongest prolate deformation of polymer coils in nematic phases, for which reason very high dimensional changes up to 400 % were found for main-chain LCE systems.[54] Selected side chain LCEs with side-on linked calamitic mesogenic units feature high shape changes of well aligned LCE samples as well, whereas substantially weaker dimensional changes were found for end-on LCEs.[55]

Beside the shape changing properties, the phase transition temperature is highly dependent on the mesogenic and polymeric structure, as well. In this manner, flexible alkyl chains around the aromatic mesogenic core, long alkyl spacers between the mesogens and the polymer chain and flexible polymer backbones generally lead to low clearing temperatures of LCEs. Furthermore, copolymerization of mesogenic units and non-mesogenic moieties can be used to systematically lower the phase transition temperatures of mesophases, which is mostly desired for the application of LCEs as actuators. However, these concepts always affect the order parameter of the LCE and therefore the magnitude of shape change, which is why reasonable compromises have to be made between the liquid crystalline order and the phase transition temperatures at the selection of the LCE structure and composition.

Synthetic Methods

Various synthetic routes have been developed for the production

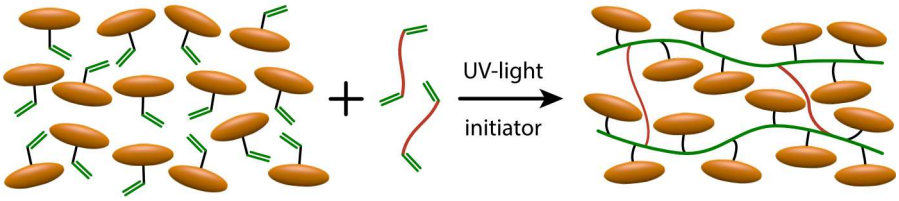

Figure 1.8 Schematic illustration of the LCE synthetic method based on polymerizable low molecular weight liquid crystalline compounds. Acrylate- or methacrylate-group containing nematic mesogens are mixed up with difunctional crosslinker moieties and a radical UV-initiator. Subsequent UV-irradiation initiates the radical polymerization and simultaneous crosslinking, which leads to the network formation of the LCE.

of shape changing LCEs to this day, which include differences in polymerization and crosslinking types, polymer architecture, as well as different sequences in polymerization and crosslinking with respect to the alignment procedure of the mesogens. The first synthetic method was introduced 1980 by the group of Heino Finkelmann, in which mesogens and crosslinker moieties are attached to polyhydrosiloxane polymer chains by palladium catalyzed addition in two steps. Two different reaction kinetics thereby enable the fast addition of vinyl group containing mesogens and crosslinker molecules to the polyhydrosiloxane polymer backbone at first. This step is followed by the slower addition of methacryloyl group containing moieties, which creates time for the alignment of the sample before the crosslinking process is finally finished.[56,57] This *one-pot* method was further developed by many groups to adopt various mesogenic types to the functionalization of polysiloxanes, resulting in many different LCE systems.

Other synthetic methods use liquid crystalline precursor polymers, which contain functional groups for subsequent crosslinking. One possibility is the network formation by addition of reactive crosslinking moieties, which undergo coupling or click-reactions with the functional groups of preformed liquid crystalline polymers[58,59]. Alternatively, crosslinkable groups are incorporated directly into the precursor polymer and the network structure is formed by external initiation of the crosslinking via thermal or UV-initiated radical polymerization of acrylate or methacrylate groups.[60,61] Beside covalent crosslinking techniques via low molecular crosslinking moieties or crosslinkable polymers, physical crosslinking has been used as well, in which ionic interaction or H-bonding enables the formation of crosslinking network points.[62,63]

Especially for this work, a further synthetic pathway plays an important role, in which the liquid crystalline polymer build up and the crosslinking are performed simultaneously (see Figure 1.8). For this method, polymerizable mesogens are mixed up with a multifunctional crosslinking compound and subsequent copolymerization

leads to the network structure in one step.[38,55,64,65] Typically, radical polymerization is used to polymerize mesogenic monomers, which contain terminal acrylate or methacrylate groups in alkyl side chains attached to the mesogenic core. These are mixed with a diacrylate crosslinker and a radical thermal or UV-initiator. Before the polymerization and crosslinking are initiated, the mixture is tempered to the liquid crystalline phase and an alignment technique is used to uniformly align the mesogens over the sample.

Beside the synthesis of side-chain LCEs by radical chain growth polymerization of reactive carbon double bond containing mesogens, main chain LCEs are formed by polyaddition chain growth polymerization via thiol-ene click chemistry or michael-addition.[37,66,67] In the case of thiol-ene based LCE, a calamitic divinyl mesogen is mixed with a dithiol comonomer, a diacrylate crosslinker and a radical initiator to form oriented main-chain LCE samples, which show large shape changes at their nematic-isotropic phase transition up to 156 %. Both synthetic methods have been utilized for the microfluidic production of shape-changing LCE microparticles in this work and are further discussed in Chapter 4, 5 and 7.

1.4 LCE ACTUATORS

Particularly with regard to the large accessible shape changes during the phase transition, the fast response to various stimuli and the tunable flexibility of their mechanical properties, liquid crystalline elastomers offer unique properties for their application as soft actuators and artificial muscles.[68–70] To enable a macroscopic shape change of LCEs in the first place, an orientation technique during the syntheses is crucial to impose a uniform alignment of the director to the LCE sample. In general, an external force is applied to the sample in the liquid crystalline state, which causes the alignment of mesogens along a defined director field before the final crosslinking of the LCE is completed.

Orientation techniques

In the case of an LCE synthesis from liquid crystalline polymer precursors, the polymer chains must be mechanically stretched to an anisotropic prolate (or oblate, see Section 1.3) shape by an externally applied force. This process generates a simultaneous alignment of the mesogens into a liquid crystalline monodomain with respect to the direction of the operating force field. If the synthesis is however carried out from a low molecular weight liquid crystalline compound (e.g. via radical chain growth polymerization), a variety of orientation methods known for the alignment of low molecular liquid crystals are available. The faster alignment of low molecular weight liquid crystals due to lower viscosities compared to liquid crystalline polymers, as well as lower phase transition temperatures, enable the use of various orientation techniques, such as magnetic or electric fields,

surface effects or optical fields. In all cases, the uniform anisotropy of the mesogens by the external force field is transferred to the emerging polymer chain conformations during the polymerization and simultaneous crosslinking process over the entire sample. Well aligned LCE samples are thereby achieved, which commonly offer polydomain structures with uniform director alignments along a well defined director field.

Irrespective of the synthetic method, the mesogen alignment along the director field as well as the deformation of the polymer chains are conserved in the network structure of the entire LCE sample after completion of the crosslinking process and disappearance of the external force. In this case, the anisotropic shape change of every single polymer chain leads to a macroscopic shape change of the aligned LCE sample during the phase transition. Furthermore, not only uniaxial shape changes (as for artificial muscles), but also complex three dimensional shape changes (*e.g.* folding or bending LCE films) are yielded from alignment techniques, which allow the generation of varying and modifiable director fields.[71]

Mechanical Stretching

The group of Finkelmann introduced mechanical stretching of liquid crystalline polymers as the first and commonly used orientation technique for the preparation of reversibly shape-changing polysiloxane LCEs.[57] For this procedure, weakly crosslinked liquid crystalline networks are exposed to an uniaxial mechanical stress, which causes a deformation of the polymer chain conformation in the direction of the applied tensile force. As a consequence of the network stretching, polymer chains unfold during their elongation along the applied physical stress and the mesogens align with respect to the polymer deformation. In the case of main-chain or side-on linked side-chain LCEs, the mesogens are aligned parallel to the direction of the polymer deformation, whereas end-on linked mesogens in side-chain LCEs can show a perpendicular alignment as well. The reorientation of the director as a result of moderately applied stresses to LCEs is expressed by the term *soft elasticity*. This phenomenon describes the rearrangement of the director by application of high strains at about constant stress in LCEs.[72–74]

After the orientation process by mechanical stretching and subsequent crosslinking of the liquid crystalline polymer, a uniform orientation of the director is received over the entire LCE sample and monodomain samples, such as nematic single liquid crystal elastomer films are obtained.[75] Especially nematic main-chain LCEs feature very high shape changes during the nematic-isotropic phase transition. Beside nematic LCEs, smectic A phases were used for the preparation of shape-changing LCEs, in which a biaxial mechanical field was applied by anisotropic deswelling during the synthesis to force a uniform homeotropic orientation to the network.[76] Furthermore, not only actuating LCE films are available by mechanical stretching, but

also highly oriented LCE fibers are accessible. The manual stretching of crosslinkable liquid crystalline polymer melts with tweezers represents an effective orientation method for the production of actuating LCE fibers, whereas electrospinning offers an automated synthesis of highly oriented entangled fibers.[60,61] Since mechanical stretching requires high viscosities of the liquid crystalline precursors, this orientation technique is limited to synthetic methods from polymeric compounds, such as crosslinkable liquid crystalline polymers and highly viscous solutions. However, the manufacturing of micro- and nanoscopic LCE actuators and their synthesis from polymerizable liquid crystalline compounds demands the application of more sophisticated orientation techniques.

Surface Effects

A widely-used method for the orientation of low molecular weight liquid crystals takes advantage of surface forces to effect a uniform director orientation in liquid crystalline samples. For this reason, surface effects reflect a suitable orientation method during the polymer synthesis of LCEs from liquid crystalline monomers. In this case, the anisotropy of a treated surface is transferred to the topography of the liquid crystalline monomer at the interface. With regard to the tendency to minimize the surface energy, nematic mesogens either adopt a parallel (homogeneous) or perpendicular (homeotropic) alignment to the surface at the interface. This director alignment extends from the surface to the inside of the liquid crystal with respect to the mesogenic interaction. However, this orientation technique is typically limited to distances in the order of 100 µm between the alignment surface and the decay of orientation inside the liquid crystal, for which reason only thin oriented LCE samples are prepared via surface effects.

Polyimide alignment layers are well known for the surface orientation of liquid crystals in display applications.[77] A planar alignment of the director is obtained by rubbing a polyimide coated surface in the desired direction of the mesogen alignment. Homogeneously aligned actuating LCE films are synthesized from acrylate or methacrylate containing mesogens by UV-initiated polymerization in liquid crystal alignment cells. In this method, rubbed polyimide or poly(vinylalcohol) (PVA) alignment layers are used to dictate the director orientation and consequently the direction of shape change after completion of the network formation.[55,78,79] By using two different alignment layers for each surface of an LCE alignment cell, homeotropic alignment on one side and planar alignment on the opposite side allows the implementation of a splayed director orientation inside the LCE film and leads to coiling and bending shape changes during the phase transition. This technique was used for the preparation of a spherically shaped self-regulating iris, which consists of an azo-benzene containing LCE and features a closing mechanism based on the bending actuation of the LCE upon the irradiation by visible light.[80]

Beside rubbing techniques, the anisotropic functionalization of surfaces with photoalignment layers represents a convenient method for the alignment of LCEs. In this case, a thin layer of chromophores (e.g. azobenzene derivates) is spin-coated on a surface and subsequently exposed to linearly polarized light, at which the molecules are oriented normal to the electric field vector. At the interface of the alignment layer to the liquid crystal, the oriented molecules transfer their anisotropic environment to the mesogenic alignment. The programmable anisotropy of the photoalignment layer by various patterning with polarized light through irradiation masks enables the modification of director fields in LCE films.[47] By this method, even very complex irradiation patterns were applied to form LCE films with complex director fields, which undergo three dimensional shape changes in terms of twisting, bending or folding actuation geometries.[66–68,81] Furthermore, the use of surfactants at interfaces enables different alignments of the director. Not only homeotropic aligned LCE films, but also polymeric colloids were synthesized by dispersion- or miniemulsion polymerization in the presence of surface-active agents which dictate a radial or bipolar director field via surface anchoring effects.[82]

Magnetic and Electric Fields

Another efficient technique for the alignment of polymerizable liquid crystalline mesogens arises from the director orientation in magnetic or electric fields. Calamitic mesogens in nematic liquid crystals exhibit strong diamagnetic properties. In a magnetic field, these mesogens align along the magnetic flux lines, which enables the preparation of uniaxially aligned LCE samples. Compared to surface effects, this method enables the uniform orientation of thicker samples and the alignment of mesogens away from the sample interface, as the magnetic field permeates the entire sample.

A common synthetic method for uniaxially actuating LCE films includes the melting of polymerizable acrylate containing nematic mesogens, crosslinker compounds and photoinitiator molecules to the isotropic state. Subsequent cooling to the nematic phase in the presence of a uniform magnetic field and UV-initiated polymerization and crosslinking yields well aligned actuating LCE films. Especially the large achievable thicknesses and consequential high actuation strains make them suitable for the application in actuator devices, such as artificial muscles and microelectromechanical systems (MEMS).[83,84]

However, the fabrication of LCE actuators with the aid of electric fields is limited to ferroelectric liquid crystals. The efficient alignment of liquid crystals in an electric field requires strong dipole moments of the mesogens and strong external electric fields. For example, crosslinkable ferroelectric liquid crystalline polymers were aligned between two electrodes in a direct current electric field. After formation of a liquid crystalline monodomain, the liquid crystalline

polmyer was crosslinked by UV-initiated radical polymerization of free standing allyl-groups, which led to well aligned ferroelectric LCEs.[85]

Actuator Processing

The development of processing techniques for LCE actuators in terms of preparation speed and practicability, defined director field integration and actuator shaping is of great interest for further applications of LCEs in actuator devices. Lithographic processes open possibilities for an automated preparation of variously shaped LCE actuators, as recently presented by Ditter *et al.* for the patterning of actuating nematic LCE films in a hard mask process.[86] In this work, very thin LCE films (300 nm to 3500 nm) are synthesized in a spin-coating process including photoalignment layers for a uniform planar director orientation. Further coating and UV-patterning of a fluorinated photoresist through a variably designable photomask enables the subsequent patterning of the actuating LCE film by oxygen-etching. Other lithographic techniques were presented, which make use of magnetic fields for the orientation of LCE films between two glass substrates. By implementation of water soluble sacrificial layers, the separation of undamaged free standing patterned LCE actuators is provided.[87]

Soft Molding

Soft molding processes utilize surface patternings to shape the surface and include a director field to LCE samples. Soft poly(dimethylsiloxane) (PDMS) molds were used in combination with a permanent magnetic field to shape the surface of polymerizable low molecular weight liquid crystalline melts and simultaneously align the nematic mesogens perpendicular to the mold. By this method, cylindrical and square shaped strongly actuating micro-pillars were prepared on the surface of LCE films, which feature switchable optical and wetting properties and enable the transport of small objects over the surface.[37,90,91] Patterned microchannels in the length scale of calamitic mesogens have been prepared by soft-lithography for the application in a molding process (Figure 1.9a to 1.9c). In this case, complex alignments of the nematic director were achieved in liquid crystalline cells by applying topological defects and director twists to the LCE films, which showed three dimensional actuating patterns during the phase transition.[88]

Printing Techniques

Printing techniques offer another effective method for the preparation of variously shaped LCE actuators. A famous utilization of ink-jet printing was presented by Broer *et al.* for the preparation of light-driven artificial cilia.[92] An azo-benzene containing low molecular weight liquid crystalline monomer mixture was printed on top of a rubbed polyimide alignment layer, to enforce parallel alignment of the director at the interface to the substrate on the bottom. By addition of a surfactant to the mixture, a splay-bend mesogen orientation was gained through the printed film, as a perpendicular alignment was achieved at the boundary surface on top of the film. In com-

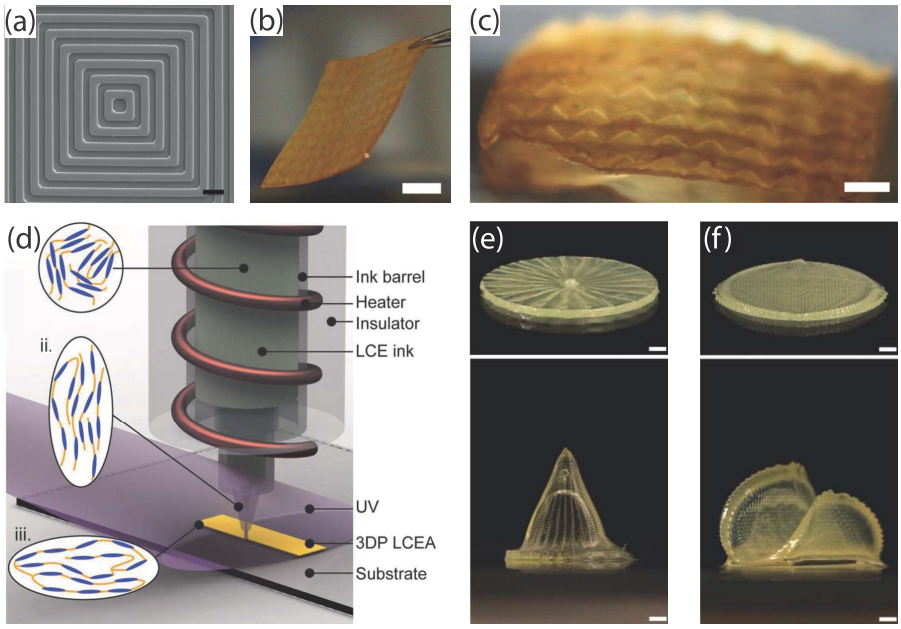

Figure 1.9 Actuator processing of LCEs by a microchannel soft molding method and a 3D-printing technique: (a) scanning electron microscopy image of a patterned 1D microchannel for LCE soft molding with a +1 defect structure and a channel width of 2 µm (scale bar: 5 µm).[88] Corresponding actuating LCE film at (b) room temperature and (c) 200 °C with a +1 and −1 defect array and a twisted liquid crystalline director by 90° (scale bars: (b) 3 mm, (c) 1 mm). (d) Schematic illustration of a heated printhead used for 3D-printing of programmable shape morphing LCE actuators.[89] Disk-shaped LCE actuators were printed via (e) layered spiral and (f) layered meander printing paths, which reversibly change their shape into a (e) cone and (f) saddle shaped morphology during the thermal phase transition (scale bars: 5 mm).

bination with a perpendicular aligned thermal actuation of a non-lightsensitive LCE, free standing cilia were produced, which show four different states of light-driven bending actuation.

Besides, 3D-printing techniques enable the simultaneous shaping and director orientation of LCE actuators (Figure 1.9d to 1.9f).[89,93] Two- and three-dimensional nematic main-chain LCE actuators are printed from liquid crystalline inks, which are polymerized and crosslinked via UV-initiated Michael-addition reaction. Multiple LCE layers are printed along a programmed path to form variously shaped objects, in which the director is oriented along the direction of the printing path. During the reversible nematic-isotropic phase transition, the LCE contraction along the direction of the printing path generates 3D-shaped changes of the objects, which are programmable by the design of the printing paths.

The microfluidic synthesis of LCE microparticles represents another effective processing technique for the preparation of aligned LCE actuators. This method is discussed in detail in Chapter 2.

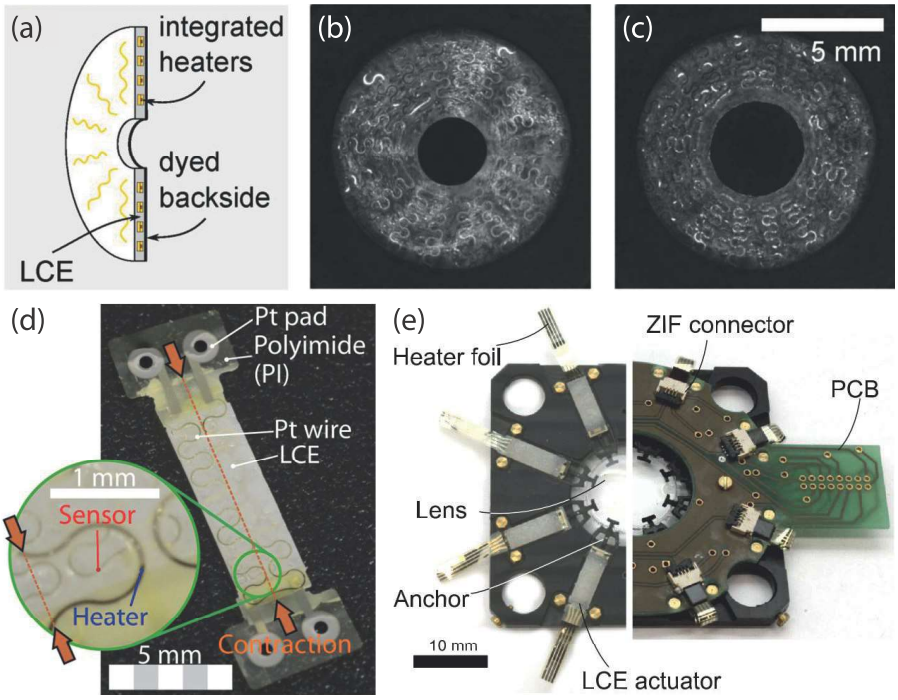

Figure 1.10 Actuator devices based on magnetically oriented nematic LCE films with integrated heating wires: (a) Schematic illustration of an actuating artificial iris with integrated polyimide-coated platinum wires, which features a nature-inspired radial contraction and expansion of the pupil during the phase transition between (b) the nematic and (c) the isotropic state.[94] (d) Stripe-shaped LCE actuator with integrated heating wires and temperature sensors, which was utilized in (e) an application for remotely controlling the strain of an elastomeric lens.[52,84]

LCE Devices

Different actuator devices have been established, in which the stimuli-responsive shape change of integrated LCEs is utilized in various ways for the application as MEMS. Recent developments of Schuhladen *et al.* presented the integration of polyimide coated platinum wires and temperature sensors in thermotropic LCE films to enable remotely controlled heating and actuation.[52,84,94] The applied voltage to the wire dictates the temperature inside the LCE as well as the consequential phase transition and shape change of the actuator. By means of this method, a spherically shaped artificial iris was fabricated, which contracts and expands similarly to a human iris while changing the pupil diameter (Figure 1.10). The variation of the aperture by change of the impressed voltage to the heating wire thereby controls the amount of the incident light. The radial director field of the LCE iris was produced by circular arranged magnets, which provided a radially symmetric magnetic field. Furthermore, uniaxially oriented remotely heatable LCE stripes were synthesized by use of a horseshoe magnet. A radial arrangement of these actuators and simultaneous heating and temperature control via integrated sensors

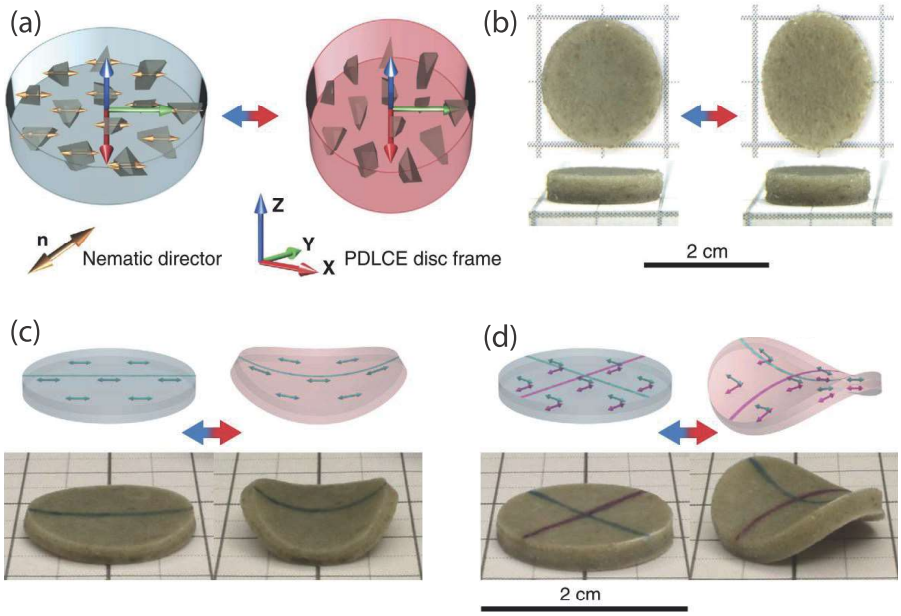

Figure 1.11 Application of oriented LCE colloids in programmable shape morphing polymer dispersed LCEs: (a) Schematic illustration and (b) photographs of the thermal shape change of a disk-shaped PDMS actuator, which appears spherical in the nematic state at 300 K (left) and changes to an elongated ellipsoidal shape in the isotropic state at 400 K (right). Bilayered actuators are formed by (c) the combination of an actuating and non-actuating elastomeric disk to yield a bend deformation during the phase transition or (d) the stack of two perpendicular aligned polymer dispersed LCE actuators, which features a saddle deformation in the isotropic state.[95]

enabled the strain of an elastomeric optical lens and subsequent control over its optical properties.

LCE Composite Materials

Another promising application of thermally actuating LCEs was introduced by Resetic *et al.*, who integrated micrometer sized actuating LCE colloids in an isotropic polymeric matrix to form actuating composite materials featuring various programmable shape changes.[95] For this purpose, an oriented nematic LCE bulk was crushed via freeze-fracturing into LCE microparticles, which were subsequently dispersed in a curable PDMS matrix. After the uniform alignment of the LCE colloid directors in a magnetic field, the isotropic PDMS matrix was cured to form an actuating elastomeric composite sample, which performed shape changes at the phase transition of the incorporated LCE particles (Figure 1.11). By applying different director orientations to the samples and combining actuating samples with non-actuating layers, various shape changes of spherical samples were achieved, such as bending, twisting, cup-like and saddle-shaped deformations. This method offers the advantages of a reduced consumption of LCE material in spite of the fabrication of large actuators at variable mechanical properties of the employed polymeric matrix.

Light Responsive Devices

Different light-responsive LCE actuators have been integrated into photomechanical devices as well, which commonly use the *trans-cis* isomerization of azo compounds to trigger an isothermal phase transition and a consequential shape change.[96] One of the most famous light-driven devices was presented by Ikeda and coworkers, who incorporated a UV-responsive LCE film to power a plastic motor.[97] In this study, an LCE laminated film was used as a belt between two pulleys to fuel their rotation. The film was irradiated by UV-light at one side of the motor to trigger a contraction along the alignment direction, whereas an irradiation by visible light caused the rearrangement of the nematic state and subsequent relaxation of the film in another area of the motor. Besides, the group introduced a bending LCE composite film, which acted as a light-driven worm-like walker to perform a lateral motion on a substrate.[98] These hybrid films were considered as propulsion systems and suitable for an application in robot arm elements. The bending actuation pattern of azo-compound containing LCE films was further utilized for the preparation of self-oscillating sunlight-driven actuators.[99] In this application, a splay-oriented nematic LCE film containing fluorinated azobenzene chromophores featured a chaotic continuous oscillatory motion in the presence of blue and green light.

2 MICROFLUIDICS

The development of microfluidic systems was initiated in the late 1980s, when the demand for small scaled mechanical devices such as micropumps and microvalves improved.[100] Microfluidics has been treated as a segment of the MEMS technology, which deals with the miniaturization of devices for the handling of microscopic amounts of fluids. Especially in the fields of chemistry and life science, the development and application of microfluidic devices is of great interest.[101] In chemistry production, microfluidics is applied for micromixing, microreaction and microseparation techniques, whereas in the field of analytical chemistry, microfluidics is utilized for microanalysis and microdetection in gas and fluid measurement devices. Furthermore, the implementation in life science techniques covers medical diagnostic systems, such as medical testing and drug-screening devices, as well as the application for scientific research, *e.g.* in the fields of genetic sequencing and drug discovery.[102,103]

General Considerations

Microfluidic systems are often referred to as lab-on-a-chip devices, which pictures the manipulation of microvolume fluids in channels with the dimension of tens to hundreds of micrometers.[104,105] In this manner, the flow physics in microfluidics covers the range of size between the macroscopic continuum regime and the molecular dominated nanoscopic regime, which brings various advantages to the fluid behavior of microfluidic small-size scales.[106] The high surface-area-to-volume ratio and the consequential large specific interface area in microfluidic systems enables an excellent control over the heat and mass transfer. Especially for the chemical production, the distributed energy supply and thermal management of microfluidics offers many advantages over the macroscopic production in bulk. For these reasons, the microfluidic production of polymeric particles plays an important role for the new design and technology of functional materials.

2.1 POLYMERIC MICROPARTICLE FABRICATION

Various microfluidic systems and technologies have been developed for the preparation of many different kinds of polymeric materials, which offer different sizes, morphologies, compositions and functionalities (see Figure 2.1).[107] Microfluidic syntheses with stable phase interfaces of immiscible liquids are subdivided into two different kinds of methods: (i) emulsion droplet systems with closed liquid-liquid interfaces and (ii) laminar flow systems with non-closed liquid-liquid

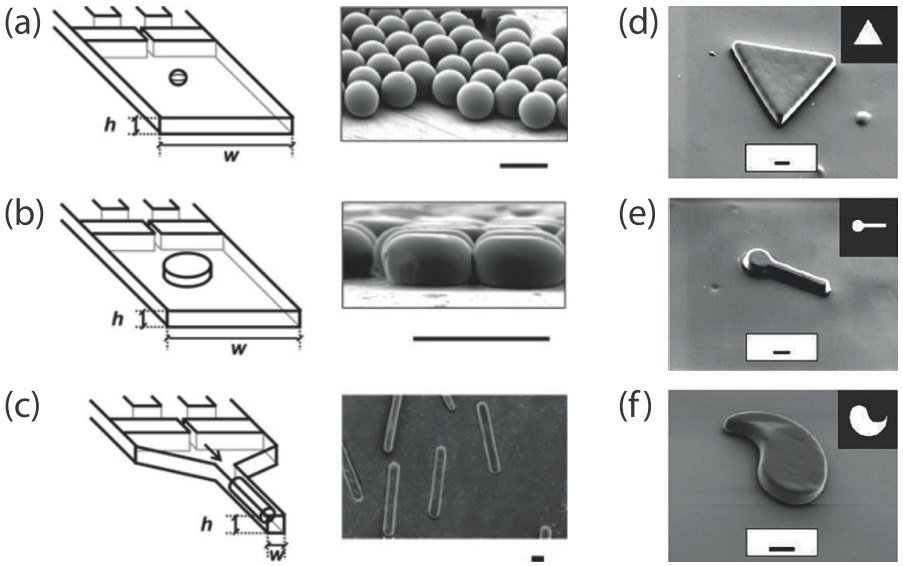

Figure 2.1 Variously shaped microparticles prepared from microchannel based microfluidic devices: Schematic illustration of flow focusing microchannel devices and corresponding microscopy images of (a) spherical, (b) disk-like and (c) rod-like polymeric microparticles obtained via photopolymerization (scale bars: 50 µm).[108] Scanning electron microscopy images of (d) triangular structured, (e) curved and (f) key-shaped microparticles and corresponding irradiation masks. These flat microparticles were produced via projection photolithography microfluidic devices (scale bars: 10 µm).[109]

interfaces. Laminar flow systems are typically used for the preparation of membranes or microfibers in microchannels, or complex colloidal structures by continuous flow projection photolithography. However, emulsion droplet systems are suitable for the production of microspheres and microcapsules, which have been used as microreactors, carriers, microseparators, structural units for drug delivery and substance encapsulation. By this method, multicomponent liquid-liquid interfaces by parallel or series microchanneling enable complex structures of microspheres, such as core-shell structures, Janus structures and multicore spheres. In this work, an emulsion droplet technique is used for the preparation of polymeric microparticles, for which reason only this technique is focused on hereinafter.

Emulsion Droplet Microfluidics

For the production of polymeric microparticles in droplet based microfluidic systems, small fluid volumes of a liquid polymerizable monomer (dispersed phase) are emulsified in an immiscible continuously flowing carrier fluid (continuous phase).[110–113] Subsequent curing of the dispersed phase and separation from the continuous phase leads to polymeric particles with typical particle size distributions below 5 %. Droplet microfluidics offers great advantages over homogeneous polymer particle preparations by suspension techniques in terms of the control over particle size, morphology and composition.

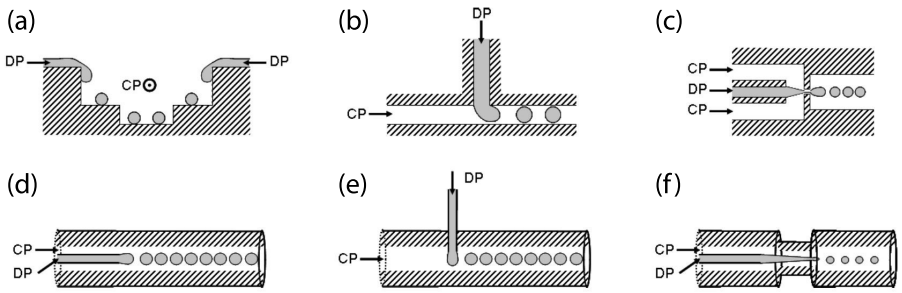

Figure 2.2 (a) Terrace-like microchannel device: The continuous phase (CP) is provided in a main channel, whereas microchannels deliver the dispersed phase (DP) from both sides at the top of the main channel. Terraces below allow the breakup of the dispersed phase. (b) T-junction microchannel device: The dispersed phase is injected by a microchannel perpendicular to the main channel and the continuous phase. (c) Flow-focusing microchannel device: The dispersed phase flows in a central microchannel, whereas the continuous phase is provided by two side channels. Hydrodynamic focusing by an orifice causes the break down of the DP jet into droplets. (d) Co-flow capillary device: The dispersed phase is delivered by a centered microcapillary inside a tube in the same direction as the continuous phase. (e) Cross-flow capillary device: The dispersed phase in injected by a microcapillary perpendicular to the continuous phase flow direction. (f) Flow-focusing capillary device: The dispersed phase is elongated by the axisymmetrical pinch of the continuous phase by reasons of a converging tube. The focused jet breaks down into droplets under capillary instabilities.[113]

Different strategies for the droplet dispersion in the continuous phase have been developed, in which the droplet formation is based on the counteraction of viscous and interfacial forces. Microfluidic droplet devices are either based on two dimensional microchannel systems or three dimensional capillary based setups, as described in Figure 2.2. In both cases, droplets are emulsified by the breakup of the dispersed phase during the shear of the continuous phase, either at the edge of a microchannel or at the tip of a capillary. Microchannel devices are fabricated by lithographic processes in silicone, glass or PDMS matrices, which enables the generation of very complex fluid paths on a small length scale with high resolutions.[114,115] The capillary based devices consist of commercially available needles, glass capillaries, polymer tubes and T-junctions and work at larger length scales.[116–119] The advantages of the microchannel devices are their complex and individual designable channel paths as well as smaller and more complex morphologies of the synthesized microparticles. On the other side, the capillary based systems provide less complex constructions and easy accessibility. Furthermore, an inverse emulsification is prevented in case of a high affinity of the dispersed phase to the channel's wall material. Each method provides the droplet formation via co-flow, cross-flow or flow-focusing devices (FFDs), which are described in detail in Figure 2.2.

Capillary Based Co-Flow Injection

The co-flow injection mode in a capillary based microfluidic device enables the continuous dispersion of symmetrically shaped droplets in the center of the carrier fluid's flow field. The droplet formation is either performed in the dripping or the jetting mode. In the dripping mode, highly monodispersed droplets are formed at the tip of a glass-capillary or an injection needle, at which the minimum droplet size is limited to the inner diameter of the providing capillary. In the jetting mode however, a continuous jet of the dispersed phase is first produced, which breaks down to dispersed droplets after a short distance from the capillary. In this case, smaller droplets with sizes below the capillary diameter are obtained, whereas the droplet size exhibits a higher polydispersity. The particle size is usually adjusted by controlling the dimensionless quantities called the *Reynolds number* R_e and the *capillary number* C_a.

$$R_e = \frac{\rho q D}{\mu} \tag{2.1}$$

$$C_a = \frac{\mu q}{\mathrm{Y}} \tag{2.2}$$

The Reynolds number R_e describes the ratio between the inertial forces and the viscous forces, which derive from the fluid density ρ, the flow velocity q, the capillary dimension D and the fluid viscosity μ. The size of R_e is therefore a measure for the tendency of the microfluids to form turbulant flow profiles. As the capillary dimensions in microfluidic systems are typically low and high viscosities of applied fluids are chosen, the Reynolds number mostly assumes low values and a laminar flow profile is consequentially generated. The capillary number however describes the ratio between the viscous forces and the interfacial tension Y between the dispersed and the continuous phase. For a droplet formation in the dripping mode, small capillary numbers are necessary, which are commonly reached by choosing dispersed and continuous phases with high interfacial tensions. The droplet size at constant and small values for R_e and C_a depends on the ratio between the flow rates of the dispersed and the continuous phase Q_d/Q_c at constant total flow rates. Furthermore, the selection of a highly viscous continuous phase raises the shear on the forming droplets and causes an early separation from the capillaries tips, which leads to smaller droplet diameters, as well.

The dispersed phase for the microfluidic generation of polymeric particles typically consists of a polymerizable monomer mixture, such as acrylate, methacrylate or vinyl group containing reactive monomers in combination with multifunctional crosslinker moieties and a radical initiator. The continuous phase commonly contains a hydrophobic silicone oil or a hydrophilic solution of a water soluble polymer with respect to the polar character of the dispersed phase.

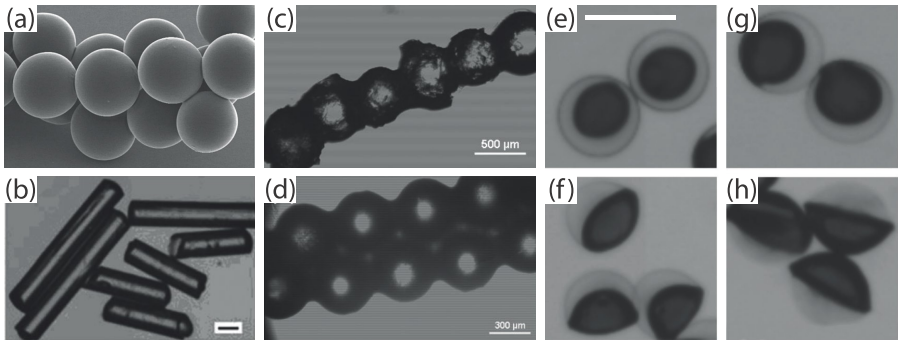

Figure 2.3 Various morphologies of microparticles produced in capillary based microfluidic devices: (a) Scanning electron microscopy image of biocatalysts containing spherical hydrogel particles with diameters of 90 µm.[120] (b) Rod-like poly(TPGDA) particles produced in a co-axial capillaries microfluidic setup (scale bar: 200 µm).[116] (c) Covalently bonded polymer bead necklace and (d) double necklace produced from stacked microparticles in a converging pipe.[117] (e) Core-shell, (f) acorn-like, (g) eccentric Janus and (h) bicompartimental Janus particles generated in a side-by-side capillaries device at different flow rate ratios of the dispersed phases (scale bar: 300 µm).[121]

After the droplet formation, the dispersed droplets are transported by the continuous phase to the polymerization zone of the microfluidic device, at which the polymer particles are formed by radical initiation of the polymerization and crosslinking process. The particle formation is commonly initiated via visible or UV-light irradiation of an included radical photoinitiator or via heat based radical formation. Besides, chemical reaction based initiation has been utilized as well, in which the polymerization is initiated only by the addition of a reacting agent to the dispersed droplets inside the microfluidic device. For instance, the radical initiation by merging two different dispersed phases each containing parts of an ARGET-ATRP (activator regeneration by electron transfer-atom transfer radical polymerization) initiator system enables the UV-free polymer particle fabrication at low temperatures.[7]

Beside the fabrication of spherical particles, other morphologies have been achieved in capillary based microfluidic reactors, as well. Figure 2.3 illustrates variously shaped particles with different morphologies, which were synthesized in capillary based microfluidic setups. Stacked particle chains were prepared by accumulation of spherical droplets and subsequent UV-polymerization in a converging capillary.[117] Rod-like particles were generated in a very thin capillary, at which the droplet volume completely fills the form of the capillary channel.[116] Furthermore, the extension of the single capillary based droplet device by a second capillary enables the formation of core-shell and Janus droplets.[121–123] In this case, the second capillary is either applied parallel or telescoped to the first one, in order to provide a second polymerizable monomer mixture, which is

immiscible with both the continuous phase and the other dispersed phase. Typically, hydrophobic monomer mixtures are used in combination with immiscible hydrophilic dispersed phases either to form the core and the shell of a corresponding core-shell droplet or to generate the two hemispheres of a Janus droplet. Transition structures between the morphology of core-shell and Janus droplets are obtained as well, such as acorn-like or so called eccentric Janus droplets. With the aid of detergents and the regulation of the ratio between the dispersed phases, the desired droplet morphology can be adjusted by stabilization of the interface between the two dispersed phases and the continuous phase. Subsequent polymerization preserves the particular droplet morphology. It has to be mentioned, that the accessible droplet morphologies and consequential particle shapes in capillary based co-flow microfluidic devices are limited to deformations of spheres.

2.2 LIQUID CRYSTALS IN MICROFLUIDICS

Microfluidic devices have been used for the processing of liquid crystals in many cases.[124] First and foremost, the possibility of producing monodispersed liquid crystalline microdroplets with a precise control over the droplet size and morphology via microfluidics enables both the study of liquid crystalline phases and the preparation of LCE microactuators. The analysis of the liquid crystalline director field and defect structures in spatial confined liquid crystalline droplets of various sizes has been executed on different kinds of droplets, such as nematic, smectic or cholesteric liquid crystals in spherical droplets or droplet shells.[125–129]

Liquid Crystal Droplets

In most of the studies, liquid crystalline droplets are dispersed in an immiscible isotropic fluid (such as aqueous solutions or silicon oils) via microchannel or capillary based microfluidics, and polarized optical microscopy is applied for the investigation of topological defect structures. Based on their anisotropic physical properties, liquid crystals cannot be treated as Newtonian fluids since the viscous stresses are not linearly proportional to the local strain rate arising during the flow over time. However, the properties of liquid crystal droplets in microfluidic environments are mostly similar to Newtonian fluids, whereas the microfluidic processing of liquid crystals in the isotropic phase ensures Newtonian behavior.

For the stabilization of liquid crystalline droplets and shells in aqueous continuous phases, surfactants are commonly used at the water/LC interface, which reduces the interfacial tension on one hand and affects the surface anchoring of the mesogens on the other hand. By choosing different kinds of surfactants, the surface anchoring conditions are predetermined and a certain director field in liquid crystalline droplets is targeted. For the specification of a homeotropic

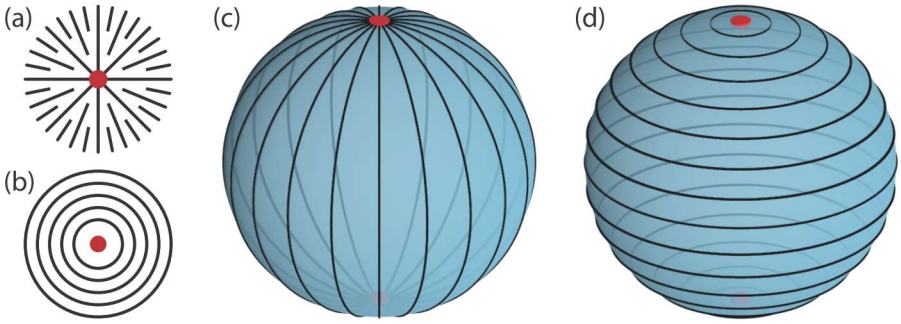

Figure 2.4 Defect singularities confined to surfaces (boojums) with (a) splay and (b) bend director field deformations and integer surface charges of $s = +1$. Commonly found defect structures for microdroplets with (c) bipolar and (d) concentric director field configuration.

alignment, low molecular weight surfactants with aliphatic chains are suitable, which extend into the hydrophobic liquid crystalline phase at the interface (*e.g.* SDS: sodium dodecyl sulfate). A planar anchoring of the mesogens at the interface is generated by polymeric surfactants, as the random coil polymer conformation favors the interfacial interaction of water molecules with the mesogenic aromatic cores. (*e.g.* PVA: polyvinylalcohol).

Defect Structures in Droplets

In emulsified droplets of liquid crystals, the volume of the mesogens is confined by the spherical boundary surface of the droplet. The anchoring conditions at the droplet interface are defined by the nature of the surrounding phase and the presence of surface-active compounds, which in turn impose topological constraints to the director field at the interface. These constraints are the reason for the inevitable occurrence of topological defects.[126] Figure 2.4 illustrates different defects and director fields, which are important for nematic liquid crystalline droplets.

In the close proximity of a defect in the liquid crystalline director field, the mesogenic order is reduced. The closer a considered region is located to the singularity of the defect, the more decreased is the liquid crystalline order parameter S. In the defect core, the liquid crystalline order disappears and the mesogens assume the isotropic state with an order parameter of $S = 0$. In nematic liquid crystalline droplets, defects in the droplet bulk (hedgehogs) and topological surface defects at the droplet interface (boojums) can occur in the director field. Hedgehogs are characterized by the topological charge Q, whereas boojums are classified by the surface charge s.

In microfluidic devices, nematic liquid crystalline droplets are commonly dispersed with the size of several micrometers right up to the scale of hundreds of micrometers. Within this scale, the surface energy predominates the bulk elastic energy, which is why the surface anchoring effects determine the director field rather than the endeavor of the liquid crystalline bulk to align parallel.[130] In the case of

a homeotropic anchoring, micrometer sized droplets assume a radial director field with a hedgehog defect in the droplet center, whereas nanodroplets show a defect free uniaxial director configuration.[82]

For microdroplets with planar anchoring conditions, two different director configurations were found. The bipolar director field is the energetically preferred orientation, in which two boojums with splay director deformation are oppositely positioned at the droplet interface (Figure 2.4c). Both defects are separated by the maximum distance of the droplet diameter and the director field in bulk shows bend deformations. In microdroplets, the concentric configuration is another possible director orientation, which however is energetically unfavored. In this case, two boojums with bend director deformation are connected by a virtual line defect and the mesogens are oriented along concentric rings around this line (Figure 2.4d). It was shown, that the high energetic concentric configuration is preferred over the bipolar configuration, if a continuous circular flow is present inside the droplet.[131]

Actuating LCE Microparticles

Beside the fundamental study of liquid crystalline phases in microdroplets, microfluidics represent an excellent method for the preparation of actuating LCE microparticles from liquid crystalline droplets. For this purpose, capillary based microfluidic devices have been proven successful in terms of chemical and high temperature stability as well as the prevention of channel wetting by the hydrophobic liquid crystalline droplets.

The first successful microfluidic synthesis of actuating LCE particles was accomplished by Ohm *et al.* by UV-initiated polymerization and crosslinking of a low molecular weight nematic side-chain monomer.[64,65,132] The particle production was performed in two different temperature zones within a fused silica capillary based microfluidic device. At first, the droplet formation occurs at temperatures above the clearing point of the liquid crystalline monomer mixture, to assure Newtonian properties and sufficient fluidity of the dispersed phase. However, the polymerization of the droplets is processed via UV-irradiation within the nematic phase of the liquid crystalline droplets to provide the generation of an ordered director field. For these particles, the unusual concentric director field was confirmed by wide-angle X-ray scattering (WAXS) measurements, which can be explained by the occurrence of a circular flow inside the droplets. As the droplet dispersion is performed in a highly viscous silicon oil continuous phase, a laminar flow at low Reynolds numbers is assumed during the transportation of the droplets in the microtube. During the continuous droplet flow, a shear gradient works perpendicular to the flow velocity on the microdroplet and causes a so-called *log-rolling* orientation of the mesogens along a concentric director field.

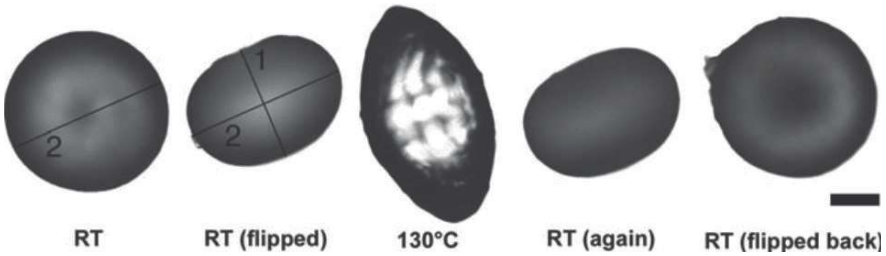

Figure 2.5 Reversible actuation of an oblate shaped LCE microparticle into a rod-like shape. The particle morphology is illustrated in the glassy phase of the LCE at room temperature from a top and a side-view. After heating up the particle to the isotropic state at 130 °C, a strong elongation along the particle main axis as well as a contraction of the particle radius is observed. By cooling down the particle to room temperature again, the former oblate shape is completely recovered (scale bar: 100 µm).[64]

LCE particles of spherical and oblate shapes were produced by this method and the particle size was varied in between diameters of 200 µm to 600 µm by modification of the flow rate ratio of the dispersed and the continuous phase. These particles feature strong shape changes during the phase transition of the LCE, at which actuations up to 80 % were measured. By heating up the particles above the LCE clearing temperature, an expansion of the particle geometry along the particle rotational axis occurs perpendicular to the concentric rings of the director configuration. Consequently, the particle contracts along the concentric director orientation at the same time, which leads to a transformation from a spherical or oblate shaped particle to a rod-like morphology. The shape change during the thermal phase transition of an exemplified oblate shaped microparticle is illustrated in Figure 2.5. This actuation is completely reversible and can be triggered by swelling of the LCE network in isotropic organic solvents, as well.

Beside the preparation of particles with concentric director configuration, this method was modified for the fabrication of elongated, fiber-like particles by strongly increasing the shear rate on the droplets during their flow in the microtube. These rod-like particles featured a bipolar director configuration and strong contractions along the particle rotational axis were found during the phase transition.

LCE Shells And Fibers

A nested glass capillary microfluidic device was utilized by Fleischmann *et al.* for the preparation of actuating LCE core-shell particles, which feature the application as one-piece micropumps.[133,134] For this approach, two cylindrical tapered capillaries are centered oppositely in a squared capillary and two immiscible dispersed phases are co-flow injected in a counter-flowing continuous phase to form a short jet in a flow-focusing constriction area. The inner dispersed phase contains glycerol whereas the outer dispersed phase consists of a polymerizable nematic monomer mixture, which forms an interface to the surrounding continuous flow of silicone oil. The jet

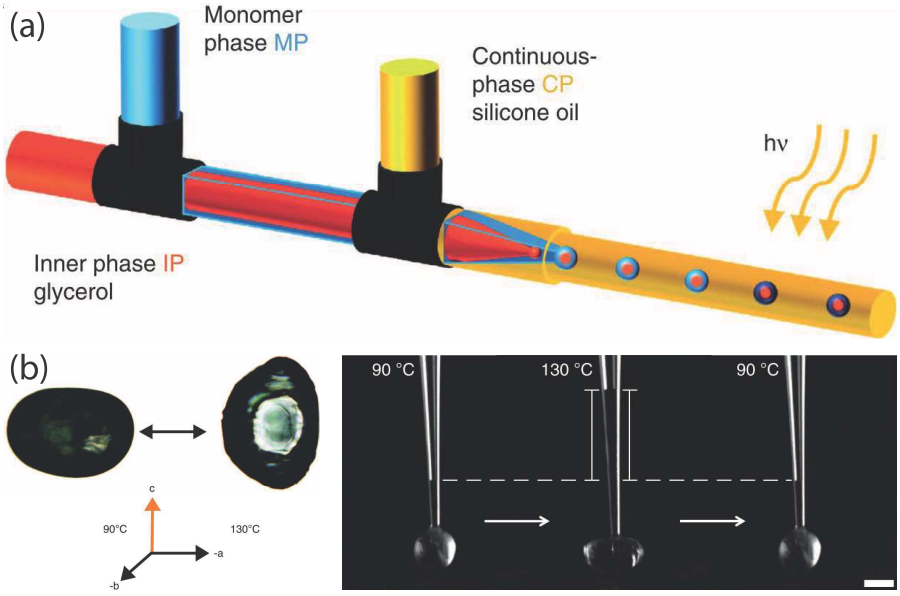

Figure 2.6 (a) Nested capillary microfluidic setup for the fabrication of LCE core-shell microparticles. (b) Shape change of an ellipsoid shaped core-shell actuator during the thermal phase transition (left) and micropump process of a capillary pierced core-shell microparticle during the nematic-isotropic phase transition (scale bar: 100 µm).[133]

breaks down into core-shell droplets inside the collection capillary and subsequent UV-irradiation leads to crosslinked LCE shells. For these shells, a bipolar director configuration was detected via WAXS measurements, which was traced back to a circular flow of the mesogens caused by the shear of the surrounding stream of the highly viscous silicon oil. Furthermore, the microshells assume an ellipsoid shape after the crosslinking process and a contraction along the ellipsoid main axis was detected during the thermal phase transition. By piercing the shell with a glass capillary and permeation into the glycerol core of the particle, the inner phase was reversibly pumped into the capillary during the contraction of the shell at the LCE phase transition. Figure 2.6 illustrates the microfluidic setup as well as the core-shell micropump actuation during the phase transition.

In addition, a crosslinkable liquid crystalline polymer precursor was used for the fabrication of actuating fibers and particles in a capillary based microfluidic device.[135] In this case, the to be dispersed polymer was dissolved in an organic solvent to reach processability despite its high viscosity. A stable jet of the dispersed phase was generated in a thin microtube, which was polymerized by UV-irradiation to yield strongly contracting LCE fibers.[136]

Further LCE particles

Research groups have worked on the microfluidic preparation of LCE particles ever after. Kim *et al.* demonstrated the preparation of spherical LCE particles with diameters below 100 µm, which showed a tangential director configuration upon uniaxial compression.[137] Be-

sides, Marshall *et al.* presented the fabrication of actuating LCE particles in two steps, one for the microfluidic droplet formation and a second step for the director alignment by mechanical stretching. At first, liquid crystalline precursor droplets were fabricated in a PDMS microchannel device, in which the droplets were dispersed in an aqueous solution of PVA. Then, the collected precursor particles are suspended in a concentrated aqueous PVA solution and the water is subsequently evaporated to obtain the liquid crystalline particles embedded in a solid PVA matrix. For the orientation step, the matrix is uniaxially stretched at temperatures of the nematic state, at which the mesogens are consequentially aligned along the direction of the mechanical stretching. Subsequent UV-irradiation and dissolution of the PVA matrix yields strongly anisotropic LCE particles, which show contractions upon heating above the LCE clearing temperature and spherical shapes in the isotropic state.[138]

3

JANUS PARTICLES

Janus particles are non-centrosymmetric patchy particles, which consist of two different phase separated materials. Each phase typically provides different chemical and physical properties, which generates an asymmetry of the colloidal characteristics within a single particle.[139] Accordingly, the advantages of two well-known disciplines are unified in the idea of Janus particles to generate a promising kind of functional material: On one side, the asymmetry of molecular structures, such as surfactants or block-copolymers, enables the self-assembly process into various aggregate structures. On the other side, the particular structure of micro and nanometer scaled colloids of various materials holds a wide range of potential functionalities, such as optical activity, magnetism or mechanical strength. Especially the broken symmetry of Janus micro- and nanoparticles offers unique properties for their use as building blocks for self-assembly approaches, which are inconvertible with homogeneous particles. The term *Janus* particle derives from the roman god Janus, who has always been pictured with two oppositely directed faces on a single head.

3.1 SYNTHETIC ROUTES TO VARIOUS JANUS PARTICLES

In his Nobel lecture about "Soft Matter" in 1991, de Gennes took the first step to realize the high potential of Janus particles for the field of advanced functional materials. Since that time, the development of synthetic strategies for Janus particles has been a big challenge for many researchers. Most of the synthetic approaches either utilize the self-assembly of smaller asymmetric components or make use of breaking the symmetry of homogeneous particles.[140] These strategies are commonly based on classical organic synthesis, macromolecular engineering and self-assembly of polymers, symmetry breaking at interfaces or within confined volumes, selective growth of second compartments or microfluidic devices with side-by-side flowing liquids. Furthermore, various morphologies of Janus particles are accessible, such as spherical, disk-like or cylindrical shapes, different dumbbell morphologies and vesicle or capsule Janus structures. Applications of Janus particles are found in the fields of solid surfactant self-assembly, electronic paper, modulated optical sensors and life-science.[141–148]

Unimolecular Janus Particles

The preparation of nanoscoped Janus particles on the smallest possible length scale is based on the synthesis of unimolecular Janus structures, such as asymmetric dendrimers, heterografted polymers

and silsesquioxanes. The classical organic synthesis of dendrimers with varying amounts of branching points as well as different branch lengths and functionalities offers a good control over the regional molecular functionalities and a possibility for the formation of Janus structured molecules. For this purpose, giant amphiphilic dendrimers have been synthesized with hydrophobic benzyl ether groups on one side and carboxylic acid groups on the other side of the molecule.[149]

Another example are heteroarm star-shaped polymers or cylindrical polymer brushes, which are grafted with two different polymers to yield spherical or cylindrical Janus nanoparticles. The prerequisite for this approach is the high incompatibility of the two applied polymers to assure the demixing within the heterografted polymer structure. Stimuli-responsive heteroarm star polymers with switchable hydrophilic-to-hydrophobic block transitions were prepared by grafting poly(*N*-isopropylacrylamide) (PNIPAAm) and poly(*N*,*N*-diethylamino-2-ethylmethacrylate) (PDEA) blocks on a precursor molecule to yield Janus structures, which self-assemble into invertible vesicles (Figure 3.1a to 3.1c).[150] Cylindrical Janus brushes were synthesized by grafting poly(styrene) (PS) and poly(isoprene) (PI) onto long reactive AB diblock copolymer backbones to generate Janus cylinders, which assemble into micellar structures.[151]

Furthermore, silsesquioxanes were functionalized with isobutyl or carboxylic groups at the corners of their cubic shaped molecular cage structures to introduce different polarities to the molecule shell. Either the combination of two silsesquioxane half cages of different functionalities or the formation of dimers leads to well defined molecular Janus structures.[152]

Janus Micelles from Block-Copolymers

Different kinds of block copolymers have been used for the formation of Janus micelles in solution. The direct formation of micellar Janus structures via simple dissolution of block-copolymers additionally demands the application of crosslinking or solubility transitions of functional polymer segments. Diblock copolymers are self-assembled into Janus micelles either by applying AB and BC block copolymers with the B block insoluble in the surrounding solvent or by using AB and CD block copolymers with attractive interaction between the blocks B and C. An example for the latter method made use of poly(ethylene oxide) (PEO) and poly(acrylamide) (PAAm) as the soluble end blocks A and D, whereas poly(*N*-methyl-2-vinylpyridinium iodide) (P2MVP) and poly(acrylic acid) (PAA) formed the attracting core blocks B and C. The asymmetric shapes of the oppositely charged soluble blocks thereby support the assembly into Janus micelles.[153]

Another synthetic route represents the assembly of ABC triblock copolymers, in which the B-block exhibits insolubility. The study of PEO-*block*-PnBuA-*block*-PNIPAAm copolymers with different lengths of the thermo-responsive end blocks showed the phase segregation

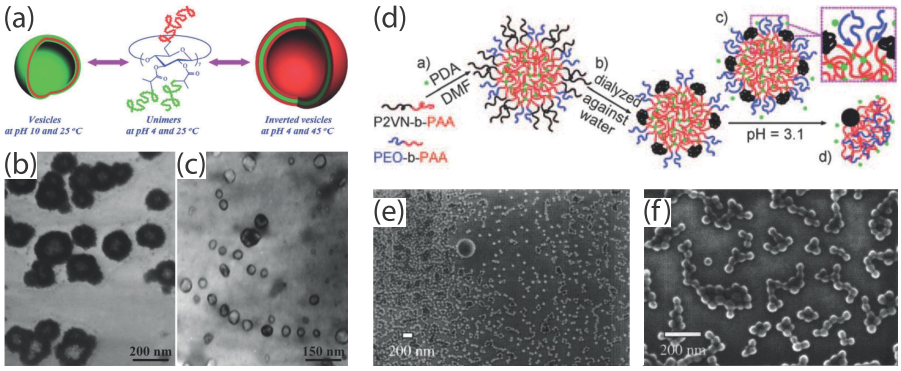

Figure 3.1 (a) Schematic illustration of the Janus structured heteroarm star polymer $(PDEA_{30})_7$-CD-$(PNIPAM_{25})_{14}$ and the reversible self-assembly process into vesicles with inverted shell structure at different pH-values. Corresponding transmission electron microscopy (TEM) images of micellar aggregates at (b) pH 4 and 45 °C and (c) pH 10 and 25 °C.[150] (d) Schematic representation of the preparation of Janus nanoparticles from mixed shell micelles: a) self-assembly in DMF, b) P2VN collapse in water, c) intramicellar complexation, d) micelle transformation into Janus nanoparticle by P2VN aggregation.[155] (e),(f) SEM images of Janus micelle aggregates prepared via crosslinking from micro phase-separated PS-*block*-PB-*block*-PMMA terpolymers in bulk.[156]

of Janus micellar structures in some cases.[154] The transformation of mixed copolymer micelles into Janus micelles has also been presented (Figure 3.1d) by applying different crosslinking reactions and solubility changes to the AB and BC block-copolymer system of PEO-*block*-PAA and PAA-*block*-poly(2-vinyl naphthalene) (P2VN).[155] Another synthesis of Janus micelles arises from selective crosslinking of spherical domains in ABC *block*-terpolymer bulk structures. In the case of the PS-*block*-PB-*block*-PMMA triblock copolymer, areas of the poly(butadiene) (PB) block are crosslinked at the interface of two lamellar domains of PS and poly(methyl methacrylate) (PMMA) blocks, which leads to spherical shaped Janus micelles (Figure 3.1e and 3.1f).[156]

Symmetry Breaking at Interfaces

The desymmetrization of homogeneous particles at interfaces has become the widely used and most effective synthetic method for the fabrication of Janus particles of micron and nanometer scale. The modification of particles at planar surfaces is the most straightforward method, in which particles are immobilized on top of a surface, followed by a symmetry breaking synthetic modification step of certain parts of the particles. Metal deposition was used from the vapor phase to generate magnetic Janus particles from polystyrene colloids. A monolayer of homogeneous particles was formed by physical attraction on top of a glass substrate and subsequent evaporation of cobalt led to Janus particles. The different Janus balances of these particles were controlled by the aid of a photoresist on top of the monolayers.[157]

For a solvent based modification of particles, a tighter connection of the particles to the surface is necessary. For this purpose, different techniques have been developed, such as the reversible embedding of particles into a PDMS matrix or the covalent immobilization of amine functionalized silica particles on poly(styrene-*ran*-acrylic acid) surfaces by ester-mediated amide formation, which further allowed the formation of triphasic Janus particles.[158]

Besides, microcontact printing offers another method for breaking the symmetry of homogeneous particles. By immobilization of negatively charged polystyrene beads in a dried glucose matrix on top of a glass substrate, a cationic surfactant was printed on top of the particle monolayer by using a stamping technique. By reasons of electrostatic adhesion, the surfactant remained on one half of the polystyrene particles after their removal from the glucose layer to form bipolar Janus particles.[159] UV-induced photografting was used to functionalize silica particles with diameters of 70 µm. For this method, a densely packed colloidal crystal layer of functionalized silica beads was formed via spin-coating and Langmuir-Blodgett array, followed by the UV-photografting and polymerization of a monomer mixture on top of the particles. Bicolor and amphiphilic Janus particles were synthesized with different polymer coatings and various sizes.[160]

Beside the desymmetrization of particles at planar surfaces, the application of Pickering emulsions represents a high performance method for the preparation of Janus particles, as well. Pickering emulsions are particle-stabilized oil-in-water emulsions, in which the particles cover the interface of the oil droplets. For this approach, a wax forming oil was used above its melting temperature to form pickering emulsions from silica particles in water. At room temperature, the oil droplets solidified and yielded the homogeneous particles immobilized on the surface of wax particles (Figure 3.2a and 3.2b). Subsequent functionalization of the silica particle hemispheres in aqueous solutions resulted in Janus particles with adjustable Janus balances by the aid of additional surfactants.[161,162]

Phase Separation and Phase Inversion

The phase separation of two homopolymers in a confined volume can be used for the symmetry breaking of droplets in emulsions and the formation of micrometer-scaled Janus particles. Surfactant stabilized emulsions of PS and PMMA homopolymer solutions in toluene were used to prepare Janus particles by slow evaporation of the toluene and consequential segregation of the two polymers. Various morphologies were obtained by the use of different kinds and concentrations of surfactants and different homopolymer molecular weights, which ranged from eccentric core-shell particles to bicompartimental Janus particles.[163,164] For the fabrication of more complex Janus structures, a modified PS-homopolymer with functional ATRP-initiator groups was used after phase separation for the growth of a poly(2-(dimethylamino)ethyl methacrylate) (PDMAEMA) hemi-

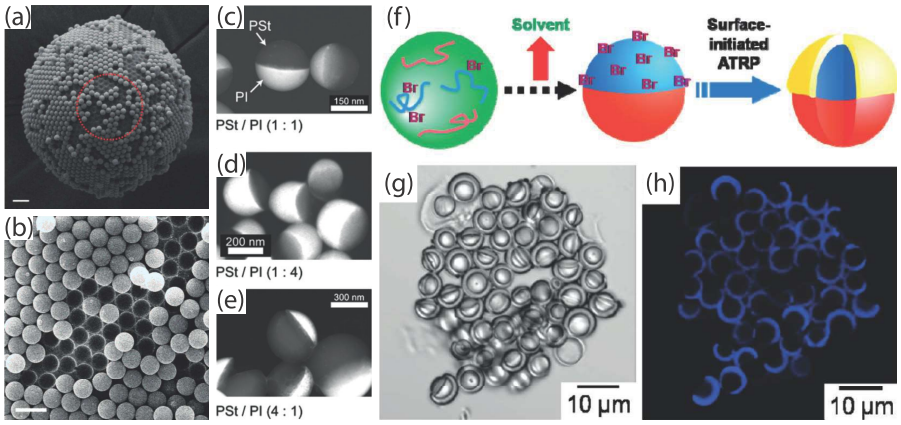

Figure 3.2 (a) SEM image of a wax particle covered with silicone microparticles, which resulted from a pickering emulsion (scale bar: 10 µm). A closer view is provided in illustration (b), in which voids are visible on the surface of the wax particle after partial removal of silicone particles via ethanol rinsing (scale bar: 5 µm).[161] (c) to (e) Dark field TEM images of Janus particles prepared by phase inversion from different amounts of PI and PS homopolymers. The Janus balance is adjusted by the ratio of PI to PS in solution during the micro-phase separation.[166] (f) Schematic illustration of the preparation of mushroom-shaped Janus particles by homopolymer phase separation in emulsified droplets via solvent evaporation and subsequent surface-initiated ATRP. (g) Optical microscopy images illustrate the Janus microparticle mushroom morphologies and (h) confocal laser scanning microscopy visualizes the labeled 2-(dimethylamino)ethyl methacrylate half-shells, which were grafted on the ATRP initiator containing PS based hemispheres of the Janus particles.[165]

spherical shell (Figure 3.2f to 3.2h). These mushroom shaped Janus particles featured a stimuli-responsive amphiphilic behavior at interfaces.[165]

The method of phase inversion represents another technique for the generation of Janus particles. In this case, polymers are dissolved in a water soluble solvent and the amount of water is slowly raised to reduce the polymer compatibility with the surrounding solvent and force the subsequent nucleation and particle growth. Either two different homopolymers or a block copolymer is used for the fabrication of Janus particles. Mixtures of PI and PS were utilized for the formation of biphasic Janus particles, at which the adjustment of the Janus balance was easily controlled by the ratio of the homopolymers in solution (Figure 3.2c to 3.2e).[166]

3.2 DROPLET BASED MICROFLUIDIC PREPARATION

Microfluidic devices provide access to droplet based synthetic methods for Janus particles, which offer micrometer sized particle preparations with excellent control over the Janus particle sizes and morphologies at high particle production volumes.[140,167,168] The princi-

ple of different microfluidic devices for the fabrication of polymeric microparticles is discussed in Section 2.1. However, the microfluidic fabrication of Janus particles requires additional conditions and adjustments concerning the microfluidic setup as well as the physical and chemical properties of the dispersed phases.

General Considerations

In general, the synthesis of Janus particles in microfluidic devices is accomplished by the dispersion of two immiscible monomer fluids in a continuous phase and subsequent curing of the Janus droplets downstream via UV-initiated polymerization. The processing and dispersion of the monomer phases is either performed via side-by-side flow and subsequent flow-focusing of the dispersed phases in a microchannel based device, or the emulsification at the tips of two parallelly proceeding capillaries in a capillary-based microfluidic device. In both cases, the monomer phases are commonly dispersed in continuous silicone oils, aqueous solutions of hydrophilic polymers or fluorinated liquids, which must be immiscible with the dispersed phases in any case. The monomer phases mostly contain a UV-initiator and the addition of surfactants is used to control the interfacial tension between the two dispersed phases as well as between the continuous and each monomer phase. To provide the formation of biphasic Janus droplets with a bicompartimental morphology, the adjustment of both the dispersed phases' viscosities and the interfacial tensions is crucial. Furthermore, the mixing of the dispersed phases by interfacial diffusion has to be considered, which is minimized by the proper selection of incompatible components for the dispersed phases, such as the choice of inverse polarities or solubilities.

Microchannel Based Fabrication

Different microchannel based devices have been developed for the fabrication of various polymeric Janus particles for more than one decade up to now. Early synthetic works in this field presented the fabrication of bicolored Janus particles, which contained carbon black and titan dioxide in separated monomer phases based on isobornyl acrylate (IBA). Janus droplets were dispersed in an aqueous PVA solution in a Y-shaped microchannel system and the curing process was achieved via thermal initiator moieties. The resulting Janus particles showed dispersities in size of less than 2 % and the successful electrical switching of black and white Janus particles demonstrated their potential application for electronic paper devices (Figure 3.3).[169,170] Similar approaches led to bipolar or hydrogel containing Janus particles via UV-initiated polymerization. Furthermore, studies of the influence of the dispersed phases' flow rates on the Janus balance of corresponding particles were carried out with the aid of incorporated fluorescent dyes to visualize one of the hemispherical compartments via fluorescent microscopy.[171,172]

Besides, magnetic-fluorescent Janus particles were recently fabricated, which contained Fe_3O_4 nanoparticles to implement magnetism on one side of the Janus particles and CdSe/ZnS quantum dots to al-

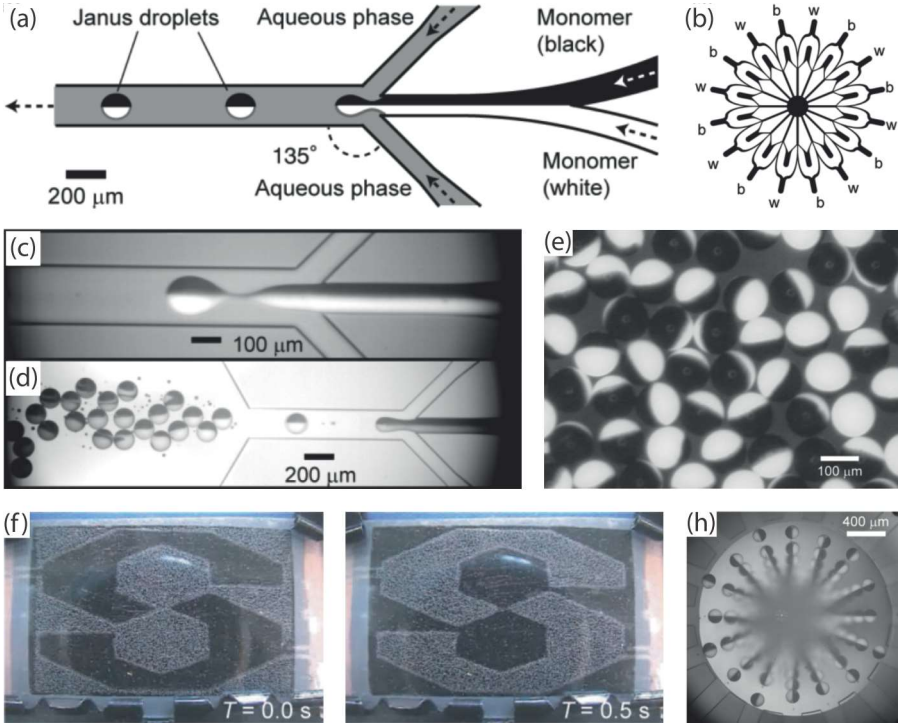

Figure 3.3 Schematic illustrations of (a) the Y-shaped microchannel device for the production of bicolored Janus particles and (b) the 16-channel module for the scale-up of the Janus particle fabrication. (c) Microscopic image of the droplet formation of IBA based Janus droplets in the co-flowing aqueous continuous phase and (d) collection of the hemispherically bicolored droplets. (e) Polymerized Janus particles with a mean diameters of 117 µm and a coefficient of variation below 2 %. (f) Electrical color switching of prepared Janus particles in between two electrodes with an applied voltage of 100 V and a switching rate of 1 Hz. (g) Janus particle convergence at the center of the microchip for the particle production scale-up.[170]

low photo-luminescence on the other side. Both monomer mixtures were based on an aqueous sodium alginate solution and the solidification of the droplets was realized by the diffusion of Ca^{2+} from the continuous phase into the Janus droplets to form a crosslinked alginate hydrogel. The resulting Janus particles allowed both, the magnetic separation and spatial enrichment of the particles as well as fluorescent labeling at the same time.[173]

Capillary Based Fabrication

An advanced capillary based microfluidic device was developed by Serra *et al.* for the production of Janus particles, in which two fused silica capillaries are applied side-by-side in the center of a poly(tetrafluoroethylene) (PTFE) microtube, each to provide one of the monomer phases.[123] Compared to the microchannel devices, the monomer phases are separated from each other until the Janus droplets are formed in the co-flowing continuous phase at the tips of the capillaries. Furthermore, the formed Janus droplets never touch the walls of the device's tubing-channels, which qualifies the capillary

based technique especially for the processing of highly wetting and reactive dispersed phases.

Drug loaded Janus particles of various morphologies and scales were fabricated in a side-by-side capillary based device by UV-initiated polymerization and crosslinking of biphasic Janus droplets. In this study, amphiphilic Janus particles with sizes from 59 µm to 240 µm were produced, which contained sodium fluoresceine in the aqueous acrylamide based hydrophilic monomer phase and ketoprofen in the methylacrylate based hydrophobic phase. The Janus morphology was thereby adjusted by variation of the surfactant amounts in the dispersed phases and the particle size was controlled by the ratio of the continuous phase to the dispersed phases flow rates in a flow-focusing channel section (Figure 3.4a to 3.4g). Furthermore, the drug release of resulting Janus particles was studied and optimized in terms of different particle shapes and sizes.[121]

In a further study, magnetic anisotropic Janus particles were synthesized in a similar capillary based device. Two UV-curable organic dispersed phases were used for the Janus droplet formation in an aqueous continuous phase. In this case, one phase contained a polymerizable siloxane-based copolymer, kerosene and magnetic nanoparticles, whereas the other one consisted of tripropylene glycol diacrylate (TPGDA). The Janus balance of the obtained particles was precisely controlled by the adjustment of the ratio between the dispersed phases flow rates. Furthermore, the particles were collectively oriented along an external applied magnetic field at which the alignment of the Janus particles' magnetic segment enforced an overall rotation of the particles (Figure 3.4h).[122]

3.3 PROPERTIES OF FUNCTIONAL JANUS PARTICLES

A wide diversity of various functional Janus particles has been developed in the past and is still the subject of present research for applications in the fields of biomedicine and life science, self-propulsion, optics and E-paper display technology.[139–142] For this work, the interfacial and self-assembly properties of amphiphilic Janus particles as well as the shape changing properties of stimuli-responsive Janus particles play an important role and are further discussed in this section.

Amphiphilic Janus Particles

Similar to amphiphilic molecules and surfactants, Janus particles with amphiphilic properties have been studied as stabilizers for liquid-liquid interfaces and Pickering emulsions. Furthermore, the surface active properties of amphiphilic Janus particles enable their self-assembly into various superstructures.[140,174–177] In general, amphiphilic Janus colloids consist of a hydrophobic material on one side and a hydrophilic compound on the other side of the particle, which both are immiscible and clearly separated by an interface.

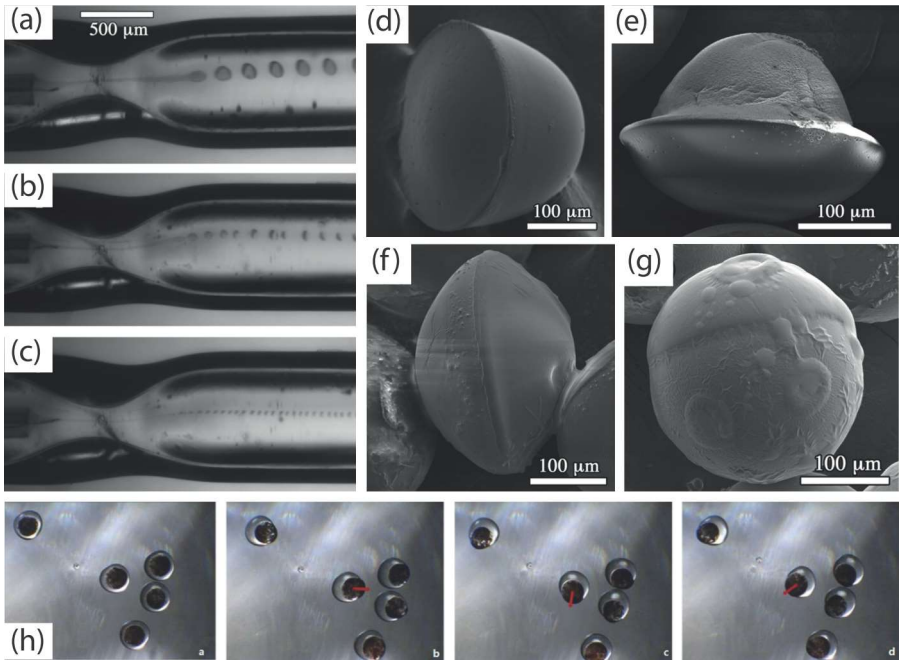

Figure 3.4 Formation of drug loaded Janus droplets with decreasing diameters from (a) to (c) in the flow focusing section of a side-by-side dual capillary based microfluidic device. SEM images of different Janus particle morphologies derived from the variation of flow rates and surfactant amounts: (d) helmet-like, (e) ufo-like, (f) rugby-like and (g) bicompartimental.[121] (h) Optical microscopy images of the alignment of anisotropic magnetic Janus particles along the direction of a rotating external magnetic field (red arrow).[122]

The surface activity of Janus particles is quantified by the detachment energy from oil-water interfaces, which represents the free energy that is necessary to remove the particle from the interface into either the water or the oil phase.[178] Compared to homogeneous particles, amphiphilic Janus particles exhibit a strongly increased surface activity and detachment energies with values up to three times higher as calculated for homogeneous particles. The detachment energy however depends on various properties of the Janus particles and the two surrounding phases, such as the interfacial tensions of both the particle materials and the two fluids, the Janus balance (particle anisotropy and ratio of the two materials), the particle morphology (spherical, disk-like, cylindrical, dumbbell) and the position of the particle concerning the fluid-fluid interface.[179]

For spherical amphiphilic Janus particles with a symmetrical Janus balance and a high affinity of each opposing material to one of the fluids, the positioning of the Janus boundary takes place at the fluid-fluid interface, which minimizes the interfacial tension of the entire system and maximizes the detachment energy. However, anisotropic Janus geometries show deviations of the Janus boundary positioning, in which one of the Janus parts reaches into both liquid phases. Fur-

thermore, different geometries and surface activities of amphiphilic Janus particles were studied in terms of thermodynamically stable formations of Pickering emulsions, whereas homogeneous particles only form kinetically stable emulsions after high energetic efforts.[180]

Solid Surfactants and Self-Assembly

The utilization of the high surface activity of Janus particles for the stabilization of emulsions was demonstrated by the application of amphiphilic Janus micelles as solid surfactants in mini-emulsion polymerization. In this study, Janus micelles with hydrophobic PS hemispheres and hydrophilic poly(methacrylic acid) (PMAA) hemispheres were exclusively applied as stabilizers for a pickering emulsion polymerization of styrene and *n*-butyl acrylate. The obtained latex particles were synthesized in different sizes, at which the average diameter was adjusted by the amount of stabilizing Janus particles during the emulsion polymerization. Furthermore, the study demonstrated the high stabilizing impact of a single Janus particle on a large interfacial area of 16 900 nm^2 in emulsified PS droplets.[181]

Furthermore, amphiphilic Janus particles were demonstrated as building blocks for the self-assembly into supermicelles and monolayer capsules (Figure 3.5a). Amphiphilic silica Janus particles were used for the stabilization of pickering emulsions and the generation of monolayerd capsules with diameters of 5 µm to 50 µm for the encapsulation of water soluble enzymes. The catalytic performance of Janus particle encapsulated lipase in organic solvents was successfully increased by a factor of 5.6 compared to the free enzyme and the stability of the capsule monolayers was demonstrated.[182]

Besides, the self-assembly of amphiphilic polymeric Janus nanoparticles into micellar structures was reported. In this work, a one-pot synthesis was used to prepare Janus particles containing *N*-isopropylacrylamide (NIPAAm) in the hydrophilic part and divinylbenzene in the hydrophobic part. These Janus particles subsequently self-assemble into supermicelles with hydrophobic cores and narrow size distributions (Figure 3.5b). Janus nanoparticles were obtained after treatment of the micelles with the molecular surfactant sodium dodecyl sulfate (SDS).[183]

Stimuli-Responsive Janus Particles

The incorporation of stimuli-responsive materials into Janus particles features the possibility of changing the colloidal properties towards an externally applied signal, such as adjustments in temperature, pH-value or light irradiation. In dependence of the integrated stimuli-responsive material, controlled changes of the Janus particles' self-assembly abilities as well as reversible transformations of the Janus particles' shape have been accomplished.[144,184]

Temperature-responsive Janus particles were synthesized from two differently concentrated aqueous NIPAAm phases in a flow-focusing microchannel device. These Janus particles consisted of an organophilic PNIPAAm rich hemisphere, which showed a reversible volume decrease upon passing the lower critical solution temperature

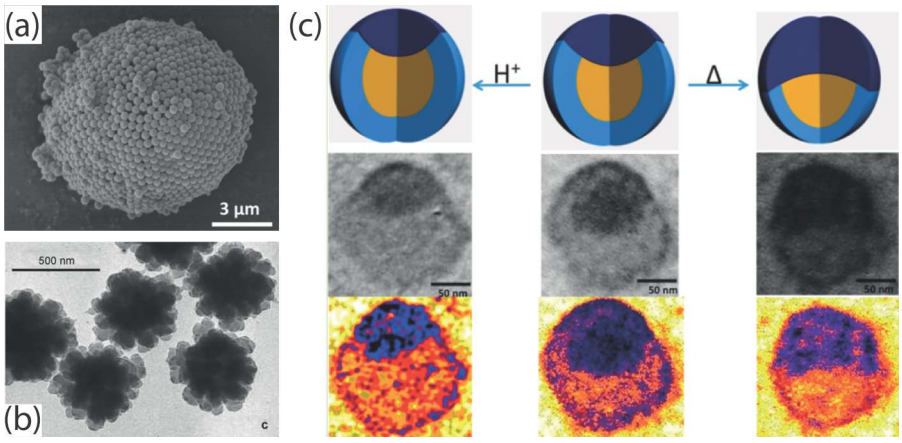

Figure 3.5 (a) SEM image of self-assembled amphiphilic Janus particles in a monolayered capsule at the interface of water and heptane.[182] (b) TEM image of supermicelles prepared by the self-assembly of amphiphilic Janus particles.[183] (c) Schematic illustrations and TEM images of triphasic temperature and ph-responsive Janus particles in the protonated state (left), at neutral pH and 25 °C (middle) and at 45 °C (right).[186]

(LCST) of 32 °C in water. However, the second part of the Janus particles contained an aqueous PNIPAAm poor phase featuring minor volume changes at the LCST, which enables an overall anisotropic temperature-responsive shape change of the entire Janus particle in water.[185]

Another study demonstrated the pH-responsive reversible change of amphiphilic Janus particle shapes and subsequent inversion of their surface activity, aggregation and dispersion behavior. In this case, Janus particles were prepared by polymerization-induced phase separation and seeded emulsion polymerization, in which the hydrophobic part was based on PS and the hydrophilic part contained PAA as the pH-responsive component. At high pH-values of the particle surrounding medium, the deprotonated PAA phase featured strong hydrophilicity and subsequent swelling caused a volume increase of the hydrophilic part. In the reverse case, the protonated PAA phase adopted a hydrophobic character and volume decreases were detected at low pH-values. Furthermore, a pH-responsive change of the particle amphiphilicity was demonstrated by analyzing the emulsification abilities of the Janus particles in Pickering emulsions. A water-in-oil emulsion was detected at pH 2.2, whereas an oil-in-water emulsion arised at pH 11.0 and an inversion of each emulsion was achieved by pH-conversion.[187]

Besides, temperature and pH-sensitive triphasic Janus particles were synthesized with tunable Janus balances from 3.78 to 0.72 and reversible stabilization properties of oil droplets in Pickering emulsions (Figure 3.5c). These particles consisted of a shape-adoptable poly(pentafluorostyrene) (PFS) / poly(*n*-butylacrylate) (PnBuA) part and a temperature and pH-responsive PDMAEMA/PnBuA hemis-

pherical corona, which collapsed at increased temperatures due to the second order LCST and assumed an increased volume in the protonated state at low pH-values.[186]

Part II

RESULTS AND DISCUSSION

4

CONTENT OVERVIEW

The main objective of this thesis is the further development of advanced microparticle actuators on the basis of liquid crystalline elastomers (LCEs) for prospective applications in functional materials and microelectromechanical systems (MEMS). This work focuses on the LCE microparticle preparation in capillary based microfluidic devices, which have been established for the processing of liquid crystalline monomers and the coincident generation of well aligned director fields in LCE particles. Two different approaches are pursued in this work to enhance the thermomechanical functionalities of LCE microparticles and to highlight the great potential of LCE actuator advancement for their application as components in smart materials.

First of all, the microfluidic preparation of Janus particles with a thermal actuating hydrophobic part based on a side-chain LCE is presented for the first time. In this study, the requirements for the microfluidic synthesis are discussed and a deeper understanding of the liquid crystalline alignment within the symmetry broken biphasic Janus morphology is obtained. Based on this elaboration, the fabrication of amphiphilic dual temperature-responsive Janus particles and their incorporation in an actuating surface application is accomplished. In this consecutive work, the functionality of actuating LCE Janus particles is expanded by the incorporation of a thermal responsive lower critical solution temperature (LCST) hydrogel. Moreover, the self-assembly of corresponding amphiphilic Janus particles at water/oil interfaces is studied and utilized as the crucial step for a molding process. Furthermore, successes in the development of main-chain LCE microparticle fabrication is achieved in terms of strong actuation improvements and microfluidic processability. In this case, the integration of a well established thiol-ene based liquid crystalline monomer mixture is used for the microfluidic preparation of actuators with component variable shape-changing properties.

In every study, the microfluidic device is adjusted to the special requirements of the particular processed monomer phases and only the fine tuning of the device parameters leads to an optimization of the actuation abilities of the LCE particles. For this reason, a comprising work about the different microfluidic devices for LCE actuator syntheses is presented with detailed setup descriptions and step-by-step video instructions to ease the initial skill adaption of future researchers in this field.

4.1 ACTUATING LCE JANUS PARTICLES

The idea for the microfluidic preparation of Janus particles with an actuating LCE part has been developed with regard to two different motivating factors. On one side, the latest achievements in the field of microfluidic LCE actuator fabrication (see Section 2.2) demonstrate the wide range of various accessible LCE particle morphologies, such as spherical, rod-like, oblate shaped and core-shell particles. These are synthesized in modified capillary-based microfluidic devices, hitherto utilized for the fabrication of non-liquid crystalline polymeric particles. From this point of view, the logical further development of actuating LCE particles is the application of the already established side-by-side dual-capillary microfluidic device, which is known as an efficient method for the preparation of polymeric Janus particles. However, this method has never been used for the fabrication of liquid crystalline actuating Janus particles before. On the other side, the new functional possibilities, which arise from breaking the symmetry of homogeneous LCE particles, create an intrinsic motivation for targeting the Janus morphology, as described in Chapter 3. For example, the incorporation of a second stimuli-responsive material beside the LCE leads to dual-responsive actuating particles with multiple remotely selectable particle states. Furthermore, the design of amphiphilic Janus particles by introducing a hydrophilic material next to the LCE enables the self-assembly of actuating particles into superstructures.

The first publication "Co-flow microfluidic synthesis of liquid crystalline actuating Janus particles" demonstrates the successful preparation of LCE Janus particles in a dual-capillary microfluidic device and discusses the necessary adjustments of various parameters for the microfluidic processing as well as the characterization of the LCE thermomechanical actuation properties (Chapter 5). In this study, a side-on connected side-chain liquid crystalline monomer is applied to form the hydrophobic actuating LCE part of the Janus particles by UV-initiated radical polymerization and simultaneous crosslinking, which has been established and optimized for the preparation of aligned LCEs in many studies before. The second part of the Janus particles consists of an aqueous hydrophilic acrylamide hydrogel with a high crosslinking density. This hydrophilic Janus part fits the necessary requirements of high mechanical stability, complete immiscibility with the hydrophobic LCE part and a high reactivity towards radical polymerization reactions to ensure a fast solidification of the droplets in the microfluidic synthesis.

As the processing of both monomer phases in the parallel capillaries of the microfluidic device yields eccentric Janus particles with poor actuation properties, two strategies are developed to fine-tune the Janus morphology and to maximize the LCE shape change during

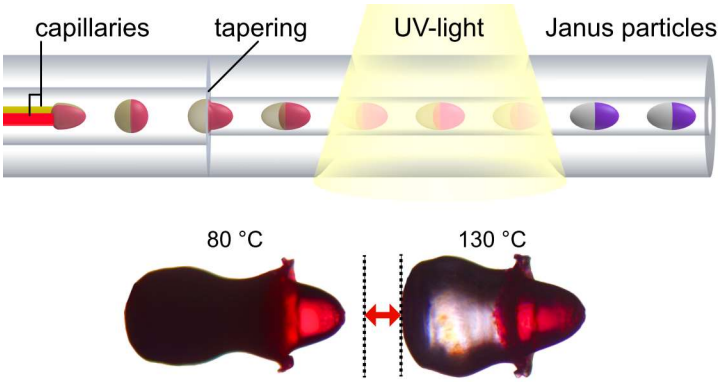

Figure 4.1 Schematic illustration of the side-by-side dual capillary microfluidic device for the preparation of rod-like LCE Janus particles (top). Shape change of the LCE part of an actuating Janus particle during the thermal induced phase transition (bottom). The LCE assumes an elongated shape at 80 °C in the nematic state, whereas a contracted shape is adopted after the phase transition at 130 °C in the isotropic state.[3]

the nematic-isotropic phase transition. At first, the interfacial tension between the aqueous monomer phase and the continuous silicone oil phase is analyzed with regard to different surfactant additives, and spherical bicompartimental Janus particles are accomplished by the aid of small amounts of a copolymer surfactant. Compared to the eccentric Janus morphology, however, the actuation properties of the LCE are just slightly increased by this method. This is traced back to mesogenic alignment restrictions caused by unintended surface anchoring influences of the copolymer surfactant as well as confined mesogenic flow patterns inside the liquid crystalline hemispherical droplet.

The second strategy implies the increase of the acting shear forces on the Janus droplets during the polymerization by application of a flow focusing tapering of the microtube after the droplet formation. This modification elongates the obtained particles along their flow direction in the microtube and subsequently applies a well aligned bipolar director field to the rod-like LCE. Furthermore, the viscosity of the aqueous monomer phase is increased by addition of a high molecular weight acrylamide homopolymer to enforce the separation of the two droplet phases and simultaneously add an additional mechanical stretching process to the liquid crystalline phase during the polymerization and crosslinking. The influence of the adjustments in shear flow and viscosity on the flow patterns inside the droplets, the consequential mesogen alignment and the Janus morphology are discussed in detail to elaborate a fundamental understanding of these correlations.

The optimized parameters of the microfluidic synthesis lead to strongly actuating rod-like Janus particles (Figure 4.1), which feature

length changes of the LCE up to 52 % during the thermal initiated nematic-isotropic phase transition. The detailed study of different morphologies of the synthesized Janus particles is carried out with special regard to the LCE volume and the interface between the LCE and the hydrogel phase via 3D computer simulations of the Janus particle shapes. The correlation of the LCE shape change with the ratio of LCE volume to the respective hydrogel/LCE boundary surface creates a guiding principle for the maximization of the actuation ability of Janus particles prepared by the described microfluidic method. Furthermore, the LCE director alignment is analyzed via wide-angle X-ray scattering (WAXS) measurements and the bipolar director field in the actuating rod-like Janus particles is confirmed. In summary, this first publication about LCE Janus particles describes the necessary boundary conditions for the successful alignment of LCEs in Janus actuators via microfluidics and lays the foundation for further developments of more sophisticated LCE Janus particles.

The second publication about actuating LCE Janus particles with the title "Interfacial Self-Assembly of Amphiphilic Dual Temperature Responsive Actuating Janus Particles" presents the preparation and characterization of advanced functional LCE Janus particles and their application as building blocks for a self-assembled stimuli-responsive surface device. After the optimization of the actuating LCE part in the first publication, this study describes the introduction of a second temperature responsive material to the hydrophilic part of the Janus particles. For this purpose, a poly(*N*-isopropylacrylamide) based hydrogel (PNIPAAm) with an LCST of 32 °C is integrated beside the previously described actuating LCE to add both temperature responsiveness to the hydrophilic Janus part and amphiphilic properties to the entire colloidal structure of the Janus particles.

To assure accurate microfluidic processing of the LCST hydrogel next to the liquid crystal, the microfluidic synthesis in the dual capillary device is optimized in terms of solvent composition and crosslinker density of the aqueous monomer phase. Furthermore, the occurring decrease of the nematic-isotropic phase transition temperature of the liquid crystalline monomer phase is compensated by adjustments of the process parameters concerning the polymerization temperature of the Janus droplets. Differential scanning calorimetry (DSC) measurements demonstrate changes in the liquid crystalline phase behavior based on different NIPAAm contamination amounts, which are assumed to occur via interfacial diffusion in the dispersed Janus droplets during the microfluidic synthesis. The impact of the polymerization temperature and different flow rates of the continuous phase on the LCE actuation properties are studied and the optimized parameters are applied to fabricate large batches of amphiphilic rod-like shaped actuating Janus particles (Figure 4.2).

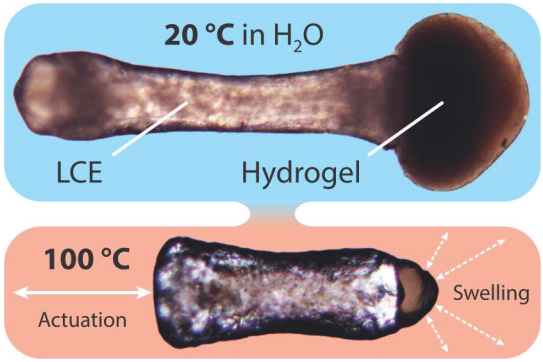

Figure 4.2 Optical images of an amphiphilic dual temperature-responsive Janus particle at two complementary morphology states. The first particle state (aqueous environment at 20 °C) features the strongly elongated LCE part in the nematic state and the voluminous hydrogel part in the swollen state. The second state (air environment at 100 °C) shows the same particle with a contracted torpedo shaped LCE part in the isotropic state and a strongly shrunken hydrogel part in the dry state.[1]

The thermal responsiveness of these Janus particles is characterized in terms of the actuation properties of the LCE part as well as the swelling behavior of the hydrogel part via heating experiments and polarized optical microscopy (POM). Four different particle morphology states are investigated, which are remotely selectable by addressing different states of each temperature responsive Janus part at different temperatures and solvent environments. Thereby, swelling and deswelling of the hydrogel part with high volumetric changes are achieved in combination with strong contractions and aspect ratio changes of the LCE shape during the nematic-isotropic phase transition. The expected bipolar director field of the rod-like LCE is confirmed via POM experiments at different rotation angles of the polarizer and analyzer. Further swelling experiments of the PNIPAAm hydrogel reveal a reduced LCST in the Janus particles compared to homogeneous hydrogel particles of the same composition, which are traced back to hydrophobic impurities of the hydrogel network by virtue of interfacial compound exchanges with the liquid crystalline phase in the biphasic Janus droplets.

For the development of a self-assembly approach, the amphiphilic properties of the dual temperature responsive Janus rods are studied in terms of different swelling properties and affinities of each Janus part towards organic and aqueous solvents. The strong swelling of the hydrogel part in aqueous environments and thereto complementary swelling of the hydrophobic LCE enables the self-assembly of the amphiphilic actuating Janus particles at water/oil interfaces into densely packed monolayers of uniformly aligned Janus rods. Thereupon, a multi-step molding process is developed, in which a monolayer of self-assembled actuating Janus rods is immobilized at a water/toluene interface by solidification of the bottom water-phase and

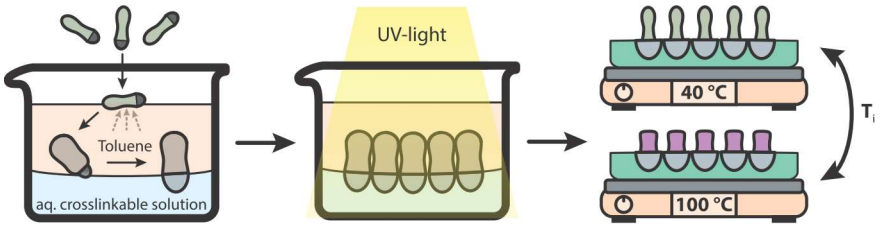

Figure 4.3 Schematic illustration of the molding process' crucial steps for the self-assembly of amphiphilic rod-like Janus particles and the subsequent preparation of an actuating surface of monolayered LCE rods. Particles are self-assembled at the water/toluene interface and the aqueous phase is cured by UV-irradiation. The resulting LCE covered hydrogel surface features actuation properties during the thermal induced nematic-isotropic phase transition.[1]

subsequent embedding of the hydrogel Janus parts (Figure 4.3). By this procedure, the modification and functionalization of a hydrogel surface is developed, which consists of a monolayer of self-assembled and uniformly aligned actuating LCE Janus rods. The preparation of these temperature responsive actuating surface devices is demonstrated with variable particle amounts and various achievable sizes and shapes of the fabricated device. Furthermore, thermal characterization experiments of the corresponding LCE rods reveal uniformly directed shape changes perpendicular to the hydrogel surface during a thermal induced phase transition. Different actuation patterns of the functionalized surfaces are achieved either by triggering a collective actuation of the entire LCE surface or by selective actuation of partial surface regions via local heating. In addition, the structural properties of the LCE covered surface devices are discussed with regard to changes of the surface properties during the phase transition.

In conclusion, the further development and functionalization of the actuating LCE Janus particles enables their successful application as building blocks for surface-active and stimuli-responsive devices via self-assembly. In this work, the concept of self-assembly is utilized not only for the microscopic alignment of liquid crystalline molecules into ordered director fields of strongly actuating LCE particles, but also for the ordered incorporation of these LCE particles into superstructured actuating devices on a macroscopic length scale.

4.2 ACTUATING MAIN-CHAIN LCE PARTICLES

In the research area of LCE actuator development, special attention has to be payed to the advancement of the mesogenic systems and the chemistry of polymerization and crosslinking of LCEs to create further improvements in their actuation properties. As described in Chapter 1, main-chain LCEs hold a great potential for the preparation of actuators, as high length changes during the phase transition are

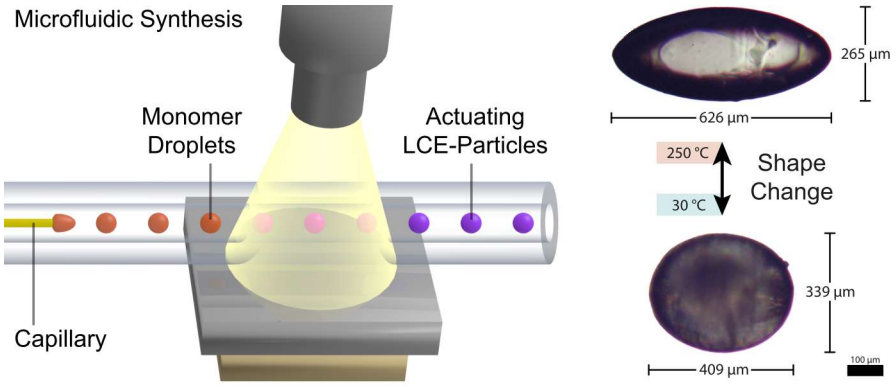

Figure 4.4 Schematic illustration of the microfluidic synthesis of main-chain LCE particles in a capillary based microreactor (left). Microscopic images of an actuating main-chain LCE particle demonstrate the strong elongation of the particle shape at 250 °C in the isotropic state (right).[4]

expected for nematic mesogens. This is based on the strong coupling of the mesogens with the LCE network structure and the parallel alignment of the director with the polymer backbone. However, former attempts on the introduction of main-chain LCEs into actuating particles via microfluidics obtained only weak actuation properties and small shape changes of corresponding LCE particles. For that reason, this work pursues the worthwhile target of the further development and optimization of a microfluidic synthesis for the effective processing of a main-chain liquid crystalline monomer system and the preparation of strongly actuating LCE microparticles.

The publication "Microfluidic Synthesis of Actuating Microparticles from a Thiol-Ene Based Main-Chain Liquid Crystalline Elastomer" describes the adaption of an already established main-chain liquid crystalline monomer mixture to the microfluidic processing in a capillary based microreactor. In this study, the dispersed phase for the microfluidic droplet formation contains a thiol-ene based nematic monomer mixture and an acrylate based liquid crystalline crosslinker, which has been proven successful for the fabrication of strongly actuating LCE films in former research studies. This mesogenic system is chosen for its fast polymerization and crosslinking in UV-initiated radical polymerization reactions as well as high expected shape changes of corresponding actuators at the nematic-isotropic phase transition. As the liquid crystalline phase behavior of the liquid crystalline dispersed phase strongly deviates from the previously processed side-chain monomer system, precise adjustments of the microfluidic process are necessarily accomplished. For this purpose, the influence of different microfluidic parameters on the actuation properties of resulting LCE particles are studied, such as the different temperature zones, the UV-irradiation times and intensities as well as the dispersed and continuous phase flow rates in the microreactor.

After the optimization of the microfluidic process, spherical and slightly ellipsoid main-chain LCE particles are obtained, which show strong elongations during the nematic-isotropic phase transition and a resulting rod-like shape of the particle in the isotropic state (Figure 4.4). An analysis of the actuation geometry leads to the conclusion of a concentric liquid crystalline director field of the fabricated particles. Further studies of the actuation process over many heating cycles are presented, which prove the complete reversibility of the particle shape change during the phase transition. To investigate the influence of the liquid crystalline crosslinker on the phase behavior of the main-chain LCE, actuating particles with different crosslinker densities are synthesized and characterized with special regard to the temperature width and the temperature shift of the nematic-isotropic phase transition. Furthermore, this study not only indicates the strong dependence of the LCE particles' actuation properties on the composition of the monomer mixture, but also the possibility of adjusting the desired particle aspect ratio change and the liquid crystalline phase behavior by choosing the proper crosslinking density is revealed.

In conclusion, the successful introduction of a thiol-ene based mesogenic monomer system is presented for the microfluidic preparation of strongly actuating main-chain LCE particles with customizable shape changing properties and different liquid crystalline phase behaviors.

4.3 MICROFLUIDIC PREPARATION OF LCE ACTUATORS

The biggest challenges for researchers in the field of LCE actuator preparation via microfluidic devices are the precise construction of the microfluidic setups and the proper handling of the liquid crystalline monomer systems. For new research groups in this area, both skills are hard to learn without the guidance of an experienced researcher, who has learned how to bypass the occurring practical issues with microreactors and is able to give skilled advices for the successful LCE actuator fabrication. For this reason, a video assisted step-by-step tutorial for the entire microfluidic fabrication process of various developed LCE actuators represents the best solution for sharing these valuable empirical values with future research groups all over the world.

The video based instructions and step-by-step protocols of the publication "Microfluidic Preparation of Liquid Crystalline Elastomer Actuators" provide detailed information about the setup of all necessary microfluidic components, the monomer phase preparation and handling as well as the fabrication process and characterization of well aligned LCE actuators. In this work, special attention is payed to the instructions of mounting different microfluidic devices for the synthesis of various actuating LCE particles. In this manner, video

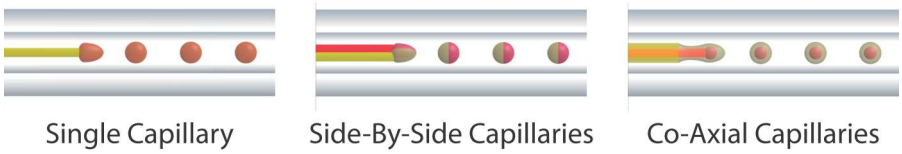

Figure 4.5 Schematic illustrations of the three types of capillary based microfluidic devices for the preparation of actuating LCE particles. The single capillary device is adapted for the preparation of homogeneous particles, the side-by-side capillaries are used for the synthesis of Janus particles and the co-axial capillaries device is suitable for the production of core-shell particles.[2]

guides and associated written protocols describe the single capillary device for the preparation of homogeneous particles, the side-by-side dual capillary device for Janus particle syntheses and the co-axial telescoped capillary device for fabrications of core-shell particles (Figure 4.5). Furthermore, detailed parameters about already approved adjustments are specified, such as the temperature zones of the microfluidic devices, the monomer mixture compositions, the flow rates of the dispersed and continuous phases, and the UV-irradiation times. In addition, different characterization methods for LCE actuators are presented and detailed examples of commonly obtained particles and their actuation properties are discussed to allow other researchers the verification of the shape-changing properties of self-produced actuators.

Finally, this article provides a comprehensive overview about the microfluidic processing methods of LCEs and the preparation of various actuating particles, which have been developed over the last decade. The detailed instructions of practical issues concerning the capillary based microfluidic devices are supposed to facilitate the establishment of these methods in other research groups and promote the further development of LCE actuating particles for future applications.

5

CO-FLOW MICROFLUIDIC SYNTHESIS OF LIQUID CRYSTALLINE ACTUATING JANUS PARTICLES

Tristan Hessberger, Lukas Braun, Franziska Henrich, Carsten Müller, Frank Gießelmann, Christoph Serra and Rudolf Zentel,
Journal of Materials Chemistry C **2016**, *4*, 8778-8786.

5.1 ABSTRACT

In this article, the microfluidic synthesis and characterization of micrometer sized actuating Janus particles containing a liquid crystalline elastomer (LCE) is presented. On one side these Janus particles consist of a hydrophobic liquid crystalline part, featuring strong shape changes during the thermotropic phase transition, whereas the other side contains a hydrophilic polyacrylamide network. The synthesis is based upon the dispersion of two immiscible monomer mixtures in a continuously flowing silicone oil, using two glass capillaries side by side to form Janus microdroplets of different morphologies. Furthermore, the systematic adjustment of the morphology of the Janus particles as well as the optimization of the actuation properties is conducted by precise control and variation of the microfluidic parameters. The actuation properties of the particles are studied by polarized optical microscopy (POM), in which relative length changes up to 52 % are investigated for the elongation of LCEs during the phase transition in rod- like Janus particles. Further wide-angle X-ray scattering (WAXS) measurements verify the mesogen's orientation in a bipolar director field, which corresponds to the observed geometry of the Janus particle's shape changes.

5.2 INTRODUCTION

The unique properties of Janus particles have attracted the attention of many researchers during the last two decades to derive advantages from the anisotropic and non-centrosymmetric architecture of these particles, which were named after the twin-headed Roman god *Janus*. The great importance and the manifold possibilities of Janus particles were already demonstrated by de Gennes in his Nobel lecture in 1991.[188] Since then, a large variety of different synthetic methods have been developed, as well as multiple applications in the fields of materials and life science.[140,142,145,146,189] Thereby, self-assembly, emulsion techniques, symmetry breaking and phase separation processes enable synthetic strategies for nanometer scaled Janus

particles, whereas microfluidic devices, biphasic electrified jetting or seeded dispersion polymerization are suitable and well-established methods for the production of various morphologies of polymeric, micrometer sized Janus particles.[123,167,168,190–192] The asymmetric architecture permits the combination of two materials in a single micro or nanometer sized object, each providing different chemical and physical properties, which offers a wide range of unique functionalities. Amphiphilic Janus particles have been studied intensely for their application as solid surfactants and interface stabilizers, catalysts and super-hydrophobic textiles and coatings.[181,193–196] Electrical and magneto-responsive Janus particles, featuring asymmetric optical properties, offer their usage for switchable display devices and electronic paper.[170,197,198] An increasing interest has grown in stimuli responsive Janus particles, which are sensitive to changes in their physical or chemical environment, such as the temperature, light or pH-value.[144,184,199] These Janus particles are able to undergo self-assembly processes, reversible shape changes or even stimuli-driven active propulsion, induced by thermophoresis or catalytic decomposition of a reactive fluid at one hemisphere of these so-called Janus motors.[200–203] In this work, we present an LCE as the stimuli responsive, actuating part of Janus particles.

LCEs are slightly crosslinked liquid crystalline polymer networks, which are capable of undergoing reversible and stimuli responsive shape transformations during their phase transition. However, LCEs have never been used as stimuli responsive materials in active Janus particles. Since de Gennes predicted the promising shape changing properties of LCEs in 1975, they have been focused and reviewed by many researchers to this day.[48,204–208] Based on the responsivity of LCEs due to temperature changes, light irradiation or solvent swelling, these materials have been identified to be suitable for applications as actuators, sensors and microelectromechanical systems (MEMS).[42,67,70,94,209,210] A co-flow microfluidic preparation of actuating particles containing an LCE represents an effective method for the synthesis of thermal shape changing, micro scaled objects.[64,65,132,133] As co-flow microfluidic setups have already been used for the production of amphiphilic Janus microparticles, the combination of hydrophobic LCEs with hydrophilic polymer networks in a microfluidic device offers a promising method for the synthesis of strongly actuating Janus particles.[121,122] In this work, we present the first microfluidic synthesis of actuating Janus particles containing an LCE and describe the control of the morphology as well as the actuation properties of the particles.

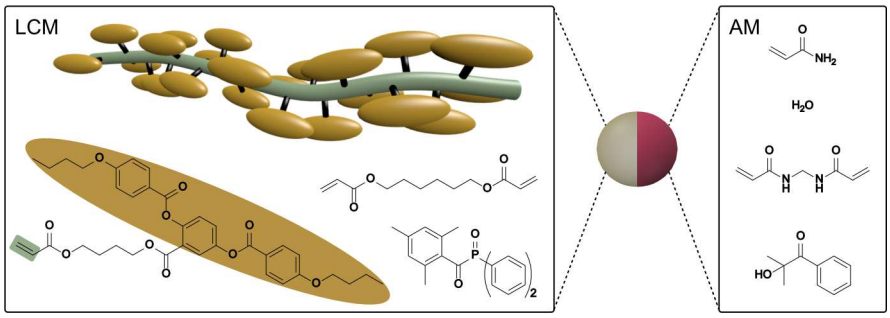

Figure 5.1 Segment of a side-on liquid crystalline polymer chain and compounds of the liquid crystalline monomer (LCM) mixture and the acrylamide monomer (AM) mixture.

5.3 RESULTS AND DISCUSSION

5.3.1 *Microfluidic preparation of Janus particles Janus*

Janus particles should be fabricated in a co-flow microfluidic reactor. The principle of the formation of Janus droplets is based on the dispersion of two monomer mixtures in a continuous phase (CP). The prerequisite for a biphasic Janus droplet formation is the immiscibility of the dispersed monomer phases with each other, in addition to the immiscibility with the continuous silicone oil phase. For this reason, a hydrophobic liquid crystalline monomer (LCM) mixture was chosen to form the actuating LCE-part of the particle, whereas an aqueous acrylamide monomer (AM) mixture was selected for the hydrophilic part. Figure 5.1 illustrates the components for both parts of the Janus particles. The LCM-mixture consists of the polymerizable nematic side-on mesogen (4″-acryloyloxybutyl)-2,5-di-(4′-butyloxybenzoyloxy) benzoate, the bifunctional crosslinking agent hexanediol diacrylate (10 mol%) and the photoinitiator ethyl(2,4,6-trimethylbenzoyl) phenylphosphinate (3 wt%). This LCM-mixture shows a monotropic nematic phase with a clearing temperature of 79 °C to 80 °C. It has already been used for the fabrication of several functional materials including actuating microparticles.[55,94,132] The AM-mixture is composed of a 40 wt% aqueous solution of acrylamide, the bifunctional crosslinker bisacrylamide (5 mol%), the photoinitiator 2-hydroxy-2-methyl propiophenone (3 wt%) and small traces of an aqueous red ink. Both monomer mixtures are immiscible with each other as well as with the CP silicone oil ($\eta_{CP} = 9.3 \times 10^{-1}$ Pa s). The dynamic viscosities of both monomer mixtures were measured at 85 °C and a shear rate of 100 s^{-1} to be $\eta_{LCM} = 5.3 \times 10^{-1}$ Pa s and $\eta_{AM} = 4.9 \times 10^{-1}$ Pa s.

The formation of the Janus droplets took place at the tips of two glass capillaries, each providing one of the monomer mixtures. Figure 5.2 shows the droplet formation and polymerization process as

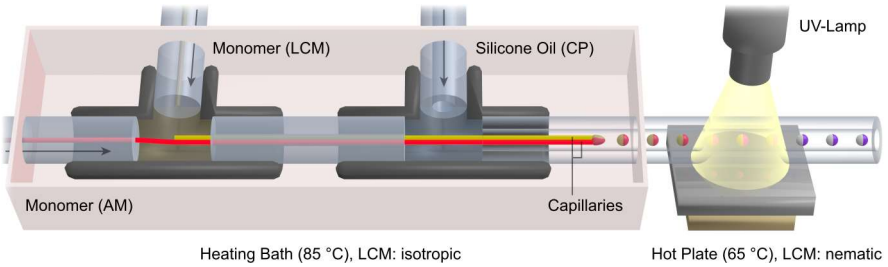

Figure 5.2 Schematic illustration of the capillary based microfluidic setup, which was used to produce liquid crystalline Janus particles in a continuous flow of silicone oil. The capillary displayed in red is directly connected to the PTFE tube on the left side, which provides the aqueous AM-mixture. The yellow capillary was charged with the hydrophobic LCM-mixture inside the T-junction on the left side. The CP silicone oil is injected into the T-junction on the right side perpendicular to the glass capillaries.

well as the microreactor's setup, which had already been described for the synthesis of polymeric particles before.[6,121–123] The flow rates of the LCM-mixture, the AM-mixture and the CP silicone oil were controlled by syringe pumps connected to the T-junctions via PTFE microtubes. The flow rates of the monomer mixtures were adjusted to magnitudes between 0.01 mL h^{-1} and 0.20 mL h^{-1}, whereas the CP flow rate was varied in a range of 0.5 mL h^{-1} and 3.0 mL h^{-1}. The morphology and geometry (volume, diameter and shape) of the Janus droplets were controlled by the ratio of the CP flow rate to the flow rates of the monomer mixtures with respect to the inner diameter of the polymerization tube. To ensure the necessary fluidity of the LCM-mixture, which is in the solid state at room temperature, the charging of the capillaries inside the T-junctions was carried out in a heating bath at 85 °C. A continuous flow of the viscous CP silicone oil surrounded the capillaries and caused the tearing of Janus droplets due to the shear rate acting on the LCM and AM dispersed phases. Transportation of the Janus droplets by the CP silicone oil over a hot plate at 65 °C cooled down the LCM-mixture from the isotropic to the nematic state. Polymerization and crosslinking of the Janus droplet's monomer mixtures were initiated by ultraviolet (UV)-irradiation on the hot plate. The resulting crosslinked Janus particles were collected at the end of the polymerization tube, removed from the silicone oil and cleaned in petroleum ether for further analysis.

5.3.2 *Control of the Janus particles' geometry and shape*

Acorn-like Janus Particles

The first synthesis of Janus particles using the co-flow micro reactor and the materials described above led to acorn-like shaped, eccentric Janus particles. This kind of particle morphology has been discov-

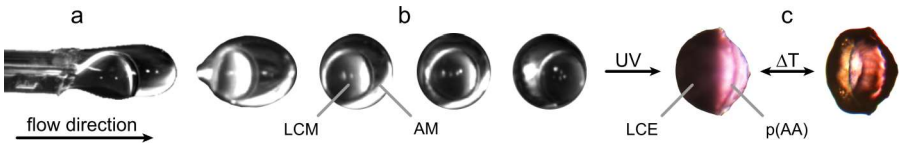

Figure 5.3 a) Formation of an acorn-like droplet at the capillaries' tips, b) development of the droplet's morphology in the continuous flow of silicone oil and c) shape change during the thermal phase transition of a crosslinked eccentric Janus particle after UV-irradiation.

ered in microfluidic syntheses before, in which different monomer mixtures were used.[121,211] Figure 5.3 illustrates the droplet formation and temporal development of its geometry in the continuous silicone oil flow, as well as a crosslinked Janus particle before and after the thermal phase transition of the LCE. The eccentric Janus droplets consisted of an aqueous core containing the AM-mixture, surrounded by a shell consisting of the LCM-mixture. This droplet morphology is formed due to the high interfacial tension between the CP silicone oil and the aqueous AM-mixture. Consequentially, the aqueous phase tries to "hide" inside the liquid crystalline phase. This core-shell structure is deformed by shear flow in the polymerization tube.[212,213] After the polymerization, the AM core forms an oblate shaped part at the front side of the crosslinked acorn-like particle, while the LCM-part with the higher viscosity forms a hemispherical shell at the back side of the particle with respect to the flow direction of the continuous phase.

The phase transition of the LCE-part is monitored via POM by exceeding the diffuse clearing temperature range between 90 °C and 130 °C. Thereby, the phase boundary inside the Janus particle is uncovered as the LCE-part got transparent in the isotropic phase. Thus, the influence of the phase transition on the shape of the Janus particle can be studied. However, it turned out that the shape changes of the LCE-part during the phase transition in these eccentric Janus particles are negligible (relative length changes $<5\,\%$) compared to actuating LCE particles composed of the same material (Figure 5.3c).[64,132] This small shape variation may be due to two reasons: (1) the director field of the LCE and (2) the LCE's movability during the phase transition.

On one side, the small actuation may be the result of a poor macroscopic director orientation in the LCE-part of the acorn like objects, especially at the interface to the AM-part. A large interface between the LCM and AM parts is assumed to decrease the order of the mesogens at the interface and thus to disturb the LCM's director field. Furthermore, the effective alignment of the mesogens and the generation of an ordered director field mainly relies on the undisturbed circulation of the fluid LC material inside the droplets, driven by the shearing of the continuously flowing poly(dimethylsiloxane) (PDMS). However, the non-spherical geometry of the LCM-part in the Janus

droplets might have a retarding influence on the LCM's flow pattern compared to microfluidicly produced almost spherical droplets of the pure LCM.[65]

Alternatively, a hindrance of the shape variation of the LCE, by "gluing" it to a non-actuating polyacrylamide network is assumed as a possible reason. The rigid and inflexible non-actuating AM-part of the Janus particles is expected to decrease the shape change of the LCE during the phase transition, since both parts get chemically fixed to each other during the UV-induced radical polymerization process. This limits the actuation process of the LCE at the interface.

Both effects depend on the particles' geometry and the size of the interface between the LCM and AM parts of the Janus particles. Thus, two different strategies to increase the magnitude of actuation during the phase transition were developed and are described in the next two subsections. The first strategy aimed at a variation of the interfacial tension between the AM-part and the CP silicone oil to change the particle's geometry from an acorn-like to a bicompartimental shaped Janus particle. This particle morphology features a smaller, more planar interface between the monomer mixtures compared to the larger, more curved interface of an acorn-like particle. The second strategy aimed at the dynamic elongation of the Janus particles' geometry perpendicular to the interface by increasing the shear rate acting on the droplets in the microfluidic setup. Especially the second strategy led to strongly asymmetric rod-like Janus particles. Both strategies were supposed to provide a higher ratio of the LCE-volume to the size of the interface in order to reduce problems in both the orientation process of the mesogens and the movability of the LCE material during the phase transition.

Bicompartimental Janus Particles

The first approach to the formation of bicompartimental Janus particles required the decrease of the interfacial tension, especially between the AM-phase and the PDMS in the continuous phase. For this purpose, two different surfactants were tested: a low molecular surfactant sodium dodecylbenzene sulfonate (SDBS) and a high molecular poly(dimethylsiloxane)-poly(ethyleneglycole) (PDMS-PEG) *graft*-copolymer, which is specially designed to reduce the surface tension between water and silicone oil. The influence of both surfactants on the interfacial tension between the AM-phase and the CP silicone oil was studied by measuring the interfacial tension as a function of the concentration of the surfactant dissolved in the aqueous AM-mixture. The measurements were carried out with a *Wilhelmy* plate tensiometer at 85 °C, which provided equal thermal conditions as the droplet formation takes place in the microfluidic reactor (see Section 5.3.1).

The measurements' results are illustrated in Figure 5.4a. As it was expected, both surfactants clearly induce a reduction of the interfa-

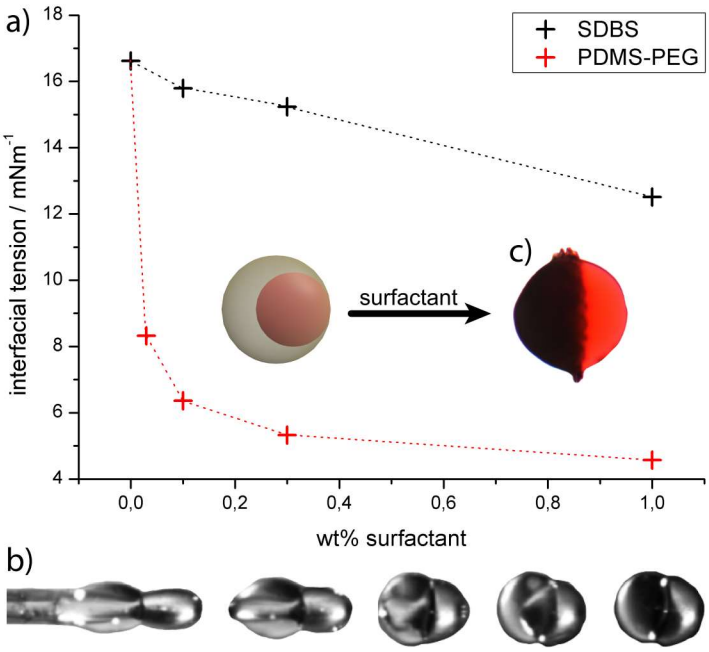

Figure 5.4 a) Interfacial tension between the AM-phase and the CP silicone oil plotted against the concentration of the surfactants SDBS (black line) and the PDMS-PEG copolymer (red line). b) Formation of bicompartimental Janus droplets in the microfluidic device and c) the morphology of resulting Janus particles after UV-polymerization and crosslinking.

cial tension. Thereby, the PDMS-PEG copolymer exhibits a strong decrease of the interfacial tension already at very low concentrations, such as the reduction of more than 60 % of its baseline value at just 0.1 wt%. By comparison, SDBS shows a smaller influence on the interfacial tension (reduction of 8.5 % at 0.1 wt% SDBS) and also a minor decrease at higher amounts of surfactant. This can be explained by the strong affinity of the PDMS-block to the silicone oil phase, which is due to the similarities in the chemical structure and polarity.

Respecting these results, the PDMS-PEG copolymer was used successfully as a surfactant in the aqueous AM-phase, which transformed the Janus particle's morphology from an acorn-like to a bicompartimental shape. The Janus particles showed an approximately planar interface, which could be observed during the droplet formation (Figure 5.4b) and after UV-polymerization (Figure 5.4c). The shape changes of the hemispherical shaped LCE-part were monitored via POM during the thermal phase transition, reaching relative length changes up to 15 % for the new particle morphology. These results represent an improvement of the actuation properties compared to the acorn-like Janus particles introduced above. However, the actuation was still smaller than the actuating LCE particles composed of the same material.[64,65,132] Thus, to further improve the particles' abilities as actuators, the second strategy was carried out, too.

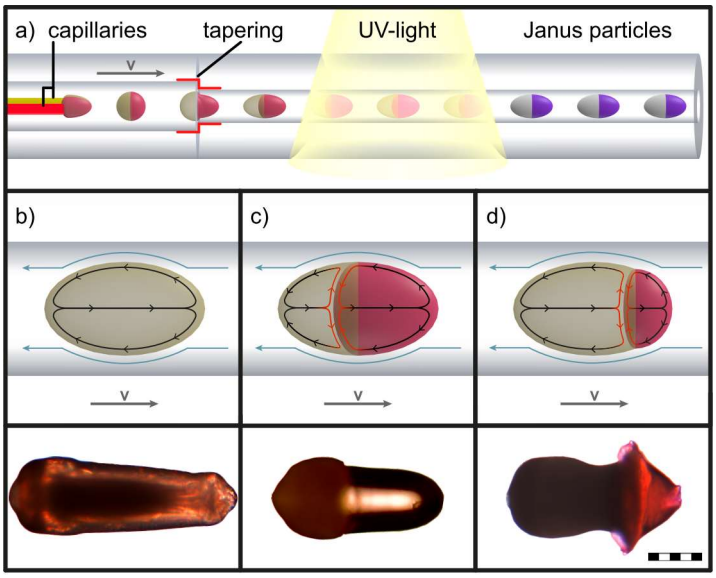

Figure 5.5 a) Formation of elongated droplets by reduction of the polymerization tube's inner diameter. The illustrations b), c) and d) schematically illustrate three different droplet morphologies during the continuous flow as well as the streaming patterns inside the droplets (grey: LCM, red: AM). The obtained particle morphologies after the UV-polymerization and crosslinking process are shown at the bottom. (scale bar: 200 µm)

Rod-like elongated Janus Particles

The formation of elongated rod-like Janus particles was enforced by increasing the shear rate acting on the Janus droplets inside the polymerization tube. Therefore, the polymerization tube's inner diameter was decreased from 750 µm to 500 µm, after the droplet formation at the capillaries' tips took place. The tapering of the tube's inner diameter by one third causes an increase of the flow velocity by the factor of 2.25 with respect to the continuity law and thus an increase of the shear gradient, too. This forced the spherical Janus droplets to transform into an elongated shape.[212,213] Figure 5.5a illustrates schematically the shape transformation and polymerization process.

Three different morphologies of rod-like particles were adjusted systematically by the variation of the microfluidic setup's parameters, in order to investigate a correlation between the particle's morphology and the magnitude of actuation, which will be discussed in Section 5.3.3. These different types of particles are illustrated in Figure 5.5b to 5.5d and can be synthesized with a wide range of the particles' axial lengths and lateral diameters as well as different ratios of the hydrophobic LCE-part to the aqueous hydrogel part by variation of the dispersed and continuous phases' flow rates.

The first type of elongated particles, produced by the described microfluidic method, contains only the LCM-mixture. Figure 5.5b shows the torpedo-shaped morphology of such a rod-like LCE par-

ticle. These exhibit an axial length of 820 µm to 860 µm and a lateral diameter up to 300 µm at the particles' back side, whereas the front side's axial diameter is reduced. The particle's morphology can be explained by means of the increased velocity gradient in the capillary, which deforms the droplets.[212,213] In our case, laminar flow can be expected due to low *Reynold* numbers, which are present at the previously described conditions in the microfluidic setup.[64] This provides a parabolic profile of the flow velocity. The details of the deformation process are, however, difficult to understand, because the viscosity inside the droplets rises quickly during the UV-irradiation as a result of the crosslinking polymerization, which transforms a low molar mass nematic droplet (liquid-like) into a soft-elastic-solid. The UV-polymerization of the droplets is completed in a short time frame (approx. 1 s to 2 s), which enables the "freezing" of the elongated non-equilibrium state of the droplet morphology. The resulting torpedo-shaped, rod-like, single-phase particles enabled the determination of the LCE's maximum actuation, which was used as the benchmark for the Janus particles' actuation (Figure 5.6d).

The morphology of the elongated Janus particles results from an even more complex situation, as both parts of the Janus droplets do not only possess different viscosities, but also different expected viscosity increases during the polymerization, which most likely follow different kinetics. From them, elongated Janus particles of two different morphologies were achieved by the variation of the aqueous phase' viscosity. These particles are displayed in Figure 5.5c and 5.5d and Figure 5.66a to 5.6c. The Janus particle 5.5c was synthesized from the same compositions of the LCM and AM mixtures as described in the previous subsections. The aqueous phase of particle 5.5d was replaced by the high viscous acrylamide monomer (pAM) mixture, which contained 0.5 wt% of a high molecular weight polyacrylamide in order to strongly increase the aqueous phase' viscosity. Particle 5.5c provides a torpedo-shaped elongated morphology of the AM part (low viscosity, colored with a red dye) and an accumulation of the LCM-part at the back side of the particle (dark colored) with respect to the flow direction. The particle features a lateral diameter of 310 µm. On the other side, the morphology of Janus particle 5.5d consists of a cone-shaped short pAM-part (high viscosity) providing a diameter of 425 µm and a strongly tapered LCM-part. The LCE shows again a lateral diameter of roughly 310 µm at the back side of the particle. Due to the viscosity increase on going from the AM (Figure 5.5c) to the pAM-mixture (Figure 5.5d), the LCM-part now gets the most strongly deformed part of the Janus particle. From the optical impression of the particle 5.5d's morphology, the LCM-part is supposed to be pulled apart from the aqueous pAM-part during the polymerization.

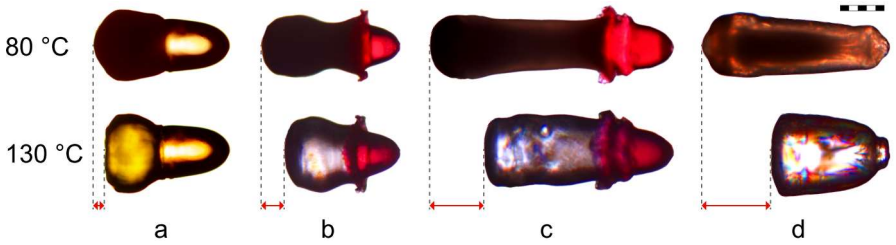

Figure 5.6 Length changes of differently shaped rod-like particles, synthesized under the same microfluidic conditions but different compositions: (a) LCM/AM, (b) and (c) LCM/pAM, (d) pure LCM. The LCE's length changes were measured parallel to the particles' long axis between the amorphous phase (at 80 °C) and the isotropic phase (at 130 °C). The calculated relative length changes are (a) 21 %, (b) 40 %, (c) 52 %, and (d) 58 % (scale bar:200 µm).

The morphological difference between the particles 5.5c and 5.5d is reasonable, as low viscosity particles are deformed most strongly in a given shear gradient. This is appropriate for either the aqueous, non-liquid crystalline AM-phase (in particle 5.5c) or the LCM-phase (in particle 5.5d). Furthermore, a special phenomenon of LCEs, the so called "soft eleasticity", may be important for the morphology of particle 5.5d.[73,214–216] Soft-elasticity is associated with the orientation of a (at first) macroscopically unoriented sample during a stretching process, as done for the microfluidic LCE particle synthesis. It leads to a situation, in which the sample can be further stretched without an increase in stress. Later on, both types of particles were produced with different ratios of the LCM-mixture to the AM/pAM-mixture, in order to investigate a correlation with the actuation properties. Thereby it turned out, that the variability of the volume ratios was larger for Janus particles produced from the LCM and pAM mixtures than for the LCM and AM combination, because Janus particles with a high amount of the LCM-phase broke up too easily in combination with the low viscous AM-phase at the capillaries' tips.

5.3.3 *Characterization of the rod-like Janus particles*

Actuation properties

The investigation of the actuation of the elongated rod-like Janus particles was carried out by observing the length changes of the LCE-part parallel to the particle's long axis at the thermal phase transition. To follow the shape change accurately, the particles were tempered on a hot stage and further analyzed via POM. A silicone oil matrix was used to guarantee a uniform heating over the whole particle. The LCE's phase transition occurred in the temperature range of 80 °C to 130 °C, featuring a length contraction along the particle's long axis and an expansion of the particle's diameter (see Figure 5.6 and Ta-

Table 5.1 Measured LCE lengths of the synthesized particles discussed in Section 5.3.3 and 5.3.2. The relative length change is defined as the ratio of the LCE length in the isotropic state (L_{Iso}) and the LCE length in the amorphous state (L_{Am}). The calculated LCE volume (V_{LC}) and polyacrylamide volume (V_A) are derived from the 3D simulations. The volume ratio between the LCM-part and the AM (or pAM) part $V_{LC} : V_A$ was evaluated from the adjusted flow rates of the dispersed phases during the microfluidic synthesis. The surface area of the LCE/polyacrylamide interface ($B_{LC/A}$) was calculated from the particle radius at the interface

Particle	L_{Iso} [µm]	L_{Am} [µm]	Relative length change	V_{LCE} [mm³]	$V_{LCE} : V_A$	$B_{LC/A}$ [mm²]
5b/6d	536.6	846.2	1.58	35	1 : 0	-
5c	223.2	271.6	1.22	14	1 : 1	0.053
5d	321.3	427.2	1.33	22	4 : 1	0.064
6a	242.3	293.8	1.21	18	2 : 1	0.047
6b	365.1	261.1	1.40	18	3 : 1	0.054
6c	473.8	720.0	1.52	40	3 : 1	0.062

ble 5.1). This leads to the conclusion, that the mesogens are oriented in a bipolar director field, which would lead to an expansion perpendicular to the director and a subsequent contraction along the director during the phase transition. Further WAXS studies proved the assumed mesogen's bipolar director field. The entire actuation process is very fast (about 1 s) and completely reversible during both, the heating and the cooling process. This process can be watched in a real-time video of an actuating Janus particle, which is placed on a hot stage at 130 °C and cooled down from the isotropic to the glassy state by cold air streams immediately (see the supporting information of the present publication).

The influence of different synthetic and microfluidic parameters on the particles' actuation properties were studied. Figure 5.6 illustrates the actuation of differently synthesized rod-like particles and highlights the length changes of the particle's LCE-part during the phase transition. The influence on the actuation properties was studied by variation of (1) the AM and pAM mixtures' viscosities (particle 5.6a and 5.6b), (2) the volume ratio between the polymerized LCM and AM (or pAM) part (particle 5.6b and 5.6c) and (3) the presence of the aqueous pAM-part and thus, the presence of an interface with the LCE (particle 5.6c and 5.6d). All particles were synthesized under the same microfluidic conditions in terms of the temperature, UV-irradiation, the polymerization tube's inner diameter and the continuous phase' viscosity and flow rate.

The different Janus particle morphologies, which were adjusted by variation of the aqueous phases' viscosities, show a strong impact

on the LCE's actuation. The relative length changes of particle 5.6b (40 %, high viscous pAM-mixture) reaches almost twice the value of particle 5.6a (21 %, low viscous AM-mixture). Especially the centrally tapered part of the LCE in particle 5.6b features a strong actuation, which is observable by the video of the corresponding Janus particle actuation. The huge difference of the actuation properties between particle 5.6a and 5.6b is probably based on the different amount of uniformly aligned mesogens along the director. In Janus droplets with the highly viscous pAM-mixture, the LCM-part is stretched most strongly during the UV-polymerization. Deformation is thereby facilitated by the soft elasticity of the LCE. This stretching improves the orientation of the LC-director and creates a bipolar orientation field. This explains the improved actuation properties of particle 5.6b as a result of an increased viscosity of the aqueous monomer mixture.

However, the spherically shaped back side of the particle's LCE exhibits a weak actuation during the phase transition for all the differently synthesized particles. This is the result of the bipolar orientation field of the mesogens, which demands the bending of the director towards the defect point located at the outermost back side of the LCE-part (Figure 5.8e). Since the volume of the poor actuating back side of the LCE is roughly constant over the different particles (at similar particle diameters), the actuation of a rod-like Janus particle should improve by increasing the total volume of the LCE. This assumption was proved by rising the volume ratio $V_{LC} : V_A$ from 2:1 (particle 5.6b) up to 4:1 (particle 5.6c), which further improved the relative length changes up to 52 %.

The third analyzed parameter was the effect of the surface area of the LCE/polyacrylamide interface ($B_{LC/A}$), whose impact on the LCE's actuation properties was studied. As mentioned in Section 5.3.3, the interface between the LCM-part and the non-actuating AM or pAM-part is supposed to be problematic for the actuation process. Since (1) the flow alignment in the area of the interface is probably less effective and (2) the direct contact between both phases hinders the deformation of the LCE. Both effects would be decreased in the absence of the interface $B_{LC/A}$. Thus, the Janus particle 5.6c was synthesized with the same volume of LCE under the same microfluidic conditions as used for the synthesis of the single phase LCE particle 5.6d. Comparing the actuation properties, particle 5.6d features an improved relative length change of 58 % in the absence of the interface $B_{LC/A}$ and sets the benchmark for the actuation process of the rod-like particles.

Both negative effects, the presence of the $B_{LC/A}$ interface and the bending director at the LCE-part's back side, are supposed to become negligible by increasing the volume of the LCE-part while keeping the area of $B_{LC/A}$ as low as possible. Thus, the actuation of differently synthesized Janus particles were correlated with the calculated quantity

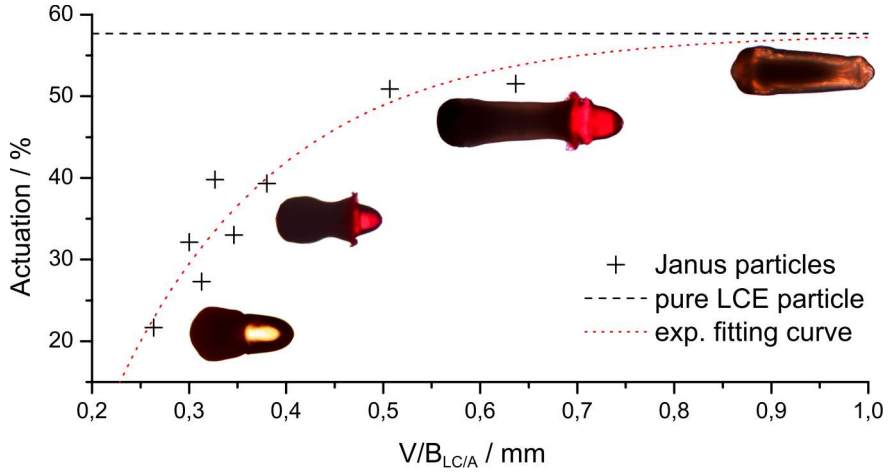

Figure 5.7 Actuation of differently shaped and composited Janus particles as a function of $V/B_{LC/A}$, which reflects the LCE volume divided by the surface area of the LCE/polyacrylamide interface. By increasing the value of $V/B_{LC/A}$, the approximate linear slope at small values flattens at higher values and converges at a constant saturation value of 58 %, reflecting the maximum actuation measured for the single phase LCE particle.

$V/B_{LC/A}$, which represents the LCE volume divided by the surface area of the LCE/polyacrylamide interface. The corresponding data are illustrated in Figure 5.7. An exponential fit function was selected to fit the data, which converge for high values of $V/B_{LC/A}$ to the actuation benchmark of the single phase LCE particle 5.6d. These data clearly illustrate, that the disturbing effects on the mesogen's alignment at the interface and the defect point can be minimized by an optimization of $V/B_{LC/A}$ and the microfluidic parameters. This establishes a systematic microfluidic synthesis of actuating Janus particles, featuring different morphologies, various sizes and high actuation values, which almost reach the length changes of single phase LCE particles.

WAXS measurements

WAXS experiments were performed on an elongated rod-like Janus particle to study the mesogen's alignment and to determine the direction of the LCE's director field. The alignment of the LCE's director dictates the actuation properties of the particles, which are discussed in Section 5.3.2. Different regions of a Janus particle were measured by using a narrow X-ray beam of roughly 100 µm diameter. Figure 5.8 illustrates the results of the X-ray measurements, carried out at three different measuring points along the particle's z-axis (Figure 5.8b). The measurement positions were chosen (1) at the actuating center of the particle's LCE, (2) at the interface of the LCE and the aqueous polymer network and (3) within the aqueous AM-part of the particle.

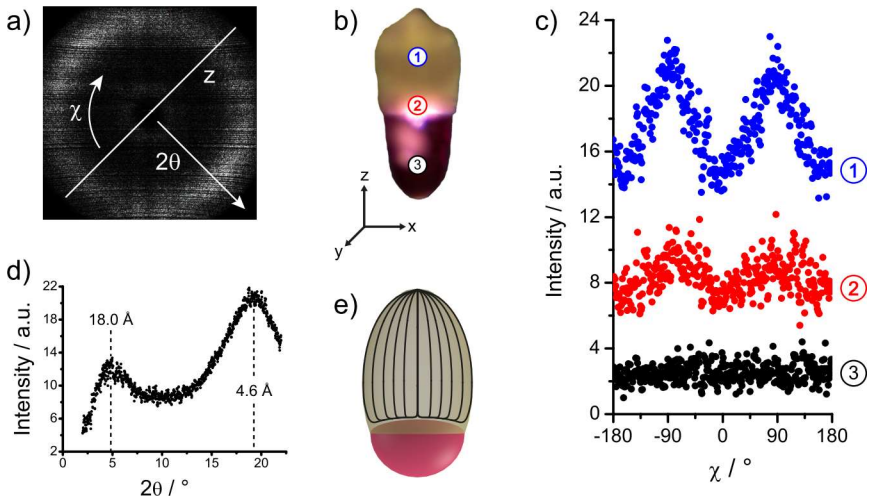

Figure 5.8 Wide-angle X-ray scattering of an elongated rod-like Janus particle. (a) X-ray scattering pattern of the measurement within the LCE (position 1). It shows two intensity maxima perpendicular to the particle's z-axis. (b) Different measurement positions on the analyzed Janus particle. (c) Radial integrated intensities over the wide angle arc χ, which depicts two intensity maxima at $-90°$ and $90°$ within the LCE. (d) Scattering intensity depending on the scattering angle 2θ, which exhibits two maxima at 4.9° and 19.2°. (e) Schematic representation of the mesogen's bipolar director field within the LCE-part of the Janus particles

The scattering pattern of the measurement within the LCE at position 1 is illustrated in Figure 5.8a. The corresponding scattering intensity profile along the scattering angle 2θ is plotted in Figure 5.8d featuring two scattering maxima, which are typically expected for nematic liquid crystals.[133] The maximum at small angles reflects the mean distance of the mesogens in the direction of the director (first peak in pair correlation function) and was calculated to be 18.0 Å using the *Bragg* equation. The second maximum at wide angles corresponds to the mean lateral distance of the mesogens, which was calculated to be 4.6 Å.

The determination of the director's orientation was performed by analysis of the azimuthal intensity distribution $I(\chi)$. This diffuse wide and small angle peaks were radially integrated over χ from $2\theta = 3°$ to $6°$ and $2\theta = 15°$ to $22°$ respectively. The results are displayed in Figure 5.8c. The measurements at position 1 exhibit two intensity maxima at wide-angle arcs of approximately $\chi = -90°$ and $\chi = 90°$, which points to the director's alignment along the z-axis of the particle and proves the assumption of the mesogen's alignment in a predicted bipolar director field (Figure 5.8e) along the particle's long axis, as described in Section 5.3.2. The examination of the results at position 2 further verifies a decrease of the mesogens' alignment along the director field, since the maxima appear clearly less

pronounced. At position 3 both maxima disappear according to the expected isotropic arrangement of the aqueous polymer network.

5.4 CONCLUSIONS

For the first time, actuating liquid crystalline Janus-particles can be synthesized in a microfluidic co-flow device by photo-polymerizing both parts of liquid Janus droplets simultaneously. Thereby a hydrophobic, shape changing LCE "half-droplet" gets glued to a hydrophilic, non-actuating "half-droplet", made of a crosslinked polymer hydrogel. To obtain the maximum shape change of the LCE at the phase transition temperature, the Janus droplet's morphology is modified by systematic variation of the microfluidic parameters. The minimization of the interface between both dispersed phases of the Janus droplets turns out to be the crucial factor to increase the actuating properties of the LCE. Beside adjusting the interfacial tensions of the dispersed monomer phases with respect to the silicone oil used as the continuous phase in the microreactor, the deformation of the Janus droplets into an elongated rod-like structure by increasing the shear rate in the polymerization tube especially leads to Janus particles with strong shape changes of the LCE during the phase transition. The resulting Janus particles feature highly reproducible and completely reversible actuation properties of the LCE, which are almost as strong as those of monophasic LCE particles processed under the same conditions. Additionally, the amphiphilic character of the presented Janus particles opens possibilities for self-organization and a further implementation of other functional materials beside the LCE as the hydrophilic part of the Janus particles.

5.5 EXPERIMENTAL

Materials and reagents

The liquid crystalline monomer was synthesized as described in the literature.[55] The UV-photoinitiators ethyl(2,4,6-trimethylbenzoyl) phenylphosphinate and 2-hydroxy-2-methylpropiophenone, the crosslinking agent *N,N*-methylenebis(acrylamide), the monomer acrylamide, the surfactant sodium dodecylbenzene sulfonate (SDBS) and the silicone oils (100 and 1000 cSt) were purchased from *Aldrich* and used as received. The PDMS–PEG (poly(dimethylsiloxane)-poly-(ethyleneglycole)) copolymer was purchased from *ABCR*. The crosslinking agent 1,6-hexanedioldiacrylate was purchased from *Aldrich* and distilled before use. The high molecular weight polyacrylamide was synthesized in a free radical polymerization using a standard procedure.[217]

The liquid crystalline monomer (LCM) mixture was prepared for the microfluidic synthesis by dissolving the LC–monomer, 10 mol% of the crosslinking agent 2-hydroxy-2-methyl propiophenone and 2 wt% of the photoinitiator ethyl(2,4,6-trimethylbenzoyl) phenylphosphinate in dichloromethane. The solution was stirred for a short time and the solvent was evaporated. The resulting mixture was melted at 90 °C and filled into a PTFE tube (inner diameter (ID): 1.59 mm), which was plugged into the microfluidic setup inside the water bath. A silicone oil (100 cSt) was used as a hydraulic fluid in a syringe to pump the LCM mixture into the microreactor.

The aqueous AM and pAM mixtures were prepared by dissolving the monomer acrylamide (40 wt%), the crosslinking agent *N*,*N*-methylenebis(acrylamide) (10 mol%), the photoinitiator 2-hydroxy-2-methylpropiophenone (2 wt%) and small traces of a red ink in distilled water. For the pAM-mixture, 0.5 wt% of polyacrylamide were added to the solution and stirred for 24 hours. The monomer mixture was filled into a 1 mL syringe, which was plugged directly into the microreactor via a PTFE tube (ID: 170 mm). For the measurements of the interfacial tension, different amounts (from 0.01 wt% to 1 wt%) of the surfactant SDBS or the PDMS-PEG copolymer were added to the solution.

Microfluidic setup

The setup of the microreactor is illustrated in Figure 5.2. Two poly(etheretherketone) (PEEK) T-junctions were connected to each other by a PEEK tube (ID: 340 mm) and tempered to 80 °C in a water bath. Two glass capillaries (ID: 100 mm, outer diameter (OD): 165 mm) were situated inside the T-junctions, one to provide the LCM-mixture from the inside of the T-junction (ID: 0.5 mm) on the left, and the other one directly connected to a PTFE tube (ID: 170 mm) to provide the AM (or pAM) mixture. The second T-junction (ID: 1.25 mm) on the right was connected to a silicone oil (1000 cSt) filled syringe by a PTFE tube (ID: 500 mm) to provide the continuous phase. Three syringe pumps (*Harvard Apparatus* Pump 33) were used for the continuous injection of the monomer mixtures (flow rates: 0.01 mL h^{-1} to 0.2 mL h^{-1}) and the silicone oil (flow rates: 0.5 mL h^{-1} to 3.0 mL h^{-1}). The tips of the glass capillaries were placed in the PTFE polymerization tube (ID: 500 mm or 750 mm), which led through the water bath and thereafter passed over a hot plate (65 °C). The polymerization tube was irradiated over a distance of 1 cm on the hot plate using an *Oriel* LSH302 (500 W) lamp equipped with a band filter (323 nm to 385 nm) and a waveguide.

Analysis

The length measurements of the LCE were carried out via POM measurements (*Olympus* BX51) at 130 °C (isotropic phase: L_{Iso}) and at 80 °C (amorphous state: L_{Am}). The heating of the particles was performed on a microscope hot-stage (*Linkam* TMS 94). Particle images were taken using a microscope camera (*Olympus* ColorView II) and analyzed using microscope imaging software (*Olympus* cell^{D}). The measured data for the LCE lengths and the calculated relative length changes are illustrated in Table 5.1. The actual LCE volume V_{LC} was determined by simulating the body of rotation from the particle's cross-sectional area, which was observed from the optical images of the particles. The simulation of the body of rotation and the calculations of V_{LC} were carried out using the open source 3D rendering program *Blender* 2.76.

The measurements of the interfacial tension between the AM-phase and the silicone oil (1000 cSt) were carried out using a DCAT 11 tensiometer (*DATAphysics*, Germany) equipped with a *Wilhelmy* plate made of platinum–iridium (PT11: length 10 mm, width 19.9 mm and thickness 0.2 mm) at 85 °C. Every measurement started with an automatic weighing of the *Wilhelmy* plate in the AM-phase. Thereafter, the silicone oil was added and the interfacial tension between the two phases was measured. Every surfactant concentration in the AM-phase was measured separately.

The WAXS studies were performed on a Janus particle, which was synthesized under the same microfluidic conditions as particle 5.6a. The measurements were carried out using a "Nanostar-System" from the company *Bruker AXS* equipped with two crossed *Goebel* mirrors, a *Kristalloflex* 770 generator with a copper anode and a *HiStar* flat panel detector with a resolution of 1024 × 1024 pixels and a diameter of 11.5 cm. The diameter of the point-shaped X-ray beam is defined by an aperture plate of 100 mm.

ACKNOWLEDGEMENTS

T. Hessberger and L. B. Braun acknowledge funding by the German Science Foundation (DFG: Ze 230/24-1). F. Henrich acknowledges funding by the ERC, Advanced grant SUPRO 340 391 (HJB).

6

INTERFACIAL SELF-ASSEMBLY OF AMPHIPHILIC DUAL TEMPERATURE RESPONSIVE ACTUATING JANUS PARTICLES

Tristan Hessberger, Lukas Braun and Rudolf Zentel,
Advanced Functional Materials **2018**, 1800629 (Early View)

6.1 ABSTRACT

Amphiphilic Janus particles feature the combination of two different functional materials in one single colloid as well as the possibility of self-assembly at interfaces into complex superstructures. In this article, the self-assembly of dual temperature-responsive amphiphilic Janus particles at liquid-liquid interfaces and their subsequent conversion into an actuating layer-shaped surface is presented. These microparticles are produced in a capillaries based continuous flow microfluidic device by photo-initiated radical polymerization. The hydrophobic part of the Janus particles contains a liquid crystalline elastomer (LCE), which performs a strong actuation up to 95 % during the nematic-isotropic phase transition. The other side consists of a poly(*N*-isopropylacrylamide) hydrogel, which features volumetric expansions up to 280 % below the lower critical solution temperature (LCST). A multi-step molding process is developed to uniformly align the Janus particles at a toluene/water interface and to embed the particles into a hydrogel matrix. A particle covered hydrogel layer is obtained, which features a collective actuation of the rod-like LCE parts on the surface and a bundling of the resulting forces during the phase transition.

6.2 INTRODUCTION

The development of new synthetic routes, as well as new concepts and applications for Janus particles has strongly increased the interest in this class of materials during the last decade.[140,142,146,189] The morphology of colloidal Janus particles is built up of two chemically different parts/phases, which are clearly distinguishable from each other and usually consist of polymeric or inorganic materials.[143,147] Therefore, Janus particles offer the advantage of (i) combining two different materials in one single colloid, thus allowing the combination of two different properties in one material. In addition, (ii) the broken symmetry of Janus particles (transition from centro to polar symmetry) makes them suitable candidates as building blocks

for self-assembly approaches and surface active applications.[218–220] Amphiphilic Janus particles are known to have a higher adsorption energy at water/oil interfaces compared to homogenous particles, which opens possibilities for their use as emulsion stabilizers and solid surfactants.[175,179,181,221] Like molecular amphiphiles, both the particle shape and the ratio of hydrophilic to hydrophobic part of the Janus particles (called Janus balance) strongly influences their properties as amphiphiles. Apart from that, the properties of Janus particles resulting from the combination of different material properties as well as their broken symmetry have been used for applications in the fields of biomedicine and drug delivery, catalysis, optical sensors, textile fibers, micromotors and electronic paper.[147,189,193,201,222–224] Furthermore, bipolar Janus particles are capable of performing self-assembly into complex structures, such as supermicelles, clusters or monolayers at interfaces.[177,182,183,225,226] This opens the possibility to increase the length scale of the broken symmetry from the individual Janus particle to the size of a superstructure.

The incorporation of stimuli-responsive materials into Janus structures offers the possibility to further increase their complexity and adds the possibility of a real-time control of their properties. For this purpose, stimuli such as changes of temperature, pH-value or irradiation by light can be used to trigger changes in size or shape, emulsifiability or amphiphilicity and even changes in their ability of self-assembly.[144,186,187] Especially dual-responsive Janus particles are expected to enable unique properties, as both parts of the particles feature structural changes at different stimuli.[165,227]

Based on these concepts, the idea for this work was the synthesis of dual-responsive amphiphilic Janus particles, which are able to self-assemble at an interface of two fluids and perform a stimuli-responsive shape change. The shape change of the individual particles should allow a directed movement, whereas the assembly of the particles into a macroscopic structure fulfills the precondition to transfer the stimuli-responsive functionalities of the individual micro objects into a directed and collective shape change of a larger actuating superstructure. Considering these requirements, LCEs offer suitable properties as actuating materials for the hydrophobic part of the Janus particles, whereas the hydrophilic part can be prepared from a hydrogel with an LCST.

Liquid crystalline elastomers are slightly crosslinked polymer networks, in which the form-anisotropic molecules of a liquid crystal (mesogens) are connected to the backbone of a polymer chain.[42,70,214] Thus, the entropic elasticity of a polymer network is combined with the anisotropic properties of a liquid crystal, which results in a stimuli-responsive material. LCE samples, which consist of uniformly aligned mesogens, perform a macroscopic shape change at the liquid crystalline-isotropic phase transition. Therefore, the interest in devel-

oping LCEs for their use as soft-actuators in micro robotics has become an important field of research.[67,78,84,228,229] For actuating LCEs, nematic liquid crystalline phases are most commonly used. The polymer network thereby consists of rod-like shaped (calamitic) mesogens, which are either connected to the polymer backbone by a flexible alkyl-spacer (side-chain LCE) or incorporated into the polymer chain (main-chain LCE).[67,215,230,231] Irrespective of the LCE type, the orientation of the mesogens along a defined director field is a crucial step during the preparation of an actuating LCE-sample. For this reason, different concepts for the mesogen orientation are known for the synthesis of actuating LCE samples and both irreversible covalent crosslinking as well as reversible ionic crosslinking techniques have been established.[63,208] Beside techniques in which the built-up of the liquid crystalline polymer and the crosslinking are performed in two sequent steps, the simultaneous radical polymerization of mesogens with polymerizable groups in the presence of multifunctional crosslinkers offers a synthetic pathway, which is very fast and easy to operate with different setups.[54,55]

Microfluidic devices offer an easy way to prepare polymeric particles of different shapes. Capillaries-based microfluidic devices also allow the production of actuating LCE particles of various types, including main-chain and side-chain LCEs as well as different particle morphologies.[4,6,64,65,124,135] Different microfluidic setups were developed to form micrometer-sized droplets from a liquid crystalline monomer mixture in a continuous flow of silicone oil, which are simultaneously polymerized and crosslinked by photo-initiation. According to various possible configurations of the capillaries in the microfluidic setup, the LCE particles can assume different shapes, such as oblate or prolate shaped, core-shell and Janus particles.[3] Furthermore, different liquid crystal director fields can be achieved by controlling the flow parameters and acting shear rates, which leads to contracting as well as elongating actuation geometries of the particles during the phase transition.

Based on these concepts, the idea of an amphiphilic dual stimuli-responsive Janus particle was developed, which contains two different temperature-responsive polymeric materials. On one side, this Janus particle contains an actuating LCE with a clearing temperature in between 95 °C to 100 °C, which performs an asymmetric shape change depending on the mesogens' director field. The other side consists of a poly(*N*-isopropylacrylamide) (PNIPAAm) hydrogel,[232–235] which changes its volume symmetrically to all spatial directions due to uniform swelling in water at temperatures below the LCST of 32 °C. Accordingly, both parts respond at different temperatures which enables an independent triggering of two geometrically different shape changes. As the swelling properties of PNIPAAm strongly depend on the degree of crosslinking, the amphiphilicity of the Janus parti-

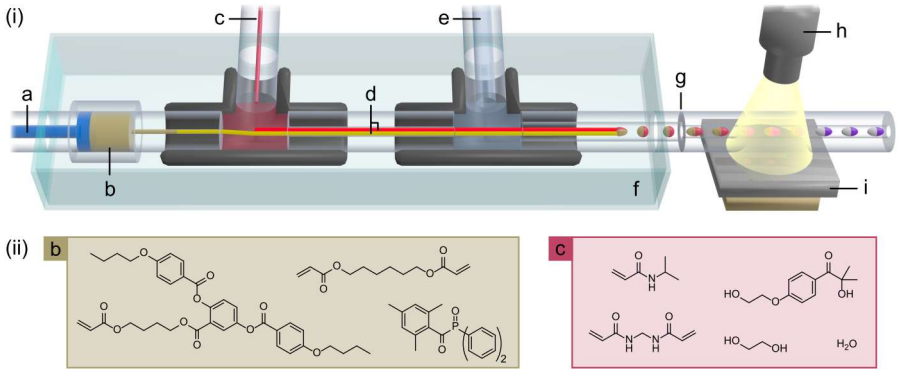

Figure 6.1 (i) Continuous flow microfluidic setup for the production of dual-temperature responsive Janus particles: a) Hydraulic silicone oil, b) reservoir of the liquid crystalline monomer mixture, c) monomer mixture for the PNIPAAm hydrogel, d) two parallelly aligned glass capillaries of different lengths, e) continuous phase silicone oil, f) heated water bath at 90 °C, g) tapering of the polymerization tube, h) UV-lamp, i) heating plate at 40 °C. (ii) Chemical compounds of b) the liquid crystalline monomer (LCM) mixture and c) the hydrogel monomer (HM) mixture.

cles can be adjusted and thus, self-assembly at fluid-fluid interfaces is enabled. By further immobilization of the uniformly aligned Janus particles, an actuating planar-shaped superstructure is formed, which provides a collective actuation of all contained LCEs in the same direction. Accordingly, we present a concept, which combines the advantages of self-assembly at two different length scales: (i) the nanoscopic alignment of form-anisotropic liquid crystalline molecules into an ordered mesophase and (ii) the macroscopic assembly of amphiphilic Janus particles at bipolar interfaces. Our concept allows the application of directed forces, which are delivered by single LCE micro objects and ordered into an actuating superlattice by breaking the symmetry of micro actuators.

6.3 RESULTS AND DISCUSSION

6.3.1 *Microfluidic Synthesis*

The preparation of actuating Janus particles was carried out in a dual capillary microfluidic setup, which was similar to our previously described microreactor.[3] Figure 6.1 illustrates the microfluidic setup and its components, which have been optimized for the production of strongly elongated Janus particles. Basically, the Janus droplets are formed in a continuous flow of a highly viscous silicone oil at the tips of two glass capillaries, which are aligned in the center of a microtube. The droplet formation is carried out in a water bath at 90 °C (which is above the clearing temperature of the liquid crystalline monomer (LCM)-mixture) to provide the sufficient fluidity of the

liquid crystalline monomer mixture in the isotropic state. However, the polymerization and crosslinking are initiated by UV-irradiation on a hot plate at 40 °C (below the clearing temperature of the LCM-mixture) to enable the alignment of the mesogens in the nematic state. Previously, we highlighted the necessity of raising the shear gradient applied on the Janus droplets during their transportation in the microtube by the continuous phase. Therefore, the spherical Janus droplets pass a tapering of the surrounding polymerization tube, at which the flow velocity as well as the shear gradient are increased, just before the UV-initiation takes place. Accordingly, an elongation of the Janus droplets along the flow direction of the continuous phase and an alignment of the mesogens during the polymerization in a bipolar director field are achieved, which have been proven as the crucial requirements for the synthesis of strongly actuating LCE Janus particles.[3]

The compounds of the hydrophobic LCM-mixture, which forms the liquid crystalline part of the Janus particles, as well as the hydrophilic monomer mixture (HM) mixture, which aims for the hydrogel part are shown in Figure 6.1. The LCM-mixture includes the nematic mesogen (4''-acryloyloxybutyl)-2,5-di-(4'-butyloxybenzoyloxy) benzoate which contains a side-on attached polymerizable acrylate group. Furthermore, 10 mol% of the difunctional crosslinker hexanediol diacrylate and 2 wt% of the radical UV-photo initiator *Lucirin TPO* are added. This monomer mixture showed a monotropic nematic phase with a clearing temperature range of 68 °C to 70 °C (note: this clearing temperature increases after polymerization). Similar monomer mixtures have been successfully established for the synthesis of various actuating microparticles, films and wires.[52,132,236] The HM-mixture contains a 40 wt% solution of the monomer *N*-isopropylacrylamide (NIPAAm) the difunctional crosslinker *N*,*N*-methylenbisacrylamide (1 mol% of NIPAAm) and the UV-photoinitiator *Irgacure* 2959 (1 mol% of NIPAAm), which are all water soluble compounds under standard conditions. As the polymerization of the Janus droplets is carried out at temperatures above the LCST of PNIPAAm in water, the aqueous HM-mixture had to contain a sufficient amount of an organic solvent, to prevent precipitation and phase separation of PNIPAAm in the hydrophilic part of the Janus droplets during the UV-polymerization. Therefore, 55 % v/v ethylene glycole was added, which complied with the requirements of a high boiling point (197.3 °C), water miscibility and a stable Janus droplet formation at the two different temperature regions in the microreactor.

Although the LCM and HM mixtures formed stable biphasic Janus droplets, a slight intermixture of both phases at the interface was detected as the liquid crystalline phase showed a reduction of the clearing temperature after contacting the hydrophilic phase. To investigate the influence of partial mixing, LCM/HM Janus particles and LCM

Table 6.1 Differential scanning calorimetry measurements of the LCM-mixture which contained different amounts of NIPAAm. The nematic-isotropip phase transition temperature (T_{NI}) was detected during cooling and heating cycles.

NIPAAm[a)] [wt%]	x(NIPAAm)[b)]	T_{NI}(cool) [°C]	T_{NI}(heat) [°C]
0	0	65.9	68.5
2.5	0.125	55.3	57.4
5.0	0.227	45.0	46.6
10.0	0.383	37.6	41.8

[a)]mass fraction and [b)]mole fraction of NIPAAm related to the liquid crystalline monomer

single phase particles (which never contacted the HM phase) were synthesized, using the previously optimized polymerization temperature of 65 °C.[3] The single phase particles showed the expected LCE actuation behavior at phase transition temperatures between 120 °C to 130 °C (clearing temperature of pure crosslinked polymer) as described in previous works. However, the Janus particle's LCE showed reduced clearing temperatures between 85 °C to 95 °C without any shape change during the phase transition. This only allows the conclusion, that the LCM-mixture gets contaminated by a guest compound originating from the HM-mixture after contact of the two phases. Thereby, the clearing temperature of the LCM-mixture gets decreased below 65 °C and the polymerization happens in the isotropic phase of the LCM, which prevents the alignment of the mesogens before polymerization. Irrespective of the partial mixing of the low molar mass compounds, the final polymer phases are segregated again. Janus particles synthesized from the more hydrophilic acrylamide monomer did not show this phenomenon.[3] However, NIPAAm includes a hydrophobic isopropyl group, which increases the solubility in the hydrophobic LCM-phase. Differential scanning calorimetry (DSC) measurements of LCM-mixtures, to which various amounts of NIPAAm had been added, were carried out to identify its influence on the LCM-phase behavior and to determine a proper polymerization temperature, at which the contaminated LCM-mixture still provides the nematic phase. Table 6.1 contains the clearing temperatures of the DSC measurements, which were determined during both cooling and heating cycles of the samples (for more detailed DSC-data see Figure 6.9 in the supporting information). The data clearly show a continuous decrease of the LCM's clearing temperatures due to a rising mole fraction of NIPAAm, which reaches down to temperature values below 40 °C. Already low amounts of NIPAAm (2.5 wt%) show a decrease

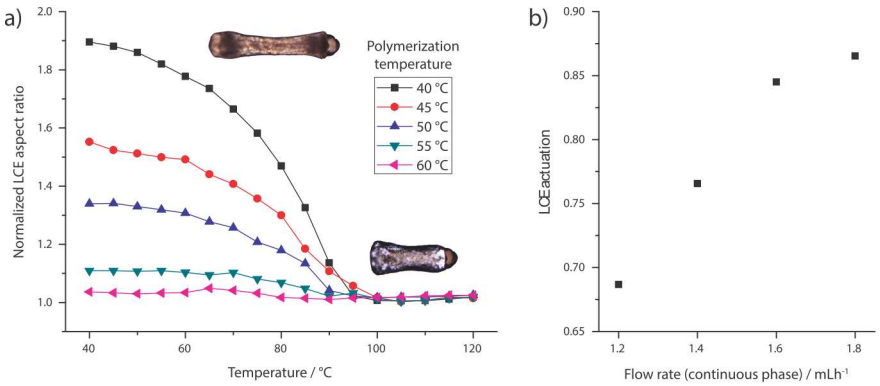

Figure 6.2 a) The normalized aspect ratio of the Janus particle's LCE is illustrated for an ambient temperature range between 40 °C and 120 °C. Heating diagrams of five different Janus particle samples are displayed, which were synthesized at different polymerization temperatures from 40 °C to 60 °C. b) The dependency of the maximum LCE actuation on the flow rate of the continuous phase during the Janus particles' syntheses is plotted.

of the clearing temperature below 60 °C. This is why the usually applied polymerization temperature of 65 °C could not be used for the preparation of actuating Janus particles anymore.

Based on these results, the polymerization temperature for Janus droplets containing both monomer mixtures (LCM and HM) was varied from 40 °C to 60 °C, to find the hot plate temperature, at which the alignment of the mesogens and subsequent actuation of the particles occurs. Janus particles were synthesized at five different polymerization temperatures from 40 °C to 60 °C and a constant flow rate of 1.8 mL h^{-1}. Further characterization was carried out on a hot stage via polarized optical microscopy (POM). Figure 6.2a illustrates the LCE actuation of Janus particles, which were heated up from 40 °C to 120 °C. The nematic-isotropic phase transition was monitored by measuring the aspect ratio of the Janus particle's anisotropically shaped LCE part in steps of 5 °C. To contrast the differences in the actuation magnitudes, the normalized aspect ratios were calculated (at which the aspect ratio in the isotropic phase was set to 1) and the average over four different particles for each polymerization temperature was determined. The heating curve for Janus particles polymerized at 40 °C shows the strongest decrease of the normalized aspect ratio from roughly 1.9 at 40 °C to 1.0 in the isotropic phase. For Janus particles polymerized at higher temperatures, the change of the normalized aspect ratio with temperature decreases continuously. An increase of the polymerization temperature to 45 °C already reduces the maximum normalized aspect ratio change to values below 1.6, whereas at polymerization temperatures of 60 °C the change of the aspect ratio with temperature becomes negligible. For all particles, the normalized LCE aspect ratio reaches its minimum value of 1 at 100 °C, which corresponds to the clearing temperature of the LCE.

This was measured independently for every Janus particle sample at all polymerization temperatures.

Furthermore, Figure 6.2b illustrates the influence of the continuous phase flow rate on the actuation of the LCE. For this purpose, the LCE actuation was defined as the fraction of the LCE's aspect ratio in the nematic state and its aspect ratio in the isotropic state. Four different Janus particle syntheses were carried out at flow rates of the continuous phase from $1.2\,\mathrm{mL\,h^{-1}}$ to $1.8\,\mathrm{mL\,h^{-1}}$ and a constant polymerization temperature of 42 °C. For every flow rate, the LCE of at least 10 Janus particles was measured and the average LCE actuation was determined. Starting at the lowest flow rate of $1.2\,\mathrm{mL\,h^{-1}}$ the LCE actuation shows a nearly linear increase from 68.7 % up to 84.5 % at $1.6\,\mathrm{mL\,h^{-1}}$. The maximum LCE actuation of 86.5 % was measured for the highest flow rate of $1.8\,\mathrm{mL\,h^{-1}}$.

Successful Janus particle syntheses at flow rates above $1.8\,\mathrm{mL\,h^{-1}}$ or polymerization temperatures below 40 °C could not be achieved, as either the increased shear gradient or the raised viscosity of the LCM-mixture caused parts of the liquid crystalline droplet to be removed from the Janus droplet during the cooling process from the isotropic to the nematic phase on the hot plate. Therefore, we regard a polymerization temperature of 40 °C at flow rates of $1.8\,\mathrm{mL\,h^{-1}}$ as the ideal parameters for the synthesis of dual responsive actuating Janus particles in the presented microfluidic setup.

6.3.2 *Thermal Responsiveness of Janus Particles*

Dual temperature-responsive Janus particles were synthesized at the optimized microfluidic conditions (as discussed in Section 6.3.1) and their responsiveness towards temperature changes was investigated in terms of actuation properties of the LCE-part as well as swelling properties of the PNIPAAm hydrogel-part via POM. Figure 6.3 illustrates the four different states of a representative Janus particle's morphology. The different particle states can be obtained in a temperature range from 40 °C to 100 °C and subsequent addition or removal of water in the particles' environment. The transitions of all morphologic states are completely reversible.

Swelling properties of the PNIPAAm hydrogel

The Janus particle state A is obtained at room temperature (20 °C) in an aqueous environment, at which the particle's shape is similar to a mushroom. The LCE on the left side of the particle in Figure 6.3A forms a strongly elongated, rod-like morphology. On the right side of the particle, the PNIPAAm hydrogel shows a spherical, slightly oblate shaped part with a lateral diameter of 410 µm, which is nearly twice the diameter of the LCE on the opposite end of the particle. As the ambient temperature is below the LCST of PNIPAAm in this state,

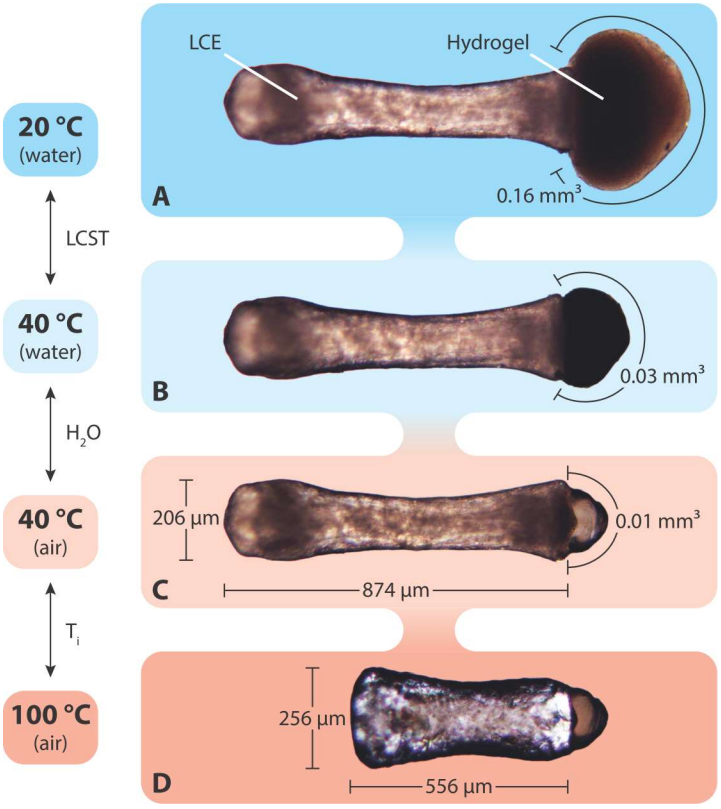

Figure 6.3 The four different states of a Janus particle's morphology at their specific environmental conditions: A. mushroom shaped (LCE: elongated, hydrogel: highly swollen), B. barbell shaped (hydrogel: less swollen), C. rod-like shaped (hydrogel: dry), D. torpedo shaped (LCE: contracted). The volume of the hydrogel part as well as the LCE's diameter and length are specified.

water strongly swells the hydrogel part of the particle, which reveals a volume of roughly 0.16 mm^3 (calculated from the cross-sectional area of the hydrogel and convergence to an elliptical area via *ImageJ*).

By heating up the particle above the LCST of PNIPAAm, the Janus particle state B is obtained at 40 °C in water. In this case, the Janus particle resembles a barbell shape, at which the volume of the hydrogel has been reduced to 0.03 mm^3. By trespassing the LCST, the major amount of water stored in the hydrogel gets released to the environment, which leads to the reduction of the hydrogel volume by more than 80 %.

Another decrease of the hydrogel volume below 0.01 mm^3 is examined at the Janus particle state C, at which the particle's surrounding water has been removed by slow evaporation at 40 °C. Exposed to air, the hydrogel dries at 40 °C and the entire water vaporizes from the hydrogel. Thus, the PNIPAAm part gets transparent and its lateral diameter shrinks below the LCE's diameter, which causes a rather rod-like shape of the Janus particle.

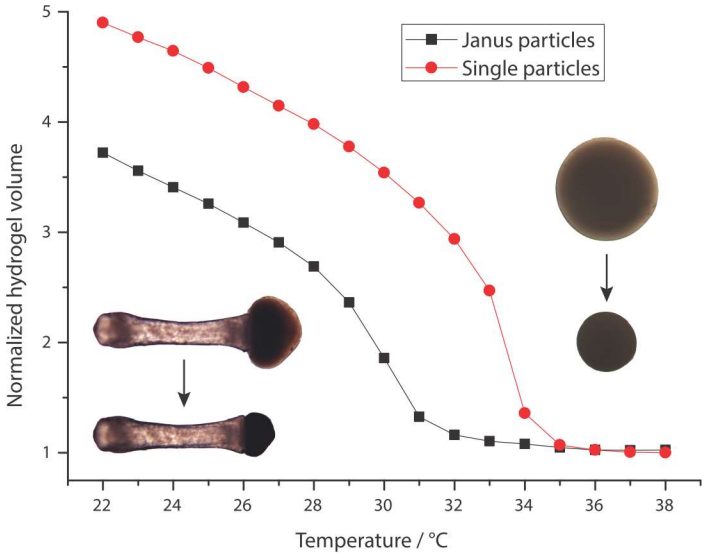

Figure 6.4 Swelling experiments of PNIPAAm hydrogel containing particles. Janus particles (black squares) and homogeneous particles (red spheres) were synthesized from the HM-mixture under equal microfluidic conditions.

To investigate the thermal response of the PNIPAAm hydrogel in the Janus particles at the LCST in detail, the hydrogel volume change of the Janus particles was compared to the swelling behavior of homogeneous PNIPAAm particles, which were synthesized from the same aqueous HM-mixture. Figure 6.4 illustrates the normalized hydrogel volume of both homogeneous and Janus particles in the temperature range from 22 °C to 38 °C. While heating up the water covered particles on a hot stage (at 3 °C min^{-1}), the hydrogel volume of the particles was determined in 1 °C steps from the cross-sectional area of the particles as described above and the average volume over 8 particle measurements was calculated. Both heating diagrams show a similar shape, containing a continuous decrease of the hydrogel volume at lower temperatures, followed by an inflection point which merges to an approximately constant minimum value of the hydrogel volume for higher temperatures.

Two major differences between the Janus particle and the homogeneous particle hydrogels turned out: (i) the LCST of the homogeneous particles can be traced at 34 °C to 35 °C, whereas the LCST for the homogeneous particles appears at lower temperatures at 31 °C to 32 °C. Furthermore, (ii) the hydrogel volume of the homogeneous particles at 22 °C is increased by 390 % (referred to the deswollen hydrogel volume above the LCST), whereas the Janus particle hydrogel expands by only 272 %. Both the lower LCST and the weaker swelling behavior of the Janus particle hydrogel can be explained by consideration of a slight solubility of the LCM's components in the hydrophilic HM-part of the Janus droplets before the polymerization takes place in the mi-

crofluidic process. Although the liquid crystalline monomer as well as the difunctional hydrophobic crosslinker are not soluble in water under standard conditions, the high amount of NIPAAm in the HM-mixture decreases the hydrophilicity, which enables the exchange of hydrophobic components at the LCM/HM interface, especially at the high temperature of 90 °C during the Janus droplet formation. The higher amount of a polymerizable crosslinker moiety as well as an incorporation of hydrophobic compounds into the PNIPAAm hydrogel network leads to a weaker tendency for the generation of hydrogen bonds and a raised crosslinking density. Accordingly, compared to the homogeneous hydrogel particles, which did not get in touch with the LCM-phase, the LCST of the Janus hydrogel network appears at lower temperatures and the amount of absorbed water gets slightly reduced.

In summary, the hydrogel part of the Janus particles shows a strong response to the environmental temperature and solvent presence, which enables a change of the Janus particle's morphology as well as the ratio of the hydrophobic and hydrophilic parts. The strong swelling of the hydrogel part at room temperature fulfills an important requirement for the further alignment of the particles at a water/hydrophobic solvent interface and the assembly of an actuating superstructure. Videos of the swelling and deswelling process of corresponding Janus particles are provided in the supporting information of this publication.

Actuation Properties of the LCE

The shape change of the strongly elongated LCE part of the Janus particles during the phase transition corresponds to a contraction along the particle rotational axis, at which the aspect ratio of the LCE gets strongly reduced. Figure 6.2a demonstrates a strong change of the aspect ratio in the temperature range from 65 °C to 95 °C and a constant remaining shape above 100 °C. Assuming a contraction of the LCE along the director and an elongation perpendicular to the director at the nematic-isotropic phase transition, the geometry of the LCE's shape change indicates a bipolar director field parallel to the particle rotational axis. The bipolar director field has already been verified by wide-angle X-ray scattering (WAXS) measurements for actuating LCE particles, which were synthesized under similar microfluidic conditions in terms of the LC monomer mixture, flow rates and the Reynolds number.[3,65]

To confirm the bipolar director field of the LCE in the case of dual-responsive Janus particles, POM images were examined in the liquid crystalline state of the LCE at 95 °C (Figure 6.5). Aligning the particle's main axis parallel to the POMs analyzer shows the tapered area in the middle of the particle to be completely dark. In this area, the mesogens are aligned uniformly along the rotational axis of the par-

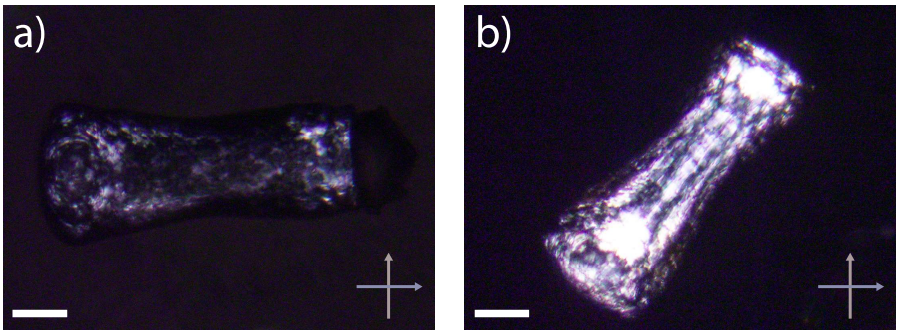

Figure 6.5 POM images of a Janus particle in the liquid crystalline state of the LCE at 95 °C. The rotational axis of the Janus particle is a) aligned parallelly with the analyzer and b) shifted by an angle of 45°. (scale bars: 100 µm)

ticle. Rotating the particle main axis by an angle of 45° towards the POMs analyzer leads to strong birefringence. This proves the bipolar director orientation of the LCE.

Figure 6.3 shows the strong shape change of the LCE from particle state C at 40 °C to particle state D at 100 °C, compared to which its shape change from state A to C is negligible. The LCE in state C is still in the glassy phase. It has a strongly elongated shape with a length of 874 µm and a lateral diameter of 206 µm, which was measured at the broadest part of the LCE at the left end of the particle. Heating up the particle from 40 °C to 100 °C leads to the torpedo shaped particle state, which is pictured in Figure 6.3D. During the nematic-isotropic phase transition, the LCE length contracts to 556 µm, whereas the lateral diameter expands to 256 µm. Accordingly, the aspect ratio of the LCE is reduced from 4.24 in the nematic phase to 2.17 in the isotropic phase, which corresponds to an actuation of roughly 95 %. During the phase transition, the LCE features a bright and colorful appearance, which vanishes by further heating until the particles appear transparent in the isotropic state. The actuation of the LCE responds immediately to temperature changes and is completely reversible during both heating as well as cooling of the Janus particle. Corresponding videos of the actuation process are provided by the supporting information of this publication.

6.3.3 *Self-Assembly of actuating Janus Particles*

The dual responsive Janus particles, which were synthesized under the optimized microfluidic conditions, feature a bipolar character as they consist of the hydrophobic LCE on one side and the hydrophilic PNIPAAm hydrogel on the other side. Accordingly, these particles enable the self-assembly at a liquid-liquid interface of water and an organic solvent to form a monolayer of uniformly aligned Janus particles. The subsequent immobilization of the particles by swelling the

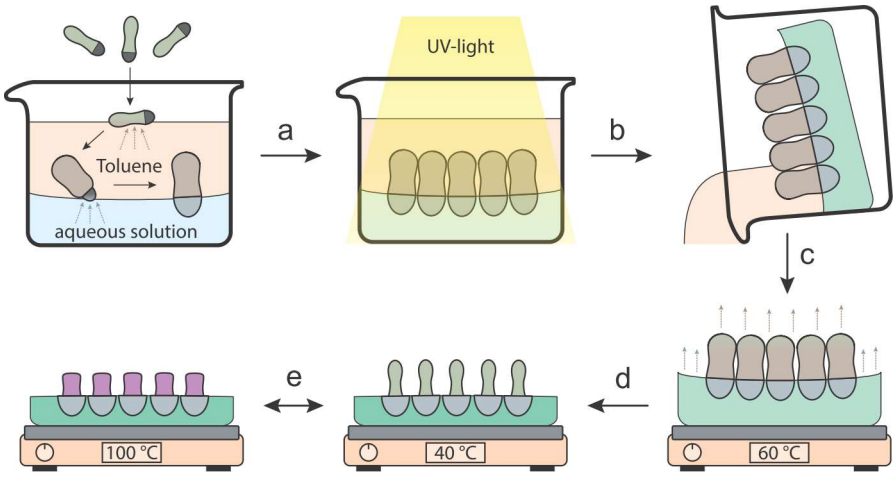

Figure 6.6 Molding process for the self-assembly of dual responsive Janus particles into an actuating monolayered surface: a) swollen Janus particles assemble at the interface b) curing of the aqueous phase by UV-irradiation c) removal of the particle structure from the beaker d) drying of the LCE/hydrogel on a heating plate at 60 °C e) reversible thermal actuation between 40 °C and 100 °C.

hydrogel part with an aqueous crosslinkable monomer solution was supposed to form a mechanically stable layer of collectively actuating particles on top of a hydrogel surface. To produce this actuating Janus monolayer, many Janus particles in the shape of the particle presented in Figure 6.3 were microfluidically synthesized and a multi-step molding process was developed, which is illustrated in Figure 6.6.

Molding process

The process starts with dispersing a variable amount of Janus particles in a biphasic mixture of toluene and an aqueous monomer solution in a small beaker glass. The LCE-part of the particles immediately swells in toluene and the LCE's length and diameter are approximately doubled. After sinking down to the toluene/water interface, the PNIPAAm hydrogel of the Janus particles swells as described in Figure 6.3.2. As the density of the toluene swollen LCE part is lower than the aqueous swollen hydrogel, the particles straight up at the interface with the LCE part pointing upwards.

Figure 6.7a and c illustrate the subsequently formed monolayer in a lateral view, which consists of uniformly aligned Janus particles at the meniscus of the interface. The swollen Janus particles are presented from the top in Figure 6.7b. It shows the densely packed alignment of the particles at the interface. Even after shaking the beaker, the Janus particles form an ordered and densely packed monolayer at the interface again, which demonstrates their high amphiphilic character and interfacial activity despite the swollen particle's size in the range of 1.2 mm to 1.4 mm.

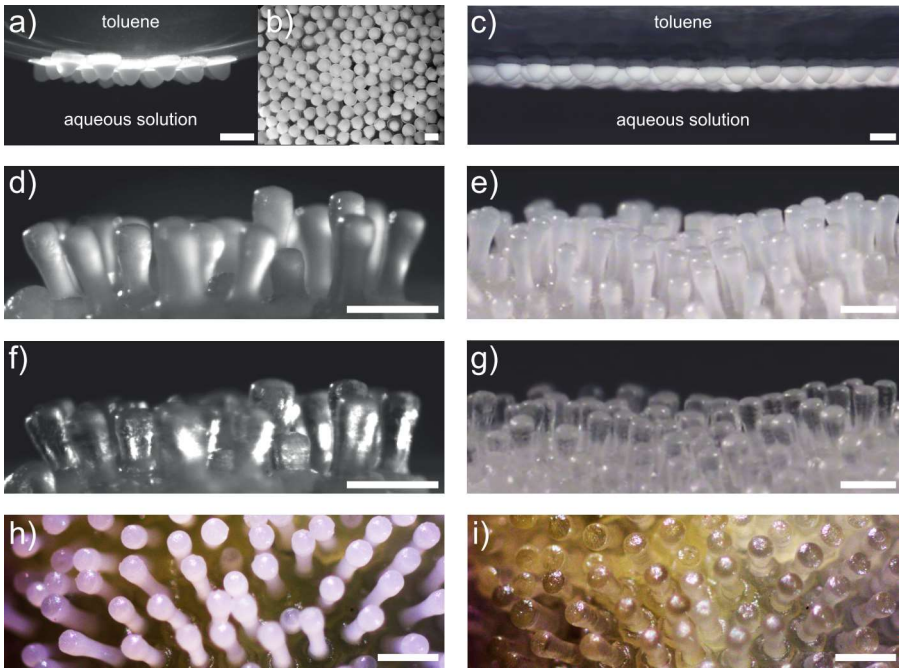

Figure 6.7 Self-assembly of a small (a) and a large number (b and c) of amphiphilic Janus particles at the interface of toluene and a crosslinkable aqueous acrylamide solution. The corresponding actuating Janus layers are displayed from different points of view in the glassy phase at room temperature (d,e and h) and after heating to the isotropic state (f,g and i). (scale bars: 500 µm)

After the Janus particle assembly, the aqueous monomer solution (containing 40 wt% acrylamide, 10 mol% *N*,*N*′-methylenebisacrylamide and 2 wt% Irgacure 2959) is cured by irradiation of the beaker glass with UV-light. Thus, the assembled monolayer of Janus particles is permanently fixed in the crosslinked polyacrylamide hydrogel, which forms an inflexible fundament for the particles due to the high amount of crosslinking agent. As only the hydrophilic parts of the Janus particles extend into the acrylamide fundament, the LCE parts are still flexible. After decanting the excessive toluene phase, the remaining Janus layer is removed from the beaker glass, placed on a glass substrate, and dried on a hot plate at 60 °C to evaporate the remaining toluene from the LCE.

Beside the circular self-assembly of the Janus particles around the meniscus of the interface in a small beaker glass, it is also possible to manufacture layers of Janus particles with variable pre-patterned shapes. For this purpose the particle alignment during the molding process has just to be carried out in a mold with the desired geometrical shape. An example for the molding process of a rectangular shaped Janus layer is illustrated in Figure 6.10 of the supporting information.

After drying at the end of the molding process, the fundamental hydrogel forms a stiff and lightly bended surface, which is covered

by colorless LCE rods. Differently sized Janus layers are obtained by varying the amount of Janus particles used for the self-assembly process. Figure 6.7d illustrates a Janus layer at the end of the molding process at room temperature, which resulted from the small number of particles pictured in Figure 6.7a, whereas the larger Janus layer in Figure 6.7e was obtained from the high amount of particles shown in Figure 6.7b and 6.7c. In these layers, some variation of the LCE rod length is noticed. This probably results from flow instabilities and uncontrolled LCE tear-off in the microfluidic capillary during preparation of the strongly elongated Janus-droplets.

The finally obtained Janus layers consist of LCE rods, which are preferably aligned perpendicular to their hydrogel fundament (the former interface). In Figure 6.7h, a Janus layer in the glassy phase is presented from above to provide an estimate of the density of the LCE rods on the hydrogel surface after the solvent evaporation. The LCE rods show some free space in between each other, which is due to the volume loss after evaporation of the toluene and subsequent deswelling. Furthermore, some deviation of the LCE rod's perpendicular alignment to the cured acrylamide fundament is noted, which is due to the slight bending of the hydrogel fundament during the curing process as well as some nonuniform deswelling of the Janus particles' embedded hydrogel part in the acrylamide fundament during the drying process.

Actuation of Janus Layers

Janus layers in the isotropic state are illustrated in Figure 6.7f, 6.7g and 6.7i. By uniformly heating up the Janus layers above the clearing temperature, the LCE rods become transparent and perform a collective actuation process, which corresponds to the actuation examined for individual LCE rods (described in Figure 6.3.2). During the phase transition of the LCE, a contraction perpendicular to the surface is noticed, which results in a reduction of the total height of the Janus layer. This can be observed by comparing the layer's height in Figure 6.7d and 6.7f as well as in Figure 6.7e and 6.7g. Furthermore, a slight expansion of the LCE rods parallel to the surface (perpendicular to the rods' rotational axis), especially at the broader top end of the rods, as well as a flattening of the rods' top end is noticed. Thus, the surface area on top of the LCE rods is supposed to be slightly increased and the free space between the rods is assumed to be decreased in the isotropic state.

Figure 6.8 illustrates two more Janus layer sections in the glassy phase, in a partially actuated state and in the isotropic phase. The flattening of the LCE rods' top end is exemplified in Figure 6.8c, which shows three particles on the left side, featuring a flat-topped shape compared to their glassy state in Figure 6.8a. Furthermore, the reduced free space between the LCE rods in the isotropic state can

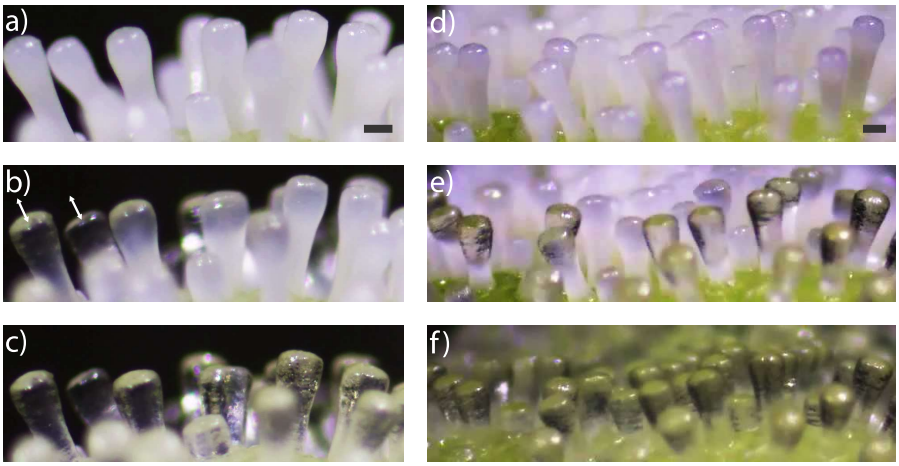

Figure 6.8 Illustration of the local and collective actuation of Janus layers. LCE rods of the layers at room temperature (a,d) are addressed by local heating from the left side (c) or the front side (e), which leads to regionally limited actuation. Uniform heating of the whole layer effects the collective actuation of all LCE rods (c,f). (scale bars: 200 µm)

be observed in Figure 6.8f, which shows more densely packed LCE rods compared to the glassy state in Figure 6.8d. To demonstrate the high speed of the reversible actuation process, a heat gun was used to quickly raise the temperature of the Janus layer, followed by cooling it down to room temperature again. The contraction of the LCE rods occurs in less than one second, whereas the reverse expansion requires about 3 to 4 seconds.

Compared to a global actuation process, at which a uniform heating over the entire LCE layer causes a simultaneous phase transition of the LCE rods, partial heating can be used to trigger a local actuation of selected parts of a Janus layer. Figure 6.8b illustrates a Janus layer section, which was partially heated on the left side. The two rods on the left side (marked with white arrows) feature a completed actuation process and the isotropic state, whereas the third particle on the left side has not entirely completed its actuation. As heating via hot air from a heat gun was used for the local heating process, the heating precision is limited and a thermal exchange through the hydrogel fundament to adjacent LCE rods could not be inhibited. Other heating patterns are also possible as demonstrated in Figure 6.8e, which shows a Janus layer heated from the front side. In this case only the first rows of LCE rods are heated to the isotropic phase featuring the contracted and transparent shape. By moving the heat gun over the Janus layer from the back to the front side, it was even possible to trigger a wave-like actuation pattern. Real-time and slow-motion videos of the collective, locally and wave-like addressed actuation of Janus layers are provided in the supporting information.

6.4 CONCLUSIONS

This work demonstrates, that the self-assembly of microfluidically produced dual temperature responsive Janus particles at a liquid-liquid interface and their conversion into an actuating layer shaped superstructure is feasible. Millimeter sized amphiphilic Janus particles can be synthesized in a capillaries based microfluidic reactor, which has been optimized for the manufacture of liquid crystalline elastomers and hydrogels. The thermic characterization of the hydrophobic rod-like LCE part of the particles offers strong shape changes during the nematic-isotropic phase transition and actuations up to 95 % are obtained with respect to the aspect ratio change. The hydrophilic part of the particles contains a PNIPAAm hydrogel, which features volumetric expansions up to 280 % by swelling in water below the lower critical solution temperature of 32 °C. By combination of the two materials in the Janus particles, four different particle shapes can be reached at temperatures between 20 °C and 100 °C and an amphiphilic character is created. Accordingly, the self-assembly at the interface of an aqueous solution and toluene can be used to uniformly align the Janus particles and to unify the direction of the LCE's actuation perpendicular to the interface. A four-step molding process is developed to obtain a layer shaped rigorous hydrogel basis, in which the hydrophilic part of a variable number of Janus particles is embedded and the actuating LCE rods are parallelized. Heating experiments of these Janus layers show very fast and reversible actuations of the entire LCE covered surface, at which the LCE rods are either addressed collectively by uniform heating or a regional response is triggered by local heating above the clearing temperature. Considering the size of the applied Janus particles, relatively high length changes and forces are generated by bundling the actuation of the particles. Accordingly, by applying a more precise heating technique to such an actuating Janus layer, complex actuation patterns of the LCE rods are assumed to enable the transport of a cargo on top of the actuating surface.

6.5 EXPERIMENTAL SECTION

Materials and Reagents

The nematic mesogen (4''-acryloyloxybutyl)-2,5-di-(4'-butyloxybenzoyloxy) benzoate was synthesized as described in the literature.[55] The crosslinking agent 1,6-hexanediol diacrylate was purchased from *Aldrich* and distilled before use. *N*-Isopropylacrylamide was purchased from *Aldrich* and recrystallized from hexanes before use. The crosslinking agent *N,N'*-methylenebisacrylamide, the photo initiators diphenyl(2,4,6-trimethylbenzoyl)phosphine oxide (*Lucerin TPO*) and 2-Hydroxy-4-(2-hydroxyethoxy)-2-methylpropiophenone

(*Irgacure* 2959), the silicone oils (100 cSt and 1000 cSt), ethylene glycole, dichloromethane and toluene were purchased from *Aldrich* and used as received. The components for the microfluidic setup (fused silica capillaries, poly(etheretherketone) (PEEK) T-junctions, fittings, ferrules, connectors, sleeves) were purchased from *Postnova Analytics* and *IDEX* and the poly(tetrafluoroethylene) (PTFE) tubes were purchased from *WICOM*.

The hydrophobic LCM-mixture was prepared before use in the microfluidic synthesis by dissolving 200 mg of (4''-acryloyloxybutyl)-2,5-di-(4'-butyloxybenzoyloxy) benzoate, 7.2 mg of 1,6-hexanediol diacrylate and 4.1 mg of diphenyl(2,4,6-trimethylbenzoyl)phosphine oxide in 250 µL dichloromethane to the exclusion of UV-light. After stirring for one minute, the solvent was removed with a rotary evaporator and the resulting mixture was heated to 110 °C. The molten mixture was drawn into a PTFE tube (inner diameter (ID): 1.59 mm, length: 8 cm) by using a syringe and plugged in the microfluidic setup as the LCM reservoir. The hydrophilic monomer mixture was prepared by dissolving 200 mg of NIPAAm, 2.7 mg of *N*,*N*'-methylenebisacrylamide and 4 mg of 2-Hydroxy-4-(2-hydroxyethoxy)-2-methylpropiophenone in a mixture of 133 mL distilled water and 158 mL ethylene glycole. After complete dissolution under stirring, the solution was drawn into a 1 mL syringe and plugged to the microfluidic reactor.

Microfluidic Setup

Figure 6.1 illustrates the setup of the microreactor. Two fused silica capillaries of different length (ID: 100 µm, outer diameter (OD): 165 µm) were inserted into a tubing sleeve (ID: 394 µm) and the left side of the sleeve was sealed with *UHU* superglue. Both ends of the sleeve were connected to a T-junction (ID: 0.5 mm) for 1/16 in tubings. The left T-junction (connected to the sealed end of the sleeve) contained the end of the shorter capillary (red) in the inside, whereas the second, longer capillary (yellow) ended at the left outlet of the T-junction. The LCM-reservoir was connected to the left outlet of the T-junction on the left side using a tube (ID: 170 µm) and the long capillary (yellow) was placed inside the tube. The second end of the LCM-reservoir was connected to a syringe with a tube (ID: 0.5 mm), which provided the hydraulic silicone oil (100 cSt). The hydraulic oil is necessary, as the mixture LCM solidifies at room temperature and cannot be processed in a syringe outside of the heated water bath. The middle outlet of the left T-junction was connected to the syringe, which was filled with the HM-mixture via a tube (ID: 170 µm). The outlet in the middle of the T-junction on the right side was connected to a syringe with the continuous phase silicone oil (1000 cSt) via a tube (ID: 0.75 mm). Both ends of the capillaries at the right outlet of the T-junction were inserted in a short PTFE tube (ID: 0.75 mm),

which was further plugged to the polymerization tube (ID: 0.5 mm) via *Luer* connectors to form the tapering of the tube's inner diameter. The polymerization tube was laid over a precision hot plate (65 °C) and an *Oriel* LSH302 (500 W) lamp equipped with a waveguide was used to irradiate 1 cm of the polymerization tube in the middle of the hot plate. The microreactor, including the LCM-reservoir and the capillaries were placed in a heating bath at 90 °C. The syringes were driven via *Harvard Apparatus* Pump 33 syringe pumps.

Analysis

The measurements of the Janus particles at different temperatures were carried out via polarized optical microscopy (*Olympus* BX51) on glass substrates. The particles were heated with a microscope hot-stage (Linkam TMS 94). Particle images were taken via microscope cameras (*Olympus* DP22, *Olympus* BX51) and analyzed by using a microscope imaging software (*Olympus* CellSens Standard V1.15, *ImageJ* V1.4.3).

The differential scanning calorimetry measurements were carried out with a *Perkin Elmer* DSC 8500 and the following temperature Program was used: 1) Hold for 1 minute at 20 °C. 2) Heat from 20 °C to 130 °C at 20 °C min^{-1}. 3) Hold for 1 minute at 130 °C. 4) Cool from 130 °C to 20 °C at 10 °C min^{-1}. 5) Hold for 3 minutes at 20 °C. 6) Heat from 20 °C to 130 °C at 10 °C min^{-1}.

6.6 SUPPORTING INFORMATION

This section contains supporting information for the present publication "Interfacial self-assembly of amphiphilic dual temperature responsive actuating Janus particles". The videos of the dual temperature-responsive Janus particle swelling and actuation processes and the videos of the Janus layer actuations are available at the *Wiley* online library (DOI: 10.1002/adfm.201 800 629).

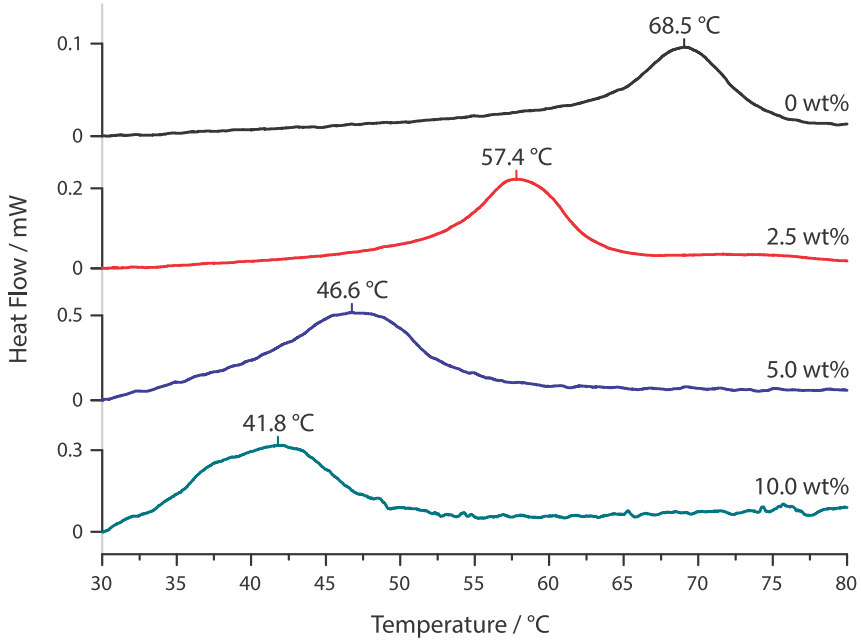

Figure 6.9 DSC measurements of the LCM-mixture containing different amounts of NIPAAm (black: 0 wt%, red: 2.5 wt%, blue: 5.0 wt%, green: 10.0 wt%). Displayed temperature program: Heating from 20 °C to 130 °C at 10 °C min^{-1}.

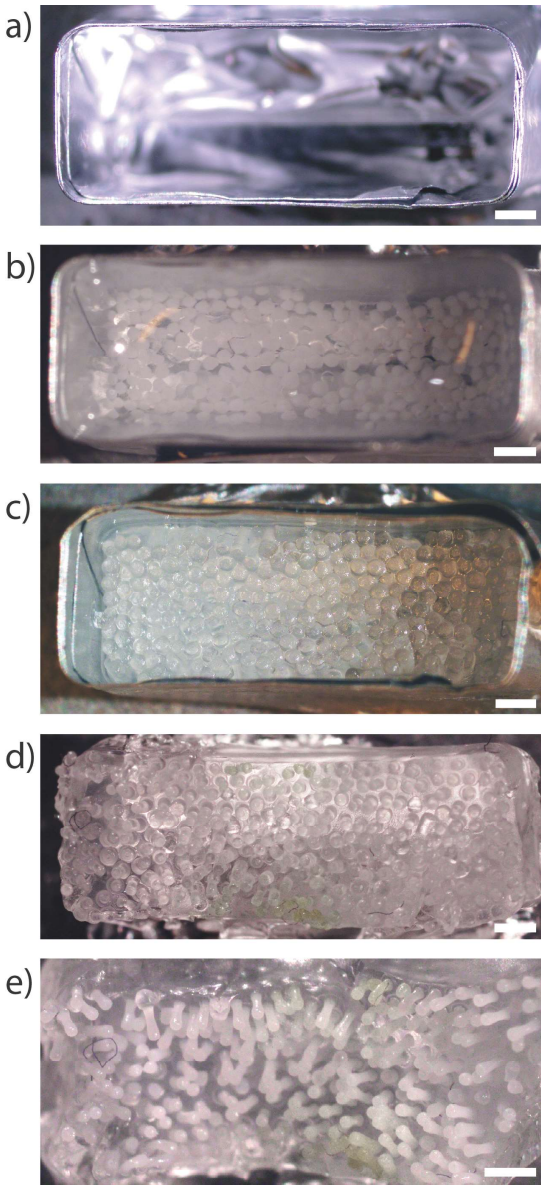

Figure 6.10 Molding process of a Janus layer in a rectangular shape. a) Rectangular shaped aluminum mold. b) Swollen Janus particles at the interface (toluene/aqueous phase) before UV-irradiation. c) Janus layer after UV-irradiation and decantation of toluene. d) Janus layer after removal from the mold (dried at room temperature). e) lightly bended deswollen Janus layer after drying with a heat gun. (scale bars: 1 mm)

7

MICROFLUIDIC SYNTHESIS OF ACTUATING MICROPARTICLES FROM A THIOL-ENE BASED MAIN-CHAIN LIQUID CRYSTALLINE ELASTOMER

Tristan Hessberger, Lukas Braun and Rudolf Zentel,
Polymers **2016**, *8*, 410-421

7.1 ABSTRACT

In this article, the microfluidic synthesis of strongly actuating particles on the basis of a liquid crystalline main-chain elastomer is presented. The synthesis is carried out in a capillary-based co-flow microreactor by photo-initiated thiol-ene click chemistry of a liquid crystalline monomer mixture. These microparticles exhibit a deformation from a spherical to a rod-like shape during the thermal-initiated phase transition of the liquid crystalline elastomer (LCE), at which the particles' aspect ratio is almost doubled. Repeated contraction cycles confirm the complete reversibility of the particles' actuation properties. The transition temperature of the LCE, the temperature range of the actuation process as well as the magnitude of the particles' aspect ratio change are studied and controlled by the systematic variation of the liquid crystalline crosslinker content in the monomer mixture. Especially the variable actuation properties of these stimuli-responsive microparticles enable the possibility of an application as soft actuators or sensors.

7.2 INTRODUCTION

LCEs have been intensely studied and enhanced during the last decades with particular regard to their unique mesophasic behavior and elasto-mechanical properties.[57,63,204,206,214,237] LCEs are slightly crosslinked liquid crystalline polymer networks, which are capable of performing a reversible macroscopic shape change during the phase transition of the liquid crystalline state. The shape anisotropic molecules of a liquid crystalline phase (mesogens) enable the molecular self-organization into mesophases, which exhibit certain grades of molecular order. Nematic liquid crystals consist of rod-shaped (calamitic) mesogens, which are aligned parallelly to a common director in the nematic phase. The deviation of the calamitic mesogens' orientation from the director orientation is expressed by the nematic order parameter, which equals 1 for the ideal crystalline state and 0 for the isotropic state. Typical values of the order parameter for a nematic

phase are between 0.3 and 0.7. In nematic LCEs, the parallel-aligned order of the mesogens is combined with the entropy-elastic properties of polymeric elastomers. The mesogens can either be linked to the polymer backbone via an alkyl spacer (side-chain LCE) or can be directly integrated into the polymer backbone (main-chain LCE). In the nematic phase, the uniform alignment of the mesogens forces the polymer chain into a deformed conformation (oblate or prolate). Heating above the clearing temperature causes the phase transition of the LCE from the nematic to the isotropic state, at which the mesogen's uniform alignment along the nematic director vanishes and a random coil conformation of the polymer chain is preferred.[238]

The interplay between the polymer network and the nematic ordering of the mesogens may also modify the phase transition between the nematic and the isotropic phase. At first, this phase transition is "weakly first-order" in low molar mass nematics. This implies the existence of strong pretransitional effects in the isotropic phase (e.g. a strong Kerr effect resulting from the interaction of local nematic ordering with the external electric field). In LCEs, the polymer network can thus induce some orientation already in the isotropic phase (para-nematic phase). For strong mechanical fields, this can change the phase transition between the nematic and the isotropic phase to become second-order. Secondly — and independent of the first effect — a broadened, continuous phase transition may also result from inhomogeneous crosslinking densities and different local clearing temperatures in the LCE sample.[239–241]

Different external stimuli are known to trigger the phase transition and, therefore, a macroscopic shape change of the LCE. Depending on the chemical structure and composition of the mesogens, heating, ultraviolet (UV) irradiation or solvent swelling can initiate the phase transition of a stimuli-responsive LCE.[6,64,78,215,242–244] The shape change of an oriented LCE as a response to an external stimulus offers the possibility for its application as actuators, sensors or microelectromechanical systems (MEMS). Recent developments of utilizing the actuating properties of LCEs in technical applications range from a bioinspired iris-like tunable aperture and flow-controlling microvalves to light-driven plastic motors.[94,97,245]

The prerequisite for a macroscopic deformation of LCEs during a phase transition is an overall orientation of the mesogens along a common director, which leads to uniformly aligned liquid crystalline domains over the whole sample. Different orientation techniques are well established for the preparation of different LCE-based materials, such as mechanical stretching, electric or magnetic fields and surface forces.[57,78,83,208,246] Microfluidic devices offer another promising orientation method for LCEs, in which the orientation process occurs mechanically in the flow field of a moving fluid. A UV-initiated on-the-fly synthesis of strongly actuating LCE microparticles with a nar-

row size distribution using a capillary-based microfluidic setup has been developed for different polymeric compositions of LCEs.[6,65,133] LCE actuators of various morphologies, such as spherical-, oblate- or rod-like-shaped particles, Janus particles, core-shell particles and actuating fibers are accessible.[3,65,133] These architectures can be synthesized in a wide range of different sizes, combined with a fast production speed within the range of several minutes, as the orientation process, the polymerization and the crosslinking occur in one step. Furthermore, the precise control of the microfluidic setup parameters enables different director fields of the LCE orientation, which features different actuation patterns and geometries.[65] Similar microfluidic setups have been used to produce different kinds of microparticles from various polymeric materials.[7,118,119]

The investigation and improvement of LCE materials in terms of their shape-changing properties (such as the magnitude of actuation, temperature range and reversibility) are still important for the development and optimization of new actuator applications. Especially main-chain elastomers are very attractive as actuators with regard to the strong coupling of the mesogens with the polymer backbone. Common synthetic pathways for main-chain LCEs are the crosslinking of liquid crystalline (LC) main-chain polymers prepared by polycondensation and poly-addition reactions. For such LCEs, contractions of up to 500 % have been reported.[54,62] However, the long reaction times needed for their synthesis represent a limiting factor for some orientation techniques, such as microfluidic devices, in which the polymerization and crosslinking process is typically initiated by UV-induced radical formation. Thiol-ene click chemistry provides an alternative synthesis route for main-chain LCEs.[35] The radical initiated addition of thiol groups to double bonds features the necessary reaction speed for fast processing in microfluidic devices. Such thiol-ene–mediated polymerizations have been used successfully for the preparation of linear polymers and — in one case — for actuating main-chain LCEs.[37,66]

In this article, the synthesis of main-chain LCE microactuators is presented, which is based on thiol-ene click reactions. Previous works by Fleischmann *et al.* already demonstrated the possibility of producing actuating particles in a microfluidic device from a monomer mixture, which contained a bifunctional liquid crystalline thiol-ene monomer and two non-mesogenic crosslinkers.[247] However, the relative length changes of these actuators during the phase transition reached merely 25 %. Moreover, the liquid crystalline phase was unstable with regard to heating and a solvent had to be added in order to reduce the monomer mixture's viscosity for the microfluidic processing. The main challenge of this study was therefore to investigate, if a recently described monomer system for the preparation of main-chain LCEs can be adopted for microfluidic procedures and

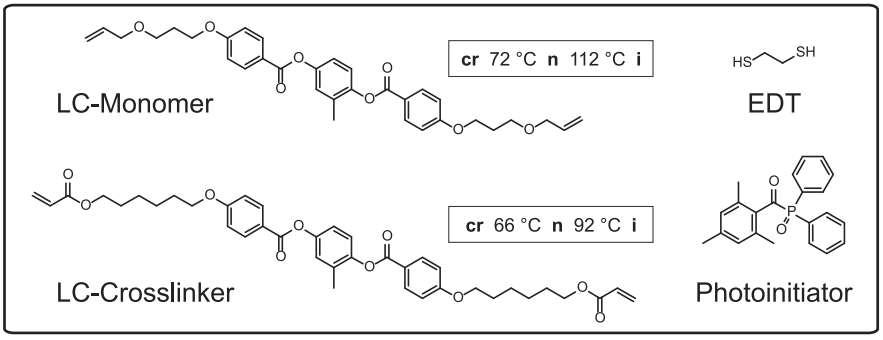

Figure 7.1 Chemical structures of the components, which were used in the liquid crystalline monomer mixture. The phase transition temperatures of the mesogenic LC-monomer and LC-crosslinker were measured via differential scanning calorimetry. (EDT: 1,2-ethanedithiol).

used successfully for the production of strongly actuating microparticles. Thus, a monomer mixture containing a liquid crystalline diacrylate crosslinker in addition to a diallyl and a dithiol monomer is used for the first time in microfluidics. It has been presented recently by White *et al.* for the preparation of programmed shape-changing LCE films.[66] By precise adjustment of the microfluidic setup, this monomer mixture provides a stable nematic phase during the polymerization process, yielding strongly actuating microactuators with changes of the particles' aspect ratio almost up to 100 % during the phase transition. Furthermore, the temperature range as well as the magnitude of the actuation process can be controlled by variation of the monomer mixture's composition, featuring a microfluidic particle synthesis that provides microactuators with variable actuating properties.

7.3 RESULTS AND DISCUSSION

7.3.1 *Liquid Crystalline Monomer Mixture*

For the synthesis of actuating LCE particles, a liquid crystalline monomer mixture was used, which was utilized for the preparation of cast films by White *et al.*[66] Figure 7.1 illustrates the components of the LC-monomer mixture. The amount of the diacrylate LC-crosslinker was varied in the range of 20 mol% to 60 mol% with respect to the LC-monomer amount. The LC-monomer and the LC-crosslinker were synthesized in our laboratory and the phase behavior was characterized by differential scanning calorimetry (DSC), in which a nematic phase of the LC-monomer (crystalline 72 °C nematic 112 °C isotropic) and a nematic phase of the LC-crosslinker (crystalline 66 °C nematic 92 °C isotropic) were observed. The mesomorphic phase behavior of the LC-monomer mixture depends on the molar parts of the LC-

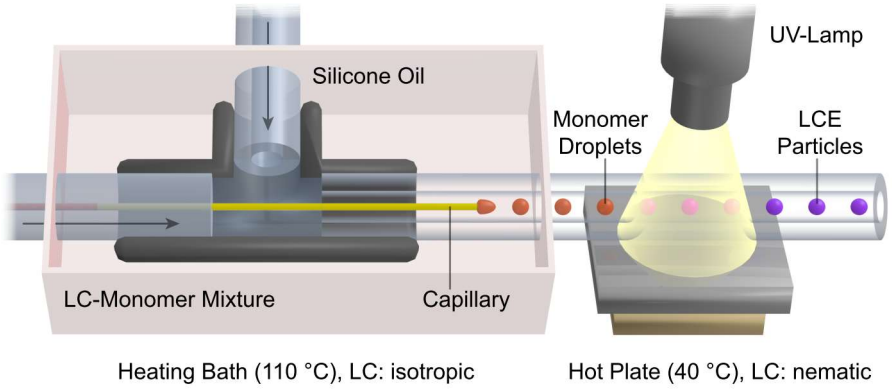

Figure 7.2 Schematic illustration of the co-flow microfluidic setup. The capillary displayed in yellow is connected to the PTFE tube on the left side of the T-junction and provides the liquid crystalline monomer mixture. The continuous silicone oil phase is injected into the T-junction via the PTFE tube on the upper side. Monomer droplets are formed at the capillary's tip and further polymerized by transportation through UV-light.

crosslinker moiety. A nematic phase with clearing temperatures in the range of 60 °C to 83 °C (at molar parts of the LC-crosslinker from 20 mol% to 60 mol%) occurs by cooling down the monomer mixture from the isotropic phase.[66]

7.3.2 *Microfluidic Preparation*

Actuating LCE particles should be fabricated in a co-flow microfluidic reactor. A schematic illustration of the microreactor and the droplet formation and polymerization process are displayed in Figure 7.2.

The basic principle of the microfluidic particle synthesis is the dispersion of a liquid monomer mixture (dispersed phase) in a continuously flowing, highly viscous silicone oil (continuous phase). The droplet formation occurs at the tip of a thin glass capillary, which is placed in the middle of a poly(tetrafluoroethylene) (PTFE) tube (polymerization tube). The monomer mixture is pumped through the glass capillary and the surrounding continuous flow of the silicone oil causes a shear strain on the developing monomer droplets. Depending on the flow velocity of the continuous phase, monomer droplets of a well-defined size are ripped off and the continuous formation of monodispersed droplets becomes accessible by the so-called dripping mode. The polymerization and crosslinking process is initiated thereafter by intensive UV-irradiation during the transportation of the monomer droplets in the polymerization tube.

To ensure a low viscosity and a sufficient fluidity of the LC-monomer mixture during the injection through the thin glass capillary, the droplet formation was carried out in the isotropic state of the monomer mixture. Therefore, the T-junction and the first part of the polymerization tube were tempered in a heating bath at 110 °C. How-

ever, the polymerization of the LC-monomer droplets was carried out in the liquid crystalline state of the monomer mixture, which enabled the formation of a preferred director orientation of the mesogens during the polymerization. For this reason, the monomer droplets were cooled down from the isotropic state to the nematic phase by transportation over a hot plate at 40 °C, at which the UV-initiation of the radical polymerization was carried out. Syringe pumps were connected to the microreactor via PTFE microtubes to allow the continuous injection of both the silicone oil and the LC-monomer mixture.

The size of the dispersed LC-monomer droplets and consequently the size of the LCE particles can be controlled by adjusting the ratio of the continuous phase's flow rate to the dispersed phase's flow rate. All LCE particles were synthesized at a constant flow rate of the LC-monomer mixture of $0.05\,\mathrm{mL\,h^{-1}}$. Due to the low *Reynold* numbers occurring under the microfluidic conditions in the presented microreactor, laminar flow can be expected to be valid for the LCE particle syntheses.[64]

7.3.3 *Adjustment of the Microfluidic Conditions*

Previous studies on microfluidic syntheses of actuating LCE particles showed a strong impact of the microfluidic conditions on the particles' morphology and shape-changing behavior.[65] To investigate the proper adjustment of the microfluidic conditions, the flow rate of the continuous phase was varied to different values. This should lead to conditions, at which the actuation properties of the particles exhibit a maximum relative length change and the highest change of the aspect ratio.

Table 7.1 summarizes the properties of LCE particles, which were synthesized at three different flow rates of the continuous phase, while the crosslinker amount was kept constant at 40 mol%. The calculated values of the particles' diameter, relative length change and aspect ratio derive from the analysis of at least 15 LCE particles, which were synthesized under equal microfluidic conditions. As expected, the averaged diameter of the LCE particles decreases at higher flow rates of the continuous phase, which is due to the increasing shear rate acting on the droplets at the tip of the capillary. Furthermore, the rapidly produced LCE particles exhibit monodispersity at the three different adjusted flow rates, which means the coefficient of variation of the particles' diameter is below 5 %.

The relative length changes of the particles' main axis during the phase transition and the aspect ratio of the particles at 30 °C and 250 °C are also listed in Table 7.1 for different flow rates of the continuous phase during the polymerization. The particles produced at $1.9\,\mathrm{mL\,h^{-1}}$ feature the strongest relative length change as well as the highest increase of the aspect ratio during the phase transition. This

Table 7.1 Properties of liquid crystalline elastomer particles synthesized at different flow rates of the continuous phase. The diameter is averaged over the particles' long and short axis at room temperature. The relative length change describes the ratio of a particle's main axis in the actuated and the non-actuated state. The aspect ratio is defined as a particle's main axis divided by the axis perpendicular to the main axis.

Flow rate [mL h^{-1}]	Diameter [µm]	CV[1] [%]	Relative length change	Aspect ratio (30 °C)	Aspect ratio (250 °C)
1.5	373.9	4.1	1.360	1.05	1.57
1.9	355.4	3.7	1.483	0.96	1.60
2.3	343.2	4.3	1.402	1.07	1.64

[1]CV derived from the averaged diameter measurements of at least 15 particles.

suggests a better orientation of the liquid crystalline director field of the LCE. At lower flow rates (1.5 mL h^{-1}) the minor amount of shear applied on the monomer droplets during the polymerization is assumed to cause less efficient alignment of the mesogens, which leads to a decrease of the actuation properties. On the other side, higher flow rates reduce the UV-irradiation time in the nematic state of the LC-monomer droplets, since the distance of irradiation inside the polymerization tube remains constant (7 cm). This may have caused an incomplete initiation of the polymerization, a minor conversion of the LC-monomers and/or small amounts of residual non-mesogenic 1,2-ethanedithiol (EDT), which explains the slight decrease of the particles' relative length changes at flow rates of 2.3 mL h^{-1} compared to the particles produced at 1.9 mL h^{-1}.

For this reason, the following particle syntheses were carried out at the medium flow rate of 1.9 mL h^{-1}, to ensure both a sufficient UV-irradiation and initiation time and high shear rates acting on the droplets during the polymerization. This consequently represents the microfluidic adjustment, which features the optimized actuation properties of the LCE particles.

7.3.4 *Actuation Properties of Liquid Crystalline Elastomer Particles*

The actuation properties of the LCE particles should be analyzed in terms of the geometry and the magnitude of the shape change during the phase transition, as well as the reversibility of the actuation process. Therefore, heating experiments of single particles were performed in the temperature range of 30 °C to 250 °C and monitored via polarized optical microscopy (POM).

LCE particles showed a shape transformation from a mostly spherical shape to an elongated rod-like shape, at which a particle expands along its main axis and decreases perpendicular to it. This process can

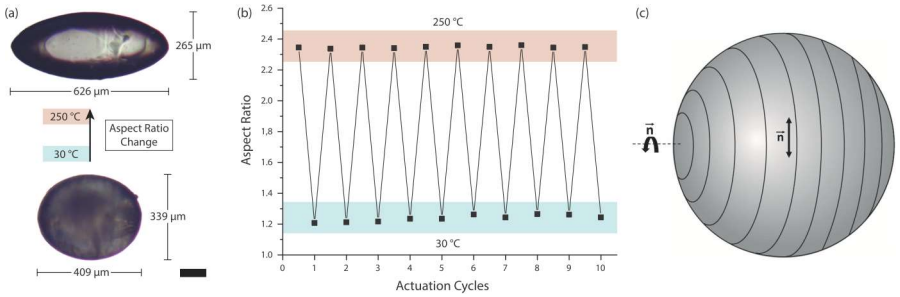

Figure 7.3 (a) Actuation of a single LCE particle before (30 °C, undercooled nematic state) and after (250 °C, isotropic state) the thermal-initiated phase transition. The aspect ratio of the particle is almost doubled during the actuation process. (b) Aspect ratio of the particle at 10 sequent actuation cycles, which demonstrates the overall reversibility of the LCE's shape change. (c) Schematic drawing of the supposed concentric director field within the particle. The director is aligned parallel to the black lines (scale bar: 100 µm).

be watched in a real-time video of an actuating LCE particle, which is placed on a hot stage at 150 °C and cooled down from the isotropic to the undercooled nematic state by cold air streams (real-time videos of the LCE particle actuation are provided in the online supporting information of this publication). This particular actuation pattern has been discovered for LCE particles produced under similar microfluidic conditions before.[65] In this case, a concentric director field orientation (Figure 7.3c) of the calamitic mesogens is reasonable, as the contraction of the LCE occurs parallel and the expansion perpendicular to the director of the mesogens.

Figure 7.3a and b illustrate the actuation process of a single LCE particle, which was synthesized at a flow rate of 1.9 mL h^{-1} for the continuous phase, and a crosslinker content of 20 mol%. At 30 °C, the particle's LCE remains in an undercooled nematic phase, in which slightly colored birefringence can be observed via POM using crossed polarizers. Heating up the LCE particle led to the elongation of the particle's morphology along its main axis and caused an intensification of the colored birefringence, which confirms the nematic state of the LCE. Further heating led to the isotropic state of the LCE at a clearing temperature of 126 °C, at which the particle became completely transparent. Thus, the LC elastomer's nematic-to-isotropic phase transition temperature could be determined as the temperature, at which a loss of birefringence and scattering was observed. At the top of Figure 7.3a, the particle is illustrated in the isotropic state at 250 °C, featuring the maximum actuation and entire transparency.

During the phase transition, the aspect ratio of this particle is almost doubled from roughly 1.2 to 2.4 and the particle's main axis exhibits a relative length change of 53 %. Compared to previously synthesized thiol-ene–based main-chain LCE particles, which featured relative length changes of up to 23 %, the actuation properties of the

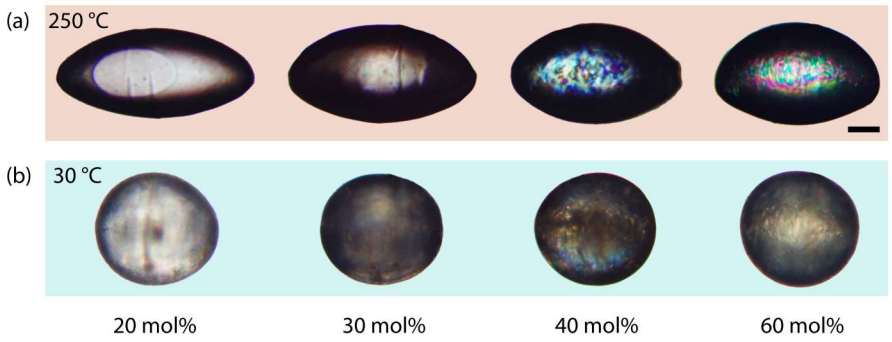

Figure 7.4 Shape transformation of LCE particles in the temperature range of 30 °C (b) and 250 °C (a). The particles contain different amounts of the liquid crystalline diacrylate crosslinker and were synthesized under the same microfluidic conditions (images were taken between crossed polarizers, scale bar: 100 µm).

presented particle show strong improvements with an additional 30 % of relative length change.[247] Furthermore, the actuation process is completely reversible during the cooling process of the particle and can be repeated without a significant change of the actuation pattern. Figure 7.3b demonstrates 10 actuation cycles, at which the particle's aspect ratio was measured alternatively at 30 °C and 250 °C. During these heating cycles, the particle's aspect ratio offers a coefficient of variation of only 0.3 % at high temperatures and 1.7 % at low temperatures. The maximum deviation from the mean value of the particle's aspect ratio reaches 0.5 % at 250 °C and 2.4 % at 30 °C, which confirms the reversibility of a soft actuator.

7.3.5 *LC-Crosslinker influence on the Thermomechanical Properties*

The actuation properties of LCEs and especially the thermomechanical phase behavior depends on the composition of the liquid crystalline monomer mixture. Since a liquid crystalline crosslinking moiety was used for the LCE particle synthesis, the amount of crosslinker is assumed to dictate the mechanical softness of the material as well as the magnitude of the actuation process.[241] As the LC-crosslinker represents a calamitic mesogen by itself, an influence on the liquid crystalline order and the phase behavior is supposed, as well. For this reason, the influence of the crosslinking density on the thermomechanical and actuation properties of the LCE particles should be analyzed.

To investigate the impact of the LC-crosslinker content on the phase behavior of the LCE, the crosslinker amount was varied to four different values (20 mol%, 30 mol%, 40 mol% and 60 mol%), whereas the flow rate of the continuous phase was held constant (1.9 mL h^{-1}) during the syntheses. Figure 7.4 illustrates the shape transformation of LCE particles, which contain different amounts of the LC-crosslinker.

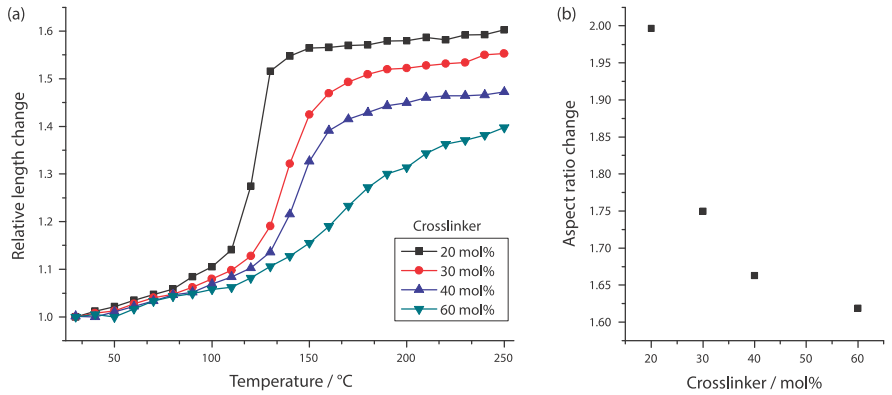

Figure 7.5 (a) Phase behavior of LCE particles, which contain different crosslinker densities. The relative length change along the particles' long axis $l(T)/l(30\,°C)$ is illustrated as a function of temperature. (b) Change of the LCE particles' aspect ratio AR(250 °C)/AR(30 °C) as a function of the crosslinker content.

The particles exhibit an elongation from a spherical to a rod-like shape by increasing the temperature from 30 °C to 250 °C, as described for the particles in Section 7.3.4. The phase transition of the LCE and the actuation process occurs in the temperature range of 125 °C to 220 °C. The relative length changes decrease for an increasing amount of the crosslinking agent. Figure 7.5b displays the change of the LCE particles' aspect ratio as a function of the crosslinker amount, which clearly demonstrates the reduction of the intensity of shape change with increasing crosslinking amounts. As expected, the stiffness of the particles rises for higher crosslinking densities, which restrains the mesogens' mobility of the LCE material and results in a decrease of the actuation ability.[241]

The LCE particles containing 40 mol% and 60 mol% of the LC-crosslinker (top right of Figure 7.4) show retained birefringence at 250 °C, which indicates a change of the phase behavior in dependence of the crosslinker amount. The behavior of the liquid crystalline phase transition was observed by analysis of the macroscopic shape change of the LCE particles, which correlates with the nematic order parameter S.[239] The relative length changes along the main axis of the LCE particles containing different crosslinker densities is illustrated in Figure 7.5a as a function of temperature. For the lowest crosslinker density of 20 mol%, the relative length change occurs in a comparatively narrow temperature range, which suggests the character of a first-order phase transition and a weak nematic ordering for temperatures above the clearing temperature (para-nematic phase), at which the length changes are indeed very low, but still existent. An increase of the crosslinker content to 30 mol% and 40 mol % broadens the temperature range, at which the relative length change and, accordingly, the decrease in the nematic order occurs. A change of the phase tran-

sition's character to a second-order phase transition is assumed. Especially for the particles with a high crosslinker content of 60 mol%, the phase transition is stretched over a wide temperature range and the relative length change is described by a flattening curve, without showing a clear inflection point. The nematic phase is no longer distinguishable from the para-nematic phase.

Two reasons can be assumed to be responsible for the change of the phase behavior with respect to the crosslinking density.[240] Firstly, a high density of the network points immobilizes the nematic order of the mesogens, which consequently prevents the disorganization of the liquid crystalline order even at higher temperatures. Secondly, the liquid crystalline network can be assumed to exhibit a highly inhomogeneous architecture, including parts with high crosslinker densities and parts with fewer network points. Since these diverse areas feature different local clearing temperatures in the LC network, the phase transition of a macroscopic LC sample is broadened.

7.4 CONCLUSIONS

A main-chain liquid crystalline elastomer was used to successfully synthesize strongly actuating microparticles with variable properties of the phase behavior and a narrow size distribution. Thiol-ene click chemistry allowed the UV-initiated polymerization of a liquid crystalline monomer mixture containing a mesogenic diallyl monomer and a mesogenic diacrylate crosslinker. The optimization of a capillary-based co-flow microfluidic device enabled the effective orientation of the liquid crystalline monomer mixture in a concentric director field. This leads to an elongation of the crosslinked LCE particles and a rod-like shape transformation during the thermal-initiated phase transition. Changes of the particle's aspect ratio of almost 100 % are thereby available and the entire reversibility of the LCE's actuation process was demonstrated over several heating and cooling cycles. Furthermore, the modification of the crosslinking density was used to adjust the particle's total length change as well as the LCE's phase behavior, such as the clearing temperature and the temperature range of the phase transition. The produced LCE particles establish the basis for further improvements of the actuation properties as well as structural developments, such as implementations in Janus particles or actuating hybrid materials.

7.5 MATERIALS AND METHODS

7.5.1 *Reagents and Materials*

The liquid crystalline monomer 2-methyl-1,4-phenylenebis(4-(3-(allyloxy)propoxy)benzoate) was synthesized by a standard *Steglich* esteri-

fication of 4-(3-(allyloxy)propoxy)benzoic acid with 2-methylbenzene-1,4-diol.[248] The 4-(3-(allyloxy)propoxy)benzoic acid was synthesized as described in the literature.[249] The liquid crystalline crosslinker 2-methyl-1,4-phenylenebis(4-((6-(acryloyloxy)hexyl)oxy)benzoate) was synthesized by a standard *Steglich* esterification[248] of 4-((6-(acryloyloxy)hexyl)oxy)benzoic acid with 2-methylbenzene-1,4-diol. The 4-((6-(acryloyloxy)hexyl)oxy)benzoic acid was synthesized as described in the literature.[250] The UV-photoinitiator diphenyl-(2,4,6-trimethyl-benzoyl)phosphine oxide (Lucerin TPO), the silicone oil (1000 cSt) and 1,2-ethanedithiol (EDT) were purchased from *Aldrich* (Sigma-Aldrich Chemie GmbH, Taufkirchen, Germany) and used as received.

The liquid crystalline monomer mixture was prepared for the microfluidic synthesis by dissolving equimolar amounts of the LC-monomer and EDT in dichloromethane. Then, 20 mol% to 60 mol% (referring to the LC-monomer) of the LC-crosslinker and 3 wt% of the photoinitiator were added to the solution. After complete solvation, the dichloromethane was removed in a rotary evaporator at 10 mbar for 30 min. The resulting mixture was heated up to 110 °C in a pear shape flask for 10 min. The hot monomer mixture was then drawn in a 1 mL syringe.

7.5.2 *Microfluidic Setup*

The setup of the capillary based co-flow microreactor is illustrated in Figure 7.2.[64,117,135] The 1 mL syringe filled with the LC-monomer mixture was connected to the T-junction (inner diameter: 1.25 mm) by a PTFE microtube (ID: 0.17 mm). A second syringe (12 mL) was filled with the silicone oil (1000 cSt) and joined to the vertical plug of the T-junction via a PTFE microtube (ID: 0.75 mm). The glass capillary (ID: 100 µm, outer diameter: 165 µm) was inserted into the PTFE tube of the monomer mixture. At the opposite plug of the T-junction, the PTFE polymerization tube (ID: 0.75 mm) was placed around the tip of the glass capillary. The T-junction including the glass capillary was placed in an oil bath and tempered to 110 °C. Two syringe pumps (*Harvard Apparatus* Model 33 Twin Syringe Pump, Instech Laboratories, Plymouth Meeting, PA, USA) were used for the continuous injection of the LC-monomer mixture (flow rate: 0.05 mL h^{-1}) and the silicone oil (flow rates: 1.5 mL h^{-1} *to* 2.3 mL h^{-1}). The polymerization tube was passed over a hot plate (40 °C) and 7 cm were irradiated by UV-light using an *Oriel* LSH302 (500 W) lamp equipped with a band filter (323 nm to 385 nm) and a waveguide. At the end of the polymerization tube, LCE particles were collected in a snap-cap bottle.

7.5.3 *Particle Analysis*

The length measurements of the LCE-particles were carried out via POM (*Olympus* BX51, Olympus Deutschland GmbH, Hamburg, Germany) in the temperature range of 30 °C to 250 °C. The heating of the particles was performed on a microscope hot-stage (*Linkam* TMS 94, Linkam Scientific Instruments, Waterfield, Tadworth, UK). Particles were placed on a glass microscope slide, embedded in a silicone oil (1000 cSt) matrix and heated at a heat rate of 30 °C min^{-1}. Thus, it took about 7 min and 20 s to measure one heating curve. Since the LCEs show an immediate response to temperature changes (less than a second), the particle's length was measured during the heating. Particle images were taken under crossed polarizers using a microscope camera (*Olympus* DP22, Olympus Deutschland GmbH, Hamburg, Germany) and analyzed with a microscope imaging software (*Olympus* CellSens Standard V1.15, Olympus Deutschland GmbH, Hamburg, Germany).

ACKNOWLEDGMENTS

The authors acknowledge funding by the German Science Foundation (DFG: Ze 230/24-1).

8

MICROFLUIDIC PREPARATION OF LIQUID CRYSTALLINE ELASTOMER ACTUATORS

Tristan Hessberger, Lukas Braun, Christophe Serra and Rudolf Zentel,
Journal of Visualized Experiments **2018**, *135*, e57715

8.1 ABSTRACT

This paper focuses on the microfluidic process (and it's parameters) to prepare actuating particles from liquid crystalline elastomers (LCEs). The preparation usually consists in the formation of droplets containing low molar mass liquid crystals at elevated temperatures. Subsequently, these particle precursors are oriented in the flow field of the capillary and solidified by a crosslinking polymerization, which produces the final actuating particles. The optimization of the process is necessary to obtain the actuating particles and the proper variation of the process parameters (respective temperature and flow rate) allows variations of size and shape (from oblate to strongly prolate morphologies) as well as the magnitude of actuation. In addition, it is possible to vary the type of actuation from elongation to contraction depending on the director profile induced to the droplets during their flow in the capillary, which again depends on the microfluidic process and its parameters. Furthermore, particles of more complex shapes, such as core-shell structures or Janus-particles, can be prepared by adjusting the setup. By variation of the chemical structure and the mode of crosslinking (solidification) of the liquid crystalline elastomer, it is additionally possible to prepare actuating particles triggered by heat or ultraviolet-visible (UV-VIS) irradiation.

8.2 INTRODUCTION

Microfluidic syntheses have become a well-known method for the fabrication of LCE actuators in the last few years.[4,64,124] This approach not only enables the production of a large number of well actuating particles, but also allows the fabrication of shapes and morphologies, which are not accessible by other methods. Since LCE actuators are promising candidates for an application as artificial muscles in micro robotics, new ways to synthesize such particles are of great importance for this future technology.[251]

In LCEs, the mesogens of a liquid crystal are attached to the polymer chains of an elastomeric network.[70,96,252,253] The linkage of the mesogens to the polymer chain can thereby happen in the form of

a side-chain, a main-chain or a combined LCE-polymer.[69,254,255] The distance between the crosslinking points should be far enough to allow a free reorientation of the polymer chain in between (in fact, this is true for any elastomer and it differentiates them from "thermosets"). Thereby, crosslinking can be permanent or reversible due to strong non-covalent interactions.[63,256,257] This kind of material combines the properties of both, the anisotropic behavior of a liquid crystal with the entropic elasticity of an elastomer. In the temperature range of its liquid crystalline phase, the polymer chains adopt a - more or less - stretched conformation caused by the anisotropy of the liquid crystalline phase, which is quantified by the nematic order parameter. If the sample is heated above the nematic-isotropic phase transition temperature, the anisotropy disappears and the network relaxes to the energetically favored random coil conformation. This leads to a macroscopic deformation and a consequential actuation.[70,258] Beside heating of the sample, this phase transition can also be induced by other stimuli, such as light or solvent diffusion in the LCEs.[5,6,80,259]

In order to obtain a strong deformation, it is necessary that the sample either forms a monodomain or features at least a preferred orientation of the single domain's directors during the crosslinking step.[57] For the production of LCE films, this is often achieved by stretching of a pre-polymerized sample, via orientation of the domains in an electric or magnetic field, with the aid of photo-alignment layers or via 3D-printing.[83,85,86,208,229,231]

A different approach is the continuous preparation of LCE particles with capillary-based microfluidic droplet generators. Liquid crystalline monomer droplets are dispersed in a highly viscous continuous phase, which flows around the droplets and applies a shear rate on the droplets' surface. Therefore, a circulation inside the monomer droplet is observed, which causes an overall alignment of the liquid crystalline phase[65]. Thereby, the magnitude of the shear rates acting on the droplets have a strong influence on both, the droplet's shape and size, as well as the orientation of the liquid crystalline director field. These well oriented droplets can then be polymerized further downstream in the microfluidic setup. Thus, the preparation of actuators with varying shapes – *e.g.* particles and fibers – and more complex morphologies like core-shell and Janus particles is possible.[3,121,133,243] It is even possible to prepare oblate LCE particles, which extend along their symmetry axis and highly prolate, fiber-like particles, which shrink at the phase transition. Both types of particles can be made with the same kind of microfluidic setup, just by variation of the shear rate.[65] Here, we present the protocol of how to produce such LCE actuators of different morphologies in self-manufactured capillary-based microfluidic devices.

Beside the effect of mesogen alignment in LCE droplets and the accessibility of polymers with varying shapes, microfluidic approaches

have further advantages. Compared to other particle fabrication methods, such as precipitation in a non-solvent or suspension polymerization (which lead to particles with a broad size-distribution), monodisperse particles (coefficient of variation of the particle size $<5\,\%$) can be synthesized via microfluidics.[123,260,261] In addition, it is easy to break the sphere symmetry of the droplets by flow. Thus, large particles with a cylindrical symmetry are accessible, which are needed for actuators. This is different from LCE-particles made by suspension polymerization.[260] Furthermore, the particle size is well adjustable by microfluidics in a range from several micrometers to hundreds of microns and additives can easily be brought into the particles or at their surface. This is why microfluidic particle preparation is often used in topics like drug delivery[262] or the manufacturing of cosmetics.[262]

The microfluidic setups used in this article were introduced by Serra *et al.*[116,123,263] These are self-manufactured and consist of high performance liquid chromatography (HPLC) poly(tetrafluoroethylene) (PTFE) tubes and T-junctions, as well as fused silica capillaries which provide the single phases. Thus, the setup can easily be modified, and single parts can simply be exchanged as they are commercially available. A photo initiator is added to the monomer mixtures, which enables the use of an appropriate light source to induce the polymerization of the droplets on-the-fly, after they left the capillary. Irradiation aside from the capillaries is necessary to prevent clogging of the setup. Other types of polymerization can be found in the literature to only start the polymerization after the droplet has left the capillary - *e.g.* with initiators based on redox processes.[7] However, due to the quickness of the photo-induced crosslinking polymerization and the ability to be remotely controlled, photo initiation is the most advantageous one.

Since the LCE's monomer mixture is crystalline at room temperature, a careful temperature control of the whole microfluidic setup is necessary. Therefore, the part of the setup in which the droplet formation occurs is placed in a water bath. Here, the droplets are formed at high temperatures in the isotropic melt of the mixture. For the orientation, the droplets must be cooled into the liquid crystalline phase. Therefore, the polymerization tube is placed on a hot plate, which is set to the lower temperature range of the LCE-phase (Figure 8.1).

Here, we describe a flexible and straightforward method for the fabrication of LCE actuators in flow. This protocol provides the steps required to build the microfluidic setup for the synthesis of single particles, as well as Janus and core-shell particles within a few minutes. Next, we describe how to run a synthesis and show the typical outcome as well as properties of the actuating particles. Finally, we discuss the advantages of this method and why we think it might bring progress to the field of LCE actuators.

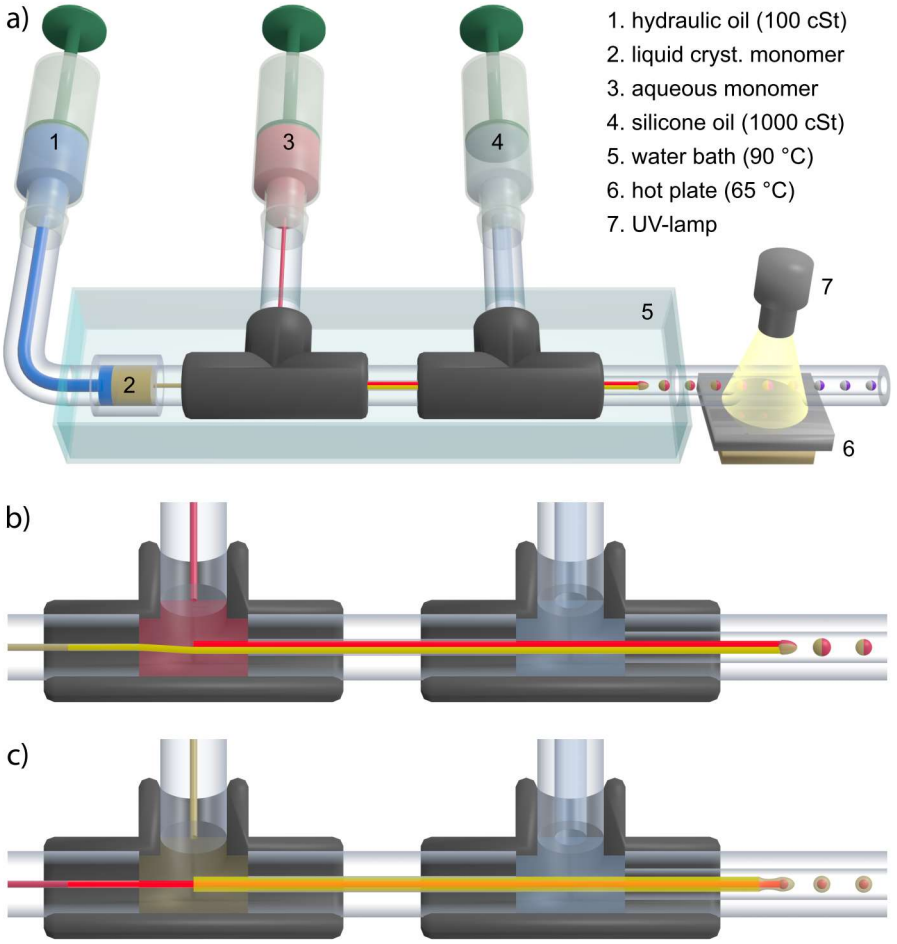

Figure 8.1 Microfluidic setups: a) The general setup includes three syringes, which contain the hydraulic silicone oil (1), the aqueous monomer mixture (3) and the continuous phase silicone oil (4). The liquid crystalline monomer mixture (2) is placed inside the water bath (5) at 90 °C, which heats up the liquid crystal to the isotropic state. The droplet's polymerization is initiated on the hot plate (6) at 65 °C in the nematic state of the liquid crystal by UV-irradiation (7). The single particle setup equals the general setup, except for the second capillary, syringe (3) and the second T-junction. Setup b) contains two capillaries side-by-side to each other, which allows the Janus droplet formation. The core-shell setup c) is composed of a capillary, which is telescoped into a broader second capillary.

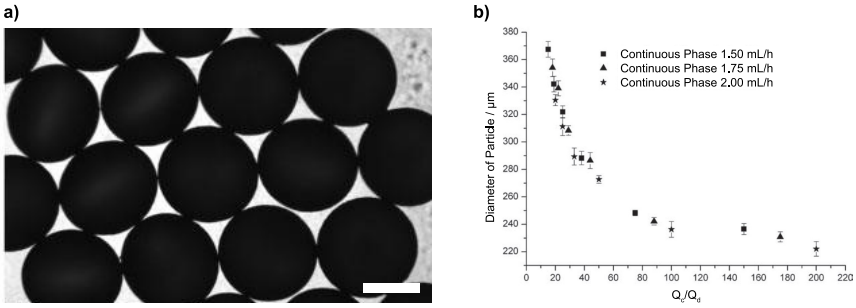

Figure 8.2 Representative particles obtained in the microfluidic single particle setup. a) Microscopy image of monodisperse LCE particles prepared in the microfluidic single particle setup. Scale bar is 200 µm. b) Dependence of the particles' diameter with respect to the ratio of the oil's flow rate (Q_c) to the monomer mixture's flow rate (Q_d). The size of the obtained particles is only dependent on the velocity ratio of both phases but not their absolute values. (This figure has been modified from previous publications[64,132])

8.3 REPRESENTATIVE RESULTS

In this protocol, we present the synthesis of LCE particles with different morphologies via a microfluidic approach. The microfluidic setups for the fabrication of single, core-shell and Janus particles are shown in Figure 8.1.[3,55,116] One advantage of the continuous flow production is the excellent control over both, size and shape of the particles. Figure 8.2a illustrates the advantage of the single droplet setup: narrow size distribution with all particles having the same shape.[55] Hereby, the size of the spheres can easily be adjusted by changing the ratio of flow rates of the different phases. Following the protocol, particle diameters between 200 µm and 400 µm can be produced in a well-controlled manner by choosing flow rate ratios shown in Figure 8.2b[64]. Best results are obtained for flow rates of the continuous phase (Q_c) between 1.5 mL h^{-1} and 2.0 mL h^{-1} and flow rate ratios of Q_c/Q_d (Q_d = flow rate of the monomer phase) between 20 and 200. For flow rates of $Q_c = 1.75\,\mathrm{mL\,h^{-1}}$ and $Q_d = 0.35\,\mathrm{mL\,h^{-1}}$, well actuating particles with a diameter of 270 µm are observed for example. If higher ratios Q_c/Q_d are selected, the droplet formation is less controlled and the particles' size distribution becomes much broader. For lower ratios, the particles are not spherical anymore. In addition to the flow rate adjustments, the distance of the UV-lamp to the polymerization tube as well as the position between the left and the right end of the precision hot plate can change the actuation properties of LCE particles, which happens for example if the polymerization kinetics change by reason of choosing monomer mixture compositions or applied polymerization temperatures different from our described values.

Figure 8.3a shows an actuating particle, which elongates up to 70 % when it is heated above its phase transition temperature. This proves.

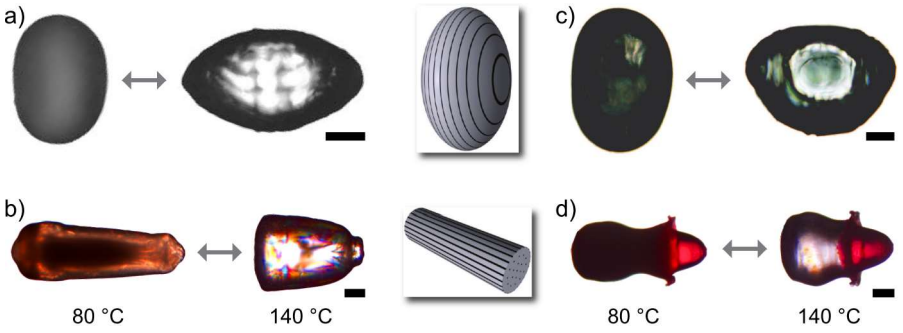

Figure 8.3 Optical microscopy images of four different particle morphologies in the nematic state (at 80 °C) and after phase transition in the isotropic state (at 140 °C). a) Elongation of an oblate shaped LCE-particle (concentric director field), b) contraction of a rod-like shaped LCE-particle (bipolar director field), c) elongation of an oblate shaped core-shell particle, d) contraction of a prolate shaped Janus particle (left part: LCE, right part: acrylamide hydrogel). (scale bars: 100 µm)

that the requirement of inducing an orientation of the liquid crystalline director before polymerization is fulfilled. This alignment of the mesogens results from the shear between the highly viscous continuous phase and the monomer droplets' surface. If silicon oils of lower viscosity are used, the particle's actuation is reduced.

Furthermore, the microfluidic device allows the control over different kinds of actuation patterns, such as elongation or contraction during the phase transition, by variation of the shear rate acting on the droplets during the polymerization. This can be processed easily at constant flow rates of the continuous phase by using different inner diameters of the polymerization tube. Figure 8.3a shows a prolate shaped particle, which elongates along its rotational axis and was synthesized at lower shear rates in a broader polymerization tube (inner diameter (ID): 0.75 mm). The liquid crystalline molecules (mesogens) are aligned along a concentric director field in this case. On the other side, rod-like particles (as illustrated in Figure 8.3b) feature a contraction during the phase transition and a bipolar alignment of the mesogens' director field. This particle was produced at higher shear rates in a thinner polymerization tube (ID: 0.5 mm).

The protocol describes another advantage of the microfluidic process. Beside single particles, samples of more complex morphologies can also be synthesized. Figure 8.3c shows an actuating core-shell particle and Figure 8.3d illustrates a Janus particle, which both were produced following part 2 and 3 of the protocol.[3,133]

If all steps of the protocol are done correctly, particles with properties shown in Figure 8.4 should be obtained.[4,132] In Figure 8.4a the heating and cooling curves are plotted for single particles, which are synthesized at different flow rates. By heating the particle from room temperature, the liquid crystalline order is – at first – slightly reduced,

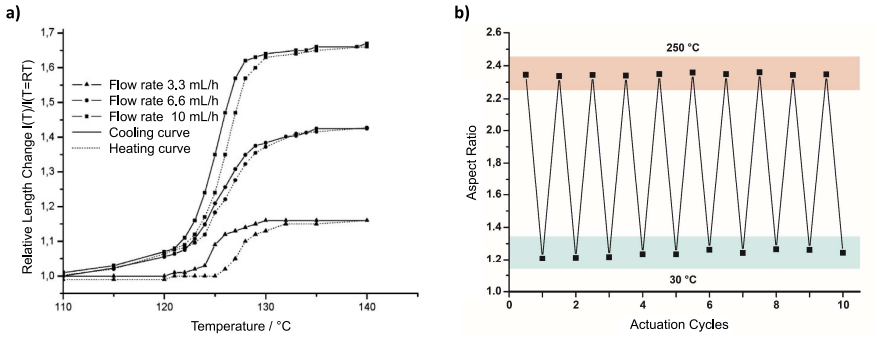

Figure 8.4 Actuation properties of representative single particles. a) Heating and cooling curves of LCE particles prepared in the single particle microfluidic setup at different flow rates for the continuous phase. The particles prepared at the highest flow rate show the strongest actuation (about 70 %) and both curves form a hysteresis, respectively. b) Plot of 10 actuation cycles of LCE particles showing no decrease of the actuation over the cycle number. This proofs, that the particles are crosslinked, and the actuation is completely reversible. Note: This graph was drawn for a particle made from a main-chain LCE system, but looks the same for the LCE system used in this article. (This figure has been modified from a previous publication[132])

which results in a small deformation of the particle. However, close to the phase transition temperature, all orientation is lost immediately and the particle shows a strong elongation just by heating it up for a few degrees. By cooling down the particle, a hysteresis can be observed, and the original shape is obtained. This process is reversible over many actuation cycles as shown in Figure 8.4b.

8.4 DISCUSSION

We have described the fabrication of particles with different morphologies via a microfluidic approach to produce LCE micro actuators. For this purpose, capillary based microfluidic setups were built, which allow droplet formation followed by photo polymerization at defined temperatures.

Here, one critical aspect of a successful synthesis is the correct mounting of the setup. All connections between the single parts must be fixed properly to prevent leaking of the liquids and the device must be clean before every synthesis, to prevent clogging. It is also crucial, that the experiment is performed under UV-free conditions since otherwise premature polymerization of the monomer mixture and consequential clogging of the setup would be the result.

To this day, our approach is the only microfluidic method, which is able to produce strongly actuating LCE particles. Hereby, the microfluidic process fulfills two requirements at the same time. Beside the fabrication of a multitude of equally sized micro objects, an orien-

tation of the liquid crystalline director is induced in these particles. In addition, it is a quite simple procedure, since a large number of actuators can be synthesized in a single step. Applying other methods, the orientation of the mesogens usually requires an additional step, such as stretching of the sample or the application of photo alignment layers. Additionally, these processes are manual, which means the production of many actuators is very time consuming. Furthermore, the LCE morphology is - in most cases - limited to polymer films. Drawbacks of the microfluidic approach are the limitation of the particle size (as the diameter is restricted to values between 200 µm and 400 µm), the vulnerability of clogging the capillary and the necessity of UV-free conditions during the particle preparation in the setup.

On-chip systems are often used for microfluidic particle fabrications, since they can easily be produced and are made out of just one piece. These setups, however, not only lack the necessary adjustability of different temperatures during the flow, but also are not flexible enough to easily exchange clogged or broken parts of the microreactor. Hence, the capillary-based setups we use are more suitable for the synthesis of LCE actuators as they fulfill the crucial requirements.

Aside from our presented results of actuating Janus-particles and core-shell micropumps, more complex actuating particles featuring new properties could be synthesized in the future and open new possibilities for soft actuator applications. The further modification of Janus-particles to a multi-responsive particle is already in progress. Therefore, the introduction of a second temperature responsive polymer beside the actuating LCE is aimed. Further possibilities for new particle designs can also arise from the use of liquid crystalline azobenzene-monomers, which results in light-driven actuation of LCE particles.[4,259] In that case, one can think of Janus particles containing both, a temperature responsive as well as a photo actuating part. The synthesis of light-driven core-shell particles or pipe-like structures offer another possible particle design, which would lead to photo-responsive micropumps. The modification of our presented basic microfluidic procedures should allow a variety of new actuators.

8.5 PROTOCOL

Synthesis of single actuating LCE particles

1.1 Mounting of the device

(All materials used for the microfluidic setup are HPLC supply and commercially available.)

1.1.1 Equip a glass water bath dish (diameter (d): 190 mm, connections: two 29/24 ground glass joints flange-mounted) with two

septa. Broach both septa with an awl to fit a tube with an outer diameter (OD) of 1/16 inch through the opening hole.

1.1.2 Attach a fitting for 1/16 inch OD tubing and the corresponding ferrule to the end of a PTFE tube (tube 1.1: OD: 1/16 inch, ID: 0.17 mm, length (L): 5 cm) and stick the tip (ca. 1 cm) of a polyimide-coated silica capillary (ID: 100 µm, OD: 165 µm, L: 7 cm) into it.

1.1.3 Screw the tube onto one of the opposing arms of a poly(ether-etherketone) (PEEK) T-junction for 1/16 inch OD tubes, which is mounted on a small metal table. Now the capillary should protrude a few centimeters out of the T-junction.

(PTFE tubes are best cut with the aid of a tube cutter and for the capillaries a cleaving stone is best to use.)

1.1.4 Attach a suitable fitting and ferrule to the end of a second PTFE tube (tube 1.2: OD: 1/16 inch, ID: 0.75 mm), which is long enough to reach a syringe pump outside the water bath, and screw it onto the lateral arm of the T-junction.

1.1.5 Stick a third PTFE tube (tube 1.3: OD: 1/16 inch, ID: 0.17 mm) through one of the septa. Tube 1.3 should be long enough to connect a second syringe pump with tube 1.1 inside the water bath. Add two female luer-locks for 1/16 inch OD tubing to the spare end of the tubes 1.1 and 1.3, respectively.

1.1.6 Prepare a fourth PTFE tube (polymerization tube 1.4: OD: 1/16 inch, ID: 0.75 mm) with a fitting plus ferrule and stick it through the second septum. Tube 1.4 should be long enough to leave the water bath and pass a precision heating plate. Connect the tube 1.4 via its fitting to the remaining arm of the T-junction and place the end of the glass capillary inside the tube.

1.1.7 Put the water bath on a hotplate equipped with a thermometer, use adhesive tape to fix tube 1.4 on top of the precision heating plate and attach a 5 mL glass vial to the end of the tube 1.4. Connect the end of tube 1.2 to a syringe filled with the continuous phase (silicone oil, viscosity: 1000 cSt), connect tube 1.3 to a syringe filled with the hydraulic oil for the monomer phase (silicone oil, viscosity: 100 cSt) and plug both syringes in a syringe pump.

(In order to connect the tubes to the syringes, barb to female luer-lock connectors for use with 3/32 inch ID tubes are best-used.)

1.1.8 Install a stereomicroscope with the focus being set on the capillary's tip to enable the observation of the droplet formation and mount a UV-light source (e.g., a 500 W mercury vapor lamp) with the light cone focused on tube 1.4.

1.2 Preparation of the monomer mixture

1.2.1 To prepare the monomer mixture,[55] add 200 mg of (4″-acryloyloxybutyl)-2,5-di-(4′-butyloxybenzoyloxy) benzoate to a 50 mL pear shaped flask.

1.2.2 Add 7.2 mg of 1,6-hexanediol dimethacrylate (10 mol%) and 6.2 mg of (2,4,6-trimethylbenzoyl) phenylphosphinate (photoinitiator, 3 wt%) to the flask. Dissolve the mixture in about 1 mL of dichloromethane.

(Starting from step 1.2.2., all steps should be performed under UV light-free conditions – *e.g.* under yellow light.)

1.2.3 Remove the solvent completely under vacuum at 40 °C and melt the residual solid at 80 °C in an oil bath.

1.2.4 Prepare a syringe with a barb to female luer-lock connector for use with 3/32 inch ID tubing and attach a PTFE tube (tube 1.5, OD: 1/8 inch, ID: 1.65 mm) via an additional connecting tube (OD: 1/16 inch, ID: 0.75 mm). Draw up the monomer mixture into the tube 1.5 with the aid of the syringe.

(The amount of monomer shouldn't be less than 70 mg since otherwise it becomes very difficult to draw enough monomer mixture into the tube 1.5. The protocol can be paused here. If so, store the tube in a refrigerator.)

1.3 Preparation of the particles

1.3.1 Attach a male luer-lock for 1/8 inch OD tubing to both ends of the tube 1.5 containing the monomer mixture. Afterwards, connect both ends of tube 1.5 with the female luer-locks on the ends of the tubes 1.1 and 1.3.

(The tubes should be rinsed with the liquids provided by the syringe pumps prior to the synthesis.)

1.3.2 Set the water bath's temperature to 90 °C and set the precision heating plate's temperature to 65 °C.

1.3.3 Make sure the capillary's tip is in the center of the polymerization tube 1.5 and doesn't touch the wall.

(The temperatures given here are optimized for this monomer mixture. In general, the water bath's temperature should be high enough to melt the monomer mixture and the heating plate's temperature should be in the temperature range of the liquid crystalline phase.)

1.3.4 After the monomer mixture is melted, set the flow rate of the continuous phase (Q_c) to a value between 1.5 mL h^{-1} and 2.0 mL h^{-1} and choose flow rate ratios of Q_c/Q_d (Q_d = flow rate of the hydraulic oil/monomer phase) between 20 and 200.

(For flow rates of $Q_c = 1.75\,\text{mL}\,\text{h}^{-1}$ and $Q_d = 0.35\,\text{mL}\,\text{h}^{-1}$, well actuating particles with a diameter of 270 µm are observed for example.)

1.3.5 After the droplet formation begins, wait until the droplets are all the same size before switching on the UV-light. For the described monomer mixture, position the UV-source 1 cm above the polymerization tube 1.4 at the right end of the precision heating plate. Collect the different fractions of the polymerized particles in the 5 mL glass vial at the end of tube 1.4. While flowing under the UV-light, the droplets' color should change from transparent to white.

(Caution: Better wear UV-protection goggles)

1.3.6 Put a shield - *e.g.* a paper box - between the light source and the water bath, in order to prevent clogging of the capillary.

(In case of a clogging polymerization tube, it might help to heat the clogged part with a heat gun.)

1.3.7 After all monomer is consumed, clean the setup by injecting acetone into tube 1.3.

Synthesis of Core-shell LCE particles

2.1 Mounting of the device

2.1.1 Follow step 1.1.1.

2.1.2 Attach a fitting and ferrule to both ends of a fluorinated ethylene propylene (FEP) tubing sleeve (ID: 395 µm, OD: 1/16 inch, L: 1.55 inch), respectively. First, stick a fused silica capillary (ID: 280 µm, OD: 360 µm, L: 8 cm) through the sleeve, in such a way that it protrudes about 3 mm out of one side. Then stick a thinner capillary (ID: 100 µm, OD: 165 µm, L: 11 cm) through the bigger one, so that it protrudes a few millimeter out of its longer side.

2.1.3 Screw the sleeve onto one of the opposing arms of a PEEK T-junction for 1/16″ OD tubes (T-junction 1) which is mounted on a small metal table, with the shorter end of the bigger capillary reaching into the T-junction.

2.1.4 Stick a PTFE tube (tube 2.1, OD: 1/16″, ID: 0.17 mm), which is long enough to connect a syringe pump with T-junction 1 through one of the water bath's septa. Attach a fitting and ferrule to the tube's end inside the water bath, connect it to the free lateral arm of T-junction 1 and stick the thinner capillary inside the tube 2.1.

2.1.5 Prepare a second PTFE tube (tube 2.2, OD: 1/16″, ID: 0.5 mm) with a fitting and a ferrule and connect it to the spare arm of T-junction 1. Stick another PTFE tube (tube 2.3, OD: 1/16″, ID: 0.5 mm) through a second hole in the septum next to tube 2.1. Tube 2.3 should be long enough to connect another syringe pump with tube 2.2.

2.1.6 Add two female luer-locks for 1/16″ OD tubing to the free ends of the tubes 2.2 and 2.3 inside the water bath, respectively.

2.1.7 Connect the free end of the sleeve to one of the opposing arms of a second PEEK T-junction (T-junction 2) which is also mounted on the small metal table. Prepare a fourth PTFE tube (tube 2.4, OD: 1/16″, ID: 0.75 mm) with a fitting plus ferrule. Tube 2.4 is long enough to reach a third syringe pump outside the water bath and connect it to the lateral arm of T-junction 2.

2.1.8 Prepare a fifth PTFE tube (polymerization tube 2.5: OD: 1/16″, ID: 0.75 mm) with a fitting plus ferrule and stick it through the other septum. Tube 2.5 should be long enough to leave the water bath and pass a high precision heating plate. Connect the fitting of tube 2.5 with the remaining arm of the T-junction. Now the glass capillaries' tips should be located inside the tube 2.5.

2.1.9 Put the water bath on a hotplate equipped with a thermometer, use adhesive tape to fix tube 2.5 on top of a precision heating plate and attach a 5 mL glass vial to the tube's end. Connect the end of tube 2.1 to a syringe filled with glycerol (inner phase), connect tube 2.3 to a syringe filled with the hydraulic oil for the monomer phase (silicone oil, viscosity: 100 cSt), connect tube 2.4 to a syringe filled with the continuous phase (silicone oil, viscosity: 1000 cSt) and plug all syringes in syringe pumps.

2.1.10 Follow step 1.1.7., but read tube 2.5 instead of tube 1.4.

2.2 Preparation of the monomer mixture

Follow all steps of 1.2.

2.3 Preparation of the core-shell particles

2.3.1 Attach a male luer-lock for 1/8″ OD tubes to both ends of the tube containing the monomer mixture, respectively. Afterwards, connect both ends of this tube with the female luer-locks on the ends of the tubes 2.2 and 2.3.

2.3.2 Follow steps 1.3.2 – 1.3.4.

2.3.3 Observe the droplet formation via a stereo microscope.

Synthesis of Janus LCE particles

3.1 Mounting of the device

3.1.1 Follow step 1.1.1.

3.1.2 Attach a fitting and ferrule to both ends of a FEP tubing sleeve (ID: 395 µm, OD: 1/16″, L: 1.55″), respectively. Stick two parallelly aligned fused silica capillaries (ID: 100 µm, OD: 165 µm, L1: 8 cm, L2: 11 cm) through the sleeve. The short capillary protrudes about 3 mm out of one side of the sleeve, on the other side of the sleeve both capillaries have the same length.

3.1.3 Super-glue the capillaries by putting some glue on one end of the sleeve and wait until it is cured.

3.1.4 Connect two PEEK T-junctions by screwing the sleeve onto one of the opposing arms, respectively, and mount both on a small metal table.

3.1.5 Follow steps 2.1.4. – 2.1.7.

3.1.6 Prepare a fifth PTFE tube (tube 3.5: OD: 1/16″, ID: 0.75 mm, L: 5 cm) with a fitting plus ferrule and connect it with the remaining arm of T-junction 2. Both tips of the glass capillaries are located inside the tube 3.5.

3.1.7 Stick another PTFE tube (tube 3.6: OD: 1/16″, ID: 0.5 mm) through the other septum. Tube 2.6 should be long enough to leave the water bath and pass a precision heating plate. Connect the tubes 3.5 and 3.6 via fitting systems for 1/16″ OD tubing.

3.1.8 Put the water bath on a hot plate, equipped with a thermometer, use adhesive tape to fix tube 3.6 on top of a precision heating plate and attach a 5 mL glass vial to the tube's end. Connect the end of tube 3.1 to a syringe filled with an aqueous monomer mixture (aq. monomer phase), connect tube 3.3 to a syringe filled with the hydraulic oil for the LC-monomer phase (silicone oil, viscosity: 100 cSt), connect tube 3.4 to a syringe filled with the continuous phase (silicone oil, viscosity: 1000 cSt) and plug all syringes in syringe pumps.

3.1.9 Follow step 1.1.7., but read tube 3.6 instead oftube 1.4.

3.2 Preparation of the LCE monomer mixture

Follow all steps of 1.2.

3.3 Preparation of the aqueous monomer mixture

3.3.1 Prepare a solution of 40 wt% acrylamide in distilled water. Add 10 mol% of the crosslinking agent *N,N'*-methylenebis(acrylamide) and 2 wt% of the initiator 2-hydroxy-2-methylpropiophenone to the solution. (Both amounts are with respect to the acrylamide)

(In order to raise the viscosity of the aqueous monomer mixture, polyacrylamide can be added.)

3.3.2 Stir the mixture for 24 h at room temperature (RT) and fill it into a 1 mL syringe, afterward.

3.4 Preparation of the Janus particles

3.4.1 Attach a male luer-lock for 1/8″ OD tubes to both ends of the tube containing the LCE monomer mixture, respectively. Afterwards, connect both ends of this tube with the female luer-locks on the ends of the tubes 3.2 and 3.3.

3.4.2 Follow steps 1.3.2 – 1.3.4.

3.4.3 Observe the droplet formation via a stereo microscope.

Analysis of the particles

4.1 Put the particles on a hot-stage under an optical microscope connected to a computer with imaging software. To analyze the particles' actuation, take pictures at temperatures above and below their phase transition temperature and measure their diameter.

(A drop of silicon oil prevents sticking of the particles on the object slide.)

4.2 To estimate the particles' clearing temperature, determine the temperature at which the particles lose their birefringence via polarized optical microscopy (POM).

ACKNOWLEDGMENTS

The authors thank the German science foundation for funding of this work (Ze 230/ 24-1)

9

CONCLUSIONS AND OUTLOOK

The present thesis deals with the advancement of microfluidicly produced temperature-responsive LCE microactuators. This unique class of soft materials holds great potential for future applications in various technologies, such as artificial muscles, microelectromechanical systems and sensors. For this reason, the further development of innovative and effective preparation methods for strongly shape-changing LCEs as well as the enhancement of functionalities of LCE actuators is of great importance for this area of research. In this work, new preparation methods are developed for the processing of novel liquid crystalline materials in this field and the achievement of LCE actuator morphologies never seen before is reached by restructuring and optimization of capillary based microfluidic devices. Furthermore, the overall goal of the incorporation of synthesized LCE actuators as building blocks into a stimuli-responsive superstructured device is successfully accomplished, which paves the way for new future applications of LCE actuators.

For the first time, this work presents the successful integration of an actuating nematic LCE into the symmetry broken colloidal morphology of Janus microparticles. These Janus particles are prepared in a microfluidic synthesis, which allows the precise control over the particle size and morphology at fast particle production speeds and simultaneous narrow size distributions. These actuating Janus particles reveal very high shape changes at the nematic-isotropic phase transition of the LCE as well as tunable Janus balances and particle shapes. The thermomechanical properties of LCE particles are extensively studied, at which not only the bipolar director field of the LCE is proved via wide-angle X-ray scattering measurements, but also the influence of the two Janus phases' viscosities, interfaces and volumes are intensively analyzed to achieve profound knowledge about the maximization of the LCE shape change.

The attained practical experience and the theoretical understanding about actuating LCE Janus particles is further used to develop multifunctional Janus particles with two different temperature-responsive Janus parts. Therefore, the microfluidic device is precisely adjusted to allow the processing of an LCST hydrogel beside the actuating LCE-part. The obtained Janus particles show strong temperature responses of both materials at different temperatures and solvent environments, at which the LCE-part offers high shape contractions and aspect ratio changes of up to 95 % during the nematic-isotropic phase transition, whereas the hydrogel shows strong volume changes of up to 280 % at

the LCST. By this advanced functionalization of the LCE Janus particles, four different Janus morphologies are remotely addressable by temperature and solvent changes for a single Janus particle, which enables the temperature controlled selection of various morphology related particle properties.

Additional to their unique temperature-responsive abilities, these rod-like Janus microparticles hold additional amphiphilic properties, which allows their self-assembly at water/oil interfaces. This self-assembly capability is intensively studied and further utilized in a specially developed molding process for the functionalization of a hydrogel surface with strongly actuating LCE Janus rods. By this sophisticated technique, the advanced amphiphilic LCE Janus particles are used as building-blocks in densely packed and uniformly aligned monolayers to form an actuating, LCE covered surface device. Various shapes and sizes of these devices are easily accessible by the proper application of the molding process. Furthermore, the detailed thermomechanical studies of different actuating surfaces not only demonstrate an accurate collective response of the LCE rods towards environmental temperature changes, but also the promising possibility of locally addressing selected parts of the LCE functionalized surface, which successfully demonstrates a remotely controlled change of the surface properties in a single region. The temperature-controlled change of the surface properties via temperature-induced phase transitions of the LCE rods allows the imagination of future applications, which would be able to make use of these unique surface properties for self-cleaning abilities, optical changes of interfaces or variable adhesive properties of functional surfaces.

Beside the studies on actuating Janus particles, the present work further demonstrates the great potential for the utilization of new liquid crystalline monomer systems in microfluidic preparation methods for LCE actuators. The successful integration of a main-chain mesogen and a liquid crystalline crosslinker into actuating LCE particles offers new possibilities for the improvement of the shape changing abilities, as well as enhanced adjustment possibilities in the chemical composition for tunable nematic-isotropic phase transitions. In this context, thiol-ene click chemistry is established as an efficient radical polymerization reaction method for the UV-initiated microparticle production in microfluidic devices. Very high shape changes of main-chain LCE particles featuring aspect ratio changes of up to 100 % are achieved and the complete reversibility of the actuation process during temperature induced phase transitions is proved over many actuation cycles. Furthermore, intensive studies regarding the impact of the liquid crystalline crosslinker density on the LCE phase behavior demonstrate the valuable opportunity of matching the phase transition temperature and the relative length changes to the user's individual demands on LCE particle properties by simple variation

of the component ratios of a single monomer system. These findings encourage for further improvements in the field of LCE actuator research and reveal the potential application of tunable LCE particles as components in stimuli-responsive smart composite materials.

As an additional ambition for this dissertation, an overview about the different capillary based microfluidic syntheses for the preparation of various LCE microparticles is compiled. To provide a comprehensive and detailed description of the most relevant practical methods in this field, step-by-step instructions are formulated as a written manual and an associated video tutorial offers many practical advices. In this manner, microfluidic devices for the preparation of homogeneous actuating LCE microparticles with different director fields as well as fabrication methods of sophisticated Janus and core-shell particle morphologies are sufficiently covered. By the disclosure of detailed empirical information, future researchers in the area of LCE actuators will get the opportunity to learn the necessary construction skills for the microfluidic setups as well as hidden tricks for the fabrication of actuating LCE microparticles, which has never been reported in its entirety before.

In conclusion, the present thesis clearly advances the spectrum of functional LCE actuators and furthers the knowledge about microfluidic preparation methods and thermomechanical properties of LCE microparticles. Furthermore, the overall goal of applying the unique stimuli-responsive abilities of advanced LCE microactuators to a macroscopic functional device is successfully achieved. Further developments of the demonstrated approaches will enable the future application of actuating LCE particles in temperature responsive composite materials or functional interfaces with temperature variable surface properties.

Part III

APPENDIX

BIBLIOGRAPHY

[1] T. Hessberger, L. Braun, R. Zentel, *Advanced Functional Materials* **2018**, 1800629 (Early View).

[2] T. Hessberger, L. B. Braun, C. A. Serra, R. Zentel, *Journal of Visualized Experiments* **2018**, *135*, e57715.

[3] T. Hessberger, L. B. Braun, F. Henrich, C. Müller, F. Gießelmann, C. Serra, R. Zentel, *Journal of Materials Chemistry C* **2016**, *4*, 8778–8786.

[4] T. Hessberger, L. Braun, R. Zentel, *Polymers* **2016**, *8*, 410.

[5] L. B. Braun, T. G. Linder, T. Hessberger, R. Zentel, *Polymers* **2016**, *8*, 435.

[6] L. B. Braun, T. Hessberger, R. Zentel, *Journal of Materials Chemistry C* **2016**, *4*, 8670–8678.

[7] L. B. Braun, T. Hessberger, C. A. Serra, R. Zentel, *Macromolecular Reaction Engineering* **2016**, *10*, 611–617.

[8] F. Reinitzer, *Liquid Crystals* **1989**, *5*, 7–18.

[9] O. Lehmann, *Zeitschrift für Physikalische Chemie* **1889**, *4*, 462–472.

[10] T. J. Sluckin, D. A. Dunmur, H. Stegemeyer, *Crystals That Flow: Classic Papers from the History of Liquid Crystals*, Taylor & Francis, London, **2004**, p. 738.

[11] G. H. Brown, W. G. Shaw, *Chemical Reviews* **1957**, *57*, 1049–1157.

[12] D. Demus, J. W. Goodby, G. W. Gray, H. W. Spiess, V. Vill, *Handbook of Liquid Crystals, Fundamentals*, Wiley, **1998**.

[13] P. G. de Gennes, J. Prost, *The Physics of Liquid Crystals*, Edition 2, Oxford University Press, Oxford, **1993**.

[14] S. Chandrasekhar, *Liquid Crystals*, Cambridge University Press, **1992**.

[15] D. Demus, J. W. Goodby, G. W. Gray, H. W. Spiess, V. Vill, *Handbook of Liquid Crystals, Volume 2A: Low Molecular Weight Liquid Crystals I: Calamitic Liquid Crystals*, Wiley, **2011**.

[16] O. V. Kruglova, *Discotic Liquid Crystals: From Dynamics to Conductivity*, IOS Press, **2007**.

[17] I. G. Voigt-Martin, P. Simon, S. Bauer, H. Ringsdorf, *Macromolecules* **1995**, *28*, 236–242.

[18] D. Haristoy, S. Mery, B. Heinrich, L. Mager, J. F. Nicoud, D. Guillon, *Liquid Crystals* **2000**, *27*, 321–328.

[19] H. Stegemeyer, *Topics in Physical Chemistry: Liquid Crystals, Vol. 3*, Steinkopff, Darmstadt, **1994**.

[20] P. J. Collings, M. Hird, *Introduction to Liquid Crystals: Chemistry and Physics*, CRC Press, **2017**.

[21] P. J. Collings, *Liquid Crystals: Nature's Delicate Phase of Matter*, Princeton University Press, **2002**.

[22] S. Singh, D. A. Dunmur, *Liquid Crystals: Fundamentals*, World Scientific, **2002**.

[23] I. Dierking, *Textures of Liquid Crystals*, Wiley, **2006**.

[24] T. N. Ruckmongathan, *Addressing Techniques of Liquid Crystal Displays*, John Wiley & Sons Ltd, Chichester, UK, **2014**.

[25] B. Bahadur, *Liquid Crystals: Applications and Uses*, World Scientific Publishing Company, **1992**.

[26] J. A. Castellano, *Liquid Gold: The Story of Liquid Crystal Displays and the Creation of an Industry*, World Scientific, **2005**.

[27] J. P. Lagerwall, G. Scalia, *Current Applied Physics* **2012**, *12*, 1387–1412.

[28] P. G. de Gennes, *Physics Letters* **1969**, *28A*, 725–727.

[29] V. K. Thakur, M. R. Kessler, *Liquid Crystalline Polymers: Volume 2 - Processing and Applications*, Springer International Publishing, **2015**.

[30] N. A. Platé, *Liquid-Crystal Polymers*, Springer US, **2013**.

[31] D. Coates, *Liquid Crystal Polymers: Synthesis, Properties and Applications*, Rapra Technology, **2000**.

[32] A. M. Donald, A. H. Windle, S. Hanna, *Liquid Crystalline Polymers*, Cambridge University Press, **2006**.

[33] G. Li in *Structure and Properties of High-Performance Fibers*, (Ed.: G. Bhat), Woodhead Publishing Series in Textiles, Woodhead Publishing, Oxford, **2017**, pp. 141–166.

[34] C. M. Yakacki, M. Saed, D. P. Nair, T. Gong, S. M. Reed, C. N. Bowman, *RSC Adv.* **2015**, *5*, 18997–19001.

[35] C. E. Hoyle, C. N. Bowman, *Angewandte Chemie - International Edition* **2010**, *49*, 1540–1573.

[36] N. P. Godman, B. A. Kowalski, A. D. Auguste, H. Koerner, T. J. White, *ACS Macro Letters* **2017**, *6*, 1290–1295.

[37] Y. Hong, A. Buguin, J. M. Taulemesse, K. Kaneko, S. Méry, A. Bergeret, P. Keller, *Journal of the American Chemical Society* **2009**, *131*, 15000–15004.

[38] M. H. Li, P. Auroy, P. Keller, *Liquid Crystals* **2000**, *27*, 1497–1502.

[39] D. Shenoy, S. Filippov, F. Aliev, P. Keller, D. Thomsen, B. Ratna, *Physical Review E - Statistical Physics Plasmas Fluids and Related Interdisciplinary Topics* **2000**, *62*, 8100–8105.

[40] H. Yang, M. X. Liu, Y. W. Yao, P. Y. Tao, B. P. Lin, P. Keller, X. Q. Zhang, Y. Sun, L. X. Guo, *Macromolecules* **2013**, *46*, 3406–3416.

[41] G. R. Mitchell, M. Coulter, F. J. Davis, W. Guo, *Journal de Physique II* **1992**, *2*, 1121–1132.

[42] E. K. Fleischmann, R. Zentel, *Angewandte Chemie - International Edition* **2013**, *52*, 8810–8827.

[43] M. Warner, E. M. Terentjev, *Liquid Crystal Elastomers*, OUP Oxford, **2003**.

[44] W. H. de Jeu, *Liquid Crystal Elastomers: Materials and Applications*, Springer Berlin Heidelberg, **2012**.

[45] M. Brehmer, R. Zentel, *Molecular Crystals and Liquid Crystals Science and Technology. Section A. Molecular Crystals and Liquid Crystals* **2006**, *243*, 353–376.

[46] D. Broer, G. P. Crawford, S. Zumer, *Cross-Linked Liquid Crystalline Systems: From Rigid Polymer Networks to Elastomers*, CRC Press, **2011**.

[47] D. Liu, D. J. Broer, *Langmuir* **2014**, *30*, 13499–13509.

[48] P. G. de Gennes, *C. R. Hebd. Seances Acad. Sci. Ser. B* **1975**, *281*, 101.

[49] M. Chambers, H. Finkelmann, M. Remškar, A. Sánchez-Ferrer, B. Zalar, S. Žumer, *J. Mater. Chem.* **2009**, *19*, 1524–1531.

[50] A. Kaiser, M. Winkler, S. Krause, H. Finkelmann, A. M. Schmidt, *J. Mater. Chem.* **2009**, *19*, 538–543.

[51] L. Yang, K. Setyowati, A. Li, S. Gong, J. Chen, *Advanced Materials* **2008**, *20*, 2271–2275.

[52] S. Petsch, R. Rix, B. Khatri, S. Schuhladen, P. Müller, R. Zentel, H. Zappe, *Sensors and Actuators A: Physical* **2015**, *231*, 44–51.

[53] T. Ikeda, O. Tsutsumi, *Science* **1995**, *268*, 1873–1875.

[54] H. Wermter, H. Finkelmann, *E-Polymers* **2001**, *1*, 111–123.

[55] D. L. Thomsen, P. Keller, J. Naciri, R. Pink, H. Jeon, D. Shenoy, B. R. Ratna, *Macromolecules* **2001**, *34*, 5868–5875.

[56] H. Finkelmann, G. Rehage, *Makromol. Chem. Rapid Commun.* **1980**, *1*, 31–34.

[57] J. Küpfer, H. Finkelmann, *Makromol. Chem. Rapid Commun.* **1991**, *12*, 717–726.

[58] Y. Xia, R. Verduzco, R. H. Grubbs, J. A. Kornfield, *Journal of the American Chemical Society* **2008**, *130*, 1735–1740.

[59] S. Bualek, R. Zentel, *Die Makromolekulare Chemie* **1988**, *189*, 791–796.

[60] S. Krause, R. Dersch, J. H. Wendorff, H. Finkelmann, *Macromolecular Rapid Communications* **2007**, *28*, 2062–2068.

[61] P. Beyer, L. Braun, R. Zentel, *Macromolecular Chemistry and Physics* **2007**, *208*, 2439–2448.

[62] S. V. Ahir, A. R. Tajbakhsh, E. M. Terentjev, *Advanced Functional Materials* **2006**, *16*, 556–560.

[63] R. Zentel, A. Wiesemann, T. Pakula, *Polymer* **1992**, *33*, 5315–5320.

[64] C. Ohm, E. K. Fleischmann, I. Kraus, C. Serra, R. Zentel, *Advanced Functional Materials* **2010**, *20*, 4314–4322.

[65] C. Ohm, N. Kapernaum, D. Nonnenmacher, F. Giesselmann, C. Serra, R. Zentel, *Journal of the American Chemical Society* **2011**, *133*, 5305–5311.

[66] T. H. Ware, Z. P. Perry, C. M. Middleton, S. T. Iacono, T. J. White, *ACS Macro Letters* **2015**, *4*, 942–946.

[67] T. H. Ware, T. J. White, *Polym. Chem.* **2015**, *6*, 4835–4844.

[68] T. J. White, D. J. Broer, *Nature Materials* **2015**, *14*, 1087–1098.

[69] M.-H. Li, P. Keller, *Philosophical Transactions of the Royal Society A: Mathematical Physical and Engineering Sciences* **2006**, *364*, 2763–2777.

[70] C. Ohm, M. Brehmer, R. Zentel, *Advanced Materials* **2010**, *22*, 3366–3387.

[71] R. S. Kularatne, H. Kim, J. M. Boothby, T. H. Ware, *Journal of Polymer Science Part B: Polymer Physics* **2017**, *55*, 395–411.

[72] A. Hotta, E. M. Terentjev, *European Physical Journal E* **2003**, *10*, 291–301.

[73] S. M. Clarke, A. R. Tajbakhsh, E. M. Terentjev, C. Remillat, G. R. Tomlinson, J. R. House, *Journal of Applied Physics* **2001**, *89*, 6530–6535.

[74] S. Dey, D. Agra-Kooijman, W. Ren, P. McMullan, A. Griffin, S. Kumar, *Crystals* **2013**, *3*, 363–390.

[75] S. Krause, F. Zander, G. Bergmann, H. Brandt, H. Wertmer, H. Finkelmann, *Comptes Rendus Chimie* **2009**, *12*, 85–104.

[76] E. Nishikawa, J. Yamamoto, H. Yokoyama, H. Finkelmann, *Macromolecular Rapid Communications* **2004**, *25*, 611–617.

[77] J. Hoogboom, T. Rasing, A. E. Rowan, R. J. M. Nolte, *J. Mater. Chem.* **2006**, *16*, 1305–1314.

[78] T. Ikeda, M. Nakano, Y. Yu, O. Tsutsumi, A. Kanazawa, *Advanced Materials* **2003**, *15*, 201–204.

[79] H. Finkelmann, S. T. Kim, A. Muñoz, P. Palffy-Muhoray, B. Taheri, *Advanced Materials* **2001**, *13*, 1069–1072.

[80] H. Zeng, O. M. Wani, P. Wasylczyk, R. Kaczmarek, A. Priimagi, *Advanced Materials* **2017**, *29*, 1–7.

[81] T. H. Ware, M. E. McConney, J. J. Wie, V. P. Tondiglia, T. J. White, *Science* **2015**, *347*, 982–984.

[82] S. Haseloh, P. van der Schoot, R. Zentel, *Soft Matter* **2010**, *6*, 4112.

[83] M. H. Li, P. Keller, J. Yang, P. A. Albouy, *Advanced Materials* **2004**, *16*, 1922–1925.

[84] S. Petsch, B. Khatri, S. Schuhladen, L. Köbele, R. Rix, R. Zentel, H. Zappe, *Smart Materials and Structures* **2016**, *25*, 1–10.

[85] M. Brehmer, R. Zentel, G. Wagenblast, K. Siemensmeyer, *Macromolecular Chemistry and Physics* **1994**, *195*, 1891–1904.

[86] D. Ditter, W.-L. Chen, A. Best, H. Zappe, K. Koynov, C. K. Ober, R. Zentel, *Journal of Materials Chemistry C* **2017**, *5*, 12635–12644.

[87] A. Komp, J. Rühe, H. Finkelmann, *Macromolecular Rapid Communications* **2005**, *26*, 813–818.

[88] Y. Xia, G. Cedillo-Servin, R. D. Kamien, S. Yang, *Advanced Materials* **2016**, *28*, 9637–9643.

[89] A. Kotikian, R. L. Truby, J. W. Boley, T. J. White, J. A. Lewis, *Advanced Materials* **2018**, *1706164*, 1–6.

[90] A. Buguin, M. H. Li, P. Silberzan, B. Ladoux, P. Keller, *Journal of the American Chemical Society* **2006**, *128*, 1088–1089.

[91] Z. L. Wu, A. Buguin, H. Yang, J. M. Taulemesse, N. Le Moigne, A. Bergeret, X. Wang, P. Keller, *Advanced Functional Materials* **2013**, *23*, 3070–3076.

[92] C. L. Van Oosten, C. W. Bastiaansen, D. J. Broer, *Nature Materials* **2009**, *8*, 677–682.

[93] C. P. Ambulo, J. J. Burroughs, J. M. Boothby, H. Kim, M. R. Shankar, T. H. Ware, *ACS Applied Materials and Interfaces* **2017**, *9*, 37332–37339.

[94] S. Schuhladen, F. Preller, R. Rix, S. Petsch, R. Zentel, H. Zappe, *Advanced materials* **2014**, *26*, 7247–7251.

[95] A. Rešetič, J. Milavec, B. Zupančič, V. Domenici, B. Zalar, *Nature Communications* **2016**, *7*, 13140.

[96] T. Ube, T. Ikeda, *Angewandte Chemie International Edition* **2014**, *53*, 10290–10299.

[97] M. Yamada, M. Kondo, J. I. Mamiya, Y. Yu, M. Kinoshita, C. J. Barrett, T. Ikeda, *Angewandte Chemie - International Edition* **2008**, *47*, 4986–4988.

[98] M. Yamada, M. Kondo, R. Miyasato, Y. Naka, J.-i. Mamiya, M. Kinoshita, A. Shishido, Y. Yu, C. J. Barrett, T. Ikeda, *J. Mater. Chem.* **2009**, *19*, 60–62.

[99] K. Kumar, C. Knie, D. Bléger, M. A. Peletier, H. Friedrich, S. Hecht, D. J. Broer, M. G. Debije, A. P.H. J. Schenning, *Nature Communications* **2016**, *7*, 11975.

[100] P. Tabeling, S. Chen, *Introduction to Microfluidics*, OUP Oxford, **2010**.

[101] N. T. Nguyen, S. T. Wereley, *Fundamentals and Applications of Microfluidics*, Artech House, **2002**.

[102] P. S. Dittrich, A. Manz, *Nature Reviews Drug Discovery* **2006**, *5*, 210–218.

[103] E. K. Sackmann, A. L. Fulton, D. J. Beebe, *Nature* **2014**, *507*, 181–189.

[104] S. Haeberle, R. Zengerle, *Lab on a Chip* **2007**, *7*, 1094–1110.

[105] D. Mark, S. Haeberle, G. Roth, F. Von Stetten, R. Zengerle, *NATO Science for Peace and Security Series A: Chemistry and Biology* **2010**, 305–376.

[106] B Lin, S Basuray, *Microfluidics: Technologies and Applications*, Springer, **2011**.

[107] L. Y. Chu, W Wang, *Microfluidics for Advanced Functional Polymeric Materials*, Wiley, **2017**.

[108] M. Seo, Z. Nie, S. Xu, M. Mok, P. C. Lewis, R. Graham, E. Kumacheva, *Langmuir* **2005**, *21*, 11614–11622.

[109] D. Dendukuri, D. C. Pregibon, J. Collins, T. A. Hatton, P. S. Doyle, *Nature Materials* **2006**, *5*, 365–369.

[110] D. Dendukuri, P. S. Doyle, *Advanced Materials* **2009**, *21*, 4071–4086.

[111] J. T. Wang, J. Wang, J. J. Han, *Small* **2011**, *7*, 1728–1754.

[112] J. H. Kim, T. Y. Jeon, T. M. Choi, T. S. Shim, S. H. Kim, S. M. Yang, *Langmuir* **2014**, *30*, 1473–1488.

[113] C. A. Serra, Z. Chang, *Chemical Engineering and Technology* **2008**, *31*, 1099–1115.

[114] J. C. McDonald, D. C. Duffy, J. R. Anderson, D. T. Chiu, H. Wu, O. J. Schueller, G. M. Whitesides, *Electrophoresis* **2000**, *21*, 27–40.

[115] E. Holczer, Z. Fekete, P. Fürjes, *Materials Science Forum* **2012**, *729*, 361–366.

[116] Z. Chang, C. A. Serra, M. Bouquey, L. Prat, G. Hadziioannou, *Lab on a Chip* **2009**, *9*, 3007–3011.

[117] M. Bouquey, C. Serra, N. Berton, L. Prat, G. Hadziioannou, *Chemical Engineering Journal* **2007**, *135*, 93–98.

[118] J. Michael Köhler, I. Kraus, J. Faerber, C. Serra, *Journal of Materials Science* **2012**, *48*, 1–9.

[119] Z. Chang, C. A. Serra, M. Bouquey, I. Kraus, S. Li, J. Michael Köhler, *Nanotechnology* **2010**, *21*, 15605.

[120] W. J. Jeong, J. Y. Kim, J. Choo, E. K. Lee, C. S. Han, D. J. Beebe, G. H. Seong, S. H. Lee, *Langmuir* **2005**, *21*, 3738–3741.

[121] I. U. Khan, C. A. Serra, N. Anton, X. Li, R. Akasov, N. Messaddeq, I. Kraus, T. F. Vandamme, *International Journal of Pharmaceutics* **2014**, *473*, 239–249.

[122] Y. T. Yang, J. Wei, X. Li, L. J. Wu, Z. Q. Chang, C. A. Serra, *Advanced Powder Technology* **2015**, *26*, 156–162.

[123] C. A. Serra, I. U. Khan, Z. Chang, M. Bouquey, R. Muller, I. Kraus, M. Schmutz, T. Vandamme, N. Anton, C. Ohm, R. Zentel, A. Knauer, M. Köhler, *Journal of Flow Chemistry* **2013**, *3*, 66–75.

[124] M. Urbanski, C. G. Reyes, J. Noh, A. Sharma, Y. Geng, V. Subba Rao Jampani, J. P. Lagerwall, *Journal of Physics Condensed Matter* **2017**, *29*, 133003.

[125] V. Tomar, S. I. Hernández, N. L. Abbott, J. P. Hernández-Ortiz, J. J. de Pablo, *Soft Matter* **2012**, *8*, 8679.

[126] O. D. Lavrentovich, *Liquid Crystals* **2014**, *24*, 117–126.

[127] F. Xu, H.-S. Kitzerow, P. P. Crooker, *Phys. Rev. E* **1994**, *49*, 3061.

[128] J. Noh, K. Reguengo De Sousa, J. P. F. Lagerwall, *Soft Matter* **2016**, *12*, 367–372.

[129] H.-L. Liang, J. Noh, R. Zentel, P. Rudquist, J. P. F. Lagerwall, *Philosophical Transactions of the Royal Society A: Mathematical Physical and Engineering Sciences* **2013**, *371*, 20120258.

[130] O. O. Prishchepa, V. Y. Zyryanov, A. P. Gardymova, V. F. Shabanov, *Molecular Crystals and Liquid Crystals* **2008**, *489*, 37–41.

[131] A. Fernández-Nieves, D. R. Link, M. Márquez, D. A. Weitz, *Physical Review Letters* **2007**, *98*, 1–4.

[132] C. Ohm, C. Serra, R. Zentel, *Advanced Materials* **2009**, *21*, 4859–4862.

[133] E.-K. Fleischmann, H.-L. Liang, N. Kapernaum, F. Giesselmann, J. Lagerwall, R. Zentel, *Nature Communications* **2012**, *3*, 1178.

[134] E.-K. Fleischmann, H.-L. Liang, J. Lagerwall, R. Zentel, *Proc. of SPIE* **2012**, *8279*, 82790M.

[135] E. K. Fleischmann, C. Ohm, C. Serra, R. Zentel, *Macromolecular Chemistry and Physics* **2012**, *213*, 1871–1878.

[136] E. K. Fleischmann, F. R. Forst, R. Zentel, *Macromolecular Chemistry and Physics* **2014**, *215*, 1004–1011.

[137] C. Kim, S. Mukherjee, P. Luchette, P. Palffy-Muhoray, *Soft Materials* **2014**, *12*, 159–165.

[138] J. E. Marshall, S. Gallagher, E. M. Terentjev, S. K. Smoukov, *Journal of the American Chemical Society* **2014**, *136*, 474–479.

[139] Z. Yang, A. H. E. Muller, C. Xu, P. S. Doyle, J. M. DeSimone, J. Lahann, F. Sciortino, S. Glotzer, L. Hong, D. A. L. Aarts, *Janus Particle Synthesis, Self-Assembly and Applications*, Royal Society of Chemistry, **2012**.

[140] A. Walther, A. H. E. Müller, *Journal of the American Chemical Society* **2013**, *113*, 5194–5261.

[141] C. Kaewsaneha, P. Tangboriboonrat, D. Polpanich, M. Eissa, A. Elaissari, *ACS Applied Materials and Interfaces* **2013**, *5*, 1857–1869.

[142] X. Pang, C. Wan, M. Wang, Z. Lin, *Angewandte Chemie - International Edition* **2014**, *53*, 5524–5538.

[143] F. Wurm, A. F. Kilbinger, *Angewandte Chemie - International Edition* **2009**, *48*, 8412–8421.

[144] M. A. Stuart, W. T. Huck, J. Genzer, M. Müller, C. Ober, M. Stamm, G. B. Sukhorukov, I. Szleifer, V. V. Tsukruk, M. Urban, F. Winnik, S. Zauscher, I. Luzinov, S. Minko, *Nature Materials* **2010**, *9*, 101–113.

[145] J. Du, R. K. O'Reilly, *Chemical Society Reviews* **2011**, *40*, 2402.

[146] J. Hu, S. Zhou, Y. Sun, X. Fang, L. Wu, *Chemical Society Reviews* **2012**, *41*, 4356.

[147] I. Schick, S. Lorenz, D. Gehrig, S. Tenzer, W. Storck, K. Fischer, D. Strand, F. Laquai, W. Tremel, *Beilstein Journal of Nanotechnology* **2014**, *5*, 2346–2362.

[148] N. Müller, C. Heinrich, K. Abersfelder, G. Kickelbick, *Chemie in unserer Zeit* **2016**, *50*, 392–399.

[149] C. J. Hawker, K. L. Wooley, J. M. J. Fréchet, *Journal of the Chemical Society Perkin Transactions 1* **1993**, 1287.

[150] Z. Ge, J. Xu, J. Hu, Y. Zhang, S. Liu, *Soft Matter* **2009**, *5*, 3932.

[151] F. Ariura, M. Schappacher, R. Borsali, A. Deffieux, *Reactive and Functional Polymers* **2009**, *69*, 402–408.

[152] Y. Li, W. B. Zhang, I. F. Hsieh, G. Zhang, Y. Cao, X. Li, C. Wesdemiotis, B. Lotz, H. Xiong, S. Z. Cheng, *Journal of the American Chemical Society* **2011**, *133*, 10712–10715.

[153] I. K. Voets, A. De Keizer, P. De Waard, P. M. Frederik, P. H. H. Bomans, H. Schmalz, A. Walther, S. M. King, F. A. M. Leermakers, M. A. Cohen Stuart, *Angewandte Chemie - International Edition* **2006**, *45*, 6673–6676.

[154] A. Walther, C. Barner-Kowollik, A. H. E. Müller, *Langmuir* **2010**, *26*, 12237–12246.

[155] L. Cheng, G. Zhang, L. Zhu, D. Chen, M. Jiang, *Angewandte Chemie - International Edition* **2008**, *47*, 10171–10174.

[156] R. Erhardt, M. Zhang, A. Böker, H. Zettl, C. Abetz, P. Frederik, G. Krausch, V. Abetz, A. H. Müller, *Journal of the American Chemical Society* **2003**, *125*, 3260–3267.

[157] R. M. Erb, N. J. Jenness, R. L. Clark, B. B. Yellen, *Advanced Materials* **2009**, *21*, 4825–4829.

[158] M. D. McConnell, M. J. Kraeutler, S. Yang, R. J. Composto, *Nano Letters* **2010**, *10*, 603–609.

[159] O. Cayre, V. N. Paunov, O. D. Velev, *Journal of Materials Chemistry* **2003**, *13*, 2445.

[160] L. Liu, M. Ren, W. Yang, *Langmuir* **2009**, *25*, 11048–11053.

[161] S. Jiang, S. Granick, *Langmuir* **2008**, *24*, 2438–2445.

[162] L. Hong, S. Jiang, S. Granick, *Langmuir* **2006**, *22*, 9495–9499.

[163] N. Saito, Y. Kagari, M. Okubo, *Langmuir* **2007**, *23*, 5914–5919.

[164] T. Tanaka, R. Nakatsuru, Y. Kagari, N. Saito, M. Okubo, *Langmuir* **2008**, *24*, 12267–12271.

[165] T. Tanaka, M. Okayama, H. Minami, M. Okubo, *Langmuir* **2010**, *26*, 11732–11736.

[166] T. Higuchi, A. Tajima, H. Yabu, M. Shimomura, *Soft Matter* **2008**, *4*, 1302.

[167] S. Lone, I. W. Cheong, *RSC Adv.* **2014**, *4*, 13322–13333.

[168] X. T. Sun, M. Liu, Z. R. Xu, *Talanta* **2014**, *121*, 163–177.

[169] T. Nisisako, T. Torii, T. Higuchi, *Chemical Engineering Journal* **2004**, *101*, 23–29.

[170] T. Nisisako, T. Torii, T. Takahashi, Y. Takizawa, *Advanced Materials* **2006**, *18*, 1152–1156.

[171] R. F. Shepherd, J. C. Conrad, S. K. Rhodes, D. R. Link, M. Marquez, D. A. Weitz, J. A. Lewis, *Langmuir* **2006**, *22*, 8618–8622.

[172] Z. Nie, W. Li, M. Seo, S. Xu, E. Kumacheva, *Journal of the American Chemical Society* **2006**, *128*, 9408–9412.

[173] J. Lan, J. Chen, N. Li, X. Ji, M. Yu, Z. He, *Talanta* **2016**, *151*, 126–131.

[174] J. Zhang, B. A. Grzybowski, S. Granick, *Langmuir* **2017**, *33*, 6964–6977.

[175] A. Kumar, B. J. Park, F. Tu, D. Lee, A. Kumar, B. J. Park, F. Tu, D. Lee, *Soft Matter* **2013**, *9*, 6604.

[176] L. C. Bradley, W. H. Chen, K. J. Stebe, D. Lee, *Current Opinion in Colloid and Interface Science* **2017**, *30*, 25–33.

[177] G. Rosenthal, K. E. Gubbins, S. H. Klapp, *Journal of Chemical Physics* **2012**, *136*, 174901.

[178] B. P. Binks, P. D. Fletcher, *Langmuir* **2001**, *17*, 4708–4710.

[179] T. M. Ruhland, A. H. Gröschel, N. Ballard, T. S. Skelhon, A. Walther, A. H. E. Müller, S. A. F. Bon, *Langmuir* **2013**, *29*, 1388–1394.

[180] R. Aveyard, *Soft Matter* **2012**, *8*, 5233.

[181] A. Walther, M. Hoffmann, A. H. E. Müller, *Angewandte Chemie - International Edition* **2008**, *47*, 711–714.

[182] W. Cao, R. Huang, W. Qi, R. Su, Z. He, *ACS Applied Materials and Interfaces* **2015**, *7*, 465–473.

[183] L. Nie, S. Liu, W. Shen, D. Chen, M. Jiang, *Angewandte Chemie - International Edition* **2007**, *46*, 6321–6324.

[184] A. Synytska, L. Ionov, *Particle and Particle Systems Characterization* **2013**, *30*, 922–930.

[185] K. D. Seo, J. Doh, D. S. Kim, *Langmuir* **2013**, *29*, 15137–15141.

[186] C. Lu, M. W. Urban, *ACS Macro Letters* **2014**, *3*, 346–352.

[187] F. Tu, D. Lee, *Journal of the American Chemical Society* **2014**, *136*, 9999–10006.

[188] P. G. de Gennes, *Science* **1992**, *256*, 495–497.

[189] C. Kaewsaneha, P. Tangboriboonrat, D. Polpanich, M. Eissa, A. Elaissari, *Colloids and Surfaces A: Physicochemical and Engineering Aspects* **2013**, *439*, 35–42.

[190] D. Baah, T. Floyd-Smith, *Microfluidics and Nanofluidics* **2014**, *17*, 431–455.

[191] S. Bhaskar, J. Hitt, S. W. L. Chang, J. Lahann, *Angewandte Chemie - International Edition* **2009**, *48*, 4589–4593.

[192] S. Y. Lee, S. Yang, *Chem. Commun.* **2015**, *51*, 1639–1642.

[193] A. Synytska, R. Khanum, L. Ionov, C. Cherif, C. Bellmann, *ACS Applied Materials and Interfaces* **2011**, *3*, 1216–1220.

[194] S. Berger, L. Ionov, A. Synytska, *Advanced Functional Materials* **2011**, *21*, 2338–2344.

[195] J. W. Kim, J. Cho, J. Cho, B. J. Park, Y. J. Kim, K. H. Choi, J. W. Kim, *Angewandte Chemie - International Edition* **2016**, *55*, 4509–4513.

[196] F. Liang, K. Shen, X. Qu, C. Zhang, Q. Wang, J. Li, J. Liu, Z. Yang, *Angewandte Chemie - International Edition* **2011**, *50*, 2379–2382.

[197] C. H. Chen, A. R. Abate, D. Lee, E. M. Terentjev, D. A. Weitz, *Advanced Materials* **2009**, *21*, 3201–3204.

[198] J. Ge, Y. Hu, T. Zhang, Y. Yin, *Journal of the American Chemical Society* **2007**, *129*, 8974–8975.

[199] S. Berger, A. Synytska, L. Ionov, K.-j. Eichhorn, M. Stamm, **2008**, *41*, 9669–9676.

[200] U. Choudhury, L. Soler, J. G. Gibbs, S. Sanchez, P. Fischer, *Chemical Communications* **2015**, *51*, 8660–8663.

[201] W. Gao, M. D'Agostino, V. Garcia-Gradilla, J. Orozco, J. Wang, *Small* **2013**, *9*, 467–471.

[202] H.-r. R. Jiang, N. Yoshinaga, M. Sano, *Physical Review Letters* **2010**, *105*, 1–4.

[203] M. Amouzadeh Tabrizi, M. Shamsipur, *RSC Adv.* **2015**, *5*, 51508–51511.

[204] R. Zentel, *Advanced Materials* **1989**, *1*, 321–329.

[205] H. Finkelmann, *Makromol. Chem.* **1981**, *2*, 317–322.

[206] P. Xie, R. Zhang, *Journal of Materials Chemistry* **2005**, *15*, 2529.

[207] G. N. Mol, K. D. Harris, C. W. Bastiaansen, D. J. Broer, *Advanced Functional Materials* **2005**, *15*, 1155–1159.

[208] P. Beyer, E. M. Terentjev, R. Zentel, *Macromolecular Rapid Communications* **2007**, *28*, 1485–1490.

[209] C. Ohm, N. Haberkorn, P. Theato, R. Zentel, *Small* **2011**, *7*, 194–198.

[210] C. L. Van Oosten, D. Corbett, D. Davies, M. Warner, C. W. M. Bastiaansen, D. J. Broer, *Macromolecules* **2008**, *41*, 8592–8596.

[211] X.-H. Ge, J.-P. Huang, J.-H. Xu, J. Chen, G.-S. Luo, *Soft Matter* **2016**, *12*, 3425–3430.

[212] A. Gupta, M. Sbragaglia, *Physical Review E* **2014**, *90*, 023305.

[213] P. Tanpaiboonkul, W. Lerdwijitjarud, A. Sirivat, R. G. Larson, *Polymer* **2007**, *48*, 3822–3835.

[214] E. M. Terentjev, *J. Phys.: Condens. Matter* **1999**, *11*, R239–R257.

[215] P. Martinoty, P. Stein, H. Finkelmann, H. Pleiner, H. R. Brand, *European Physical Journal E* **2004**, *14*, 311–321.

[216] H. R. Brand, H. Pleiner, P. Martinoty, *Soft Matter* **2006**, *2*, 182.

[217] T. J. Suen, Y. Jen, J. V. Lockwood, *Journal of Polymer Science* **1958**, *31*, 481–497.

[218] Y. Jiang, T. I. Löbling, C. Huang, Z. Sun, A. H. Müller, T. P. Russell, *ACS Applied Materials and Interfaces* **2017**, *9*, 33327–33332.

[219] S. C. Glotzer, M. J. Solomon, *Nature Materials* **2007**, *6*, 557–562.

[220] H. M. Gao, Z. Y. Lu, H. Liu, Z. Y. Sun, L. J. An, *Journal of Chemical Physics* **2014**, *141*, 134907.

[221] J. H. Schröder, M. Doroshenko, D. Pirner, M. E. Mauer, B. Förster, V. Boyko, B. Reck, K. J. Roschmann, A. H. Müller, S. Förster, *Polymer (United Kingdom)* **2016**, *106*, 208–217.

[222] Z. Wu, J. Li, B. E. F. De Ávila, T. Li, W. Gao, Q. He, L. Zhang, J. Wang, *Advanced Functional Materials* **2015**, *25*, 7497–7501.

[223] M. D. McConnell, M. J. Kraeutler, S. Yang, R. J. Composto, *Nano Letters* **2010**, *10*, 603–609.

[224] M.-J. Huang, J. Schofield, R. Kapral, *Soft Matter* **2016**, *12*, 5581–5589.

[225] T. S. Skelhon, Y. Chen, S. A. F. Bon, *Soft Matter* **2014**, *10*, 7730–7735.

[226] A. Walther, M. Drechsler, A. H. E. Müller, *Soft Matter* **2009**, *5*, 385–390.

[227] Z. Cao, G. Wang, Y. Chen, F. Liang, Z. Yang, *Macromolecules* **2015**, *48*, 7256–7261.

[228] H. Jiang, C. Li, X. Huang, *Nanoscale* **2013**, *5*, 5225.

[229] M. López-Valdeolivas, D. Liu, D. J. Broer, C. Sánchez-Somolinos, *Macromolecular Rapid Communications* **2017**, *39*, 1700710.

[230] J. C. Wittmann, S. Meyer, P. Damman, M. Dosière, H. W. Schmidt, *Polymer* **1998**, *39*, 3545–3550.

[231] G. H. F. Bergmann, H. Finkelmann, V. Percec, M. Zhao, *Macromol. Rapid Comm.* **1997**, *18*, 353–360.

[232] J. W. Kim, A. S. Utada, A. Fernández-Nieves, Z. Hu, D. A. Weitz, *Angewandte Chemie - International Edition* **2007**, *46*, 1819–1822.

[233] C. Boutris, E. G. Chatzi, C. Kiparissides, *Polymer* **1997**, *38*, 2567–2570.

[234] K. D. Seo, A. Choi, J. Doh, D. S. Kim, *J. Vis. Exp.* **2016**, *108*, e52813.

[235] Y. Hu, G. Azadi, A. M. Ardekani, *Carbohydrate Polymers* **2015**, *120*, 38–45.

[236] R. Wei, Y. He, X. Wang, P. Keller, *Macromolecular Rapid Communications* **2013**, *34*, 330–334.

[237] D. J. Broer, J. Boven, G. N. Mol, *Makromol. Chem.* **1989**, *190*, 3201–3215.

[238] I. Dierking, *Handbook of liquid crystals*, *Vol. 24*, Edition 3, (Eds.: D. Demus, J. Goodby, G. W. Gray, H. W. Spiess), WILEY-VCH, Weinheim, Germany, **2015**, pp. 25–27.

[239] J. Schatzle, W. Kaufhold, H. Finkelmann, *Makromol. Chem.* **1989**, *190*, 3269–3284.

[240] J. Küpfer, E. Nishikawa, H. Finkelmann, *Polymers for Advanced Technologies* **1994**, *5*, 110–115.

[241] J. Küpfer, H. Finkelmann, *Macromolecular Chemistry and Physics* **1994**, *195*, 1353–1367.

[242] J. Naciri, A. Srinivasan, H. Jeon, N. Nikolov, P. Keller, B. R. Ratna, *Macromolecules* **2003**, *36*, 8499–8505.

[243] C. Ohm, M. Morys, F. R. Forst, L. Braun, A. Eremin, C. Serra, R. Stannarius, R. Zentel, *Soft Matter* **2011**, *7*, 3730.

[244] H. Finkelmann, E. Nishikawa, G. G. Pereira, M. Warner, *Physical Review Letters* **2001**, *87*, 015501.

[245] A. Sánchez-Ferrer, A. Merekalov, H. Finkelmann, *Macromolecular Rapid Communications* **2011**, *32*, 671–678.

[246] M. Portugall, H. Ringsdorf, R. Zentel, *Makromol. Chem.* **1982**, *183*, 2311–2321.

[247] E.-K. Fleischmann, F. R. Forst, K. Köder, N. Kapernaum, R. Zentel, K. Koeder, N. Kapernaum, R. Zentel, *Journal of Materials Chemistry C* **2013**, *1*, 5885.

[248] B. Neises, W. Steglich, *Angewandte Chemie International Edition in English* **1978**, *17*, 522–524.

[249] C. Zhang, T. J. Bunning, R. M. Laine, *Chem. Mater.* **2001**, *13*, 3653–3662.

[250] J. Cowie, H. Hunter, *Canadian Journal of Chemistry* **1995**, *73*, 1811–1817.

[251] S. Palagi, A. G. Mark, S. Y. Reigh, K. Melde, T. Qiu, H. Zeng, C. Parmeggiani, D. Martella, A. Sanchez-Castillo, N. Kapernaum, F. Giesselmann, D. S. Wiersma, E. Lauga, P. Fischer, *Nature Materials* **2016**, *15*, 647–653.

[252] T. J. White, D. J. Broer, *Nature Materials* **2015**, *14*, 1087–1098.

[253] D. Liu, D. J. Broer, *Langmuir* **2014**, *30*, 13499–13509.

[254] R. Zentel, G. F. Parker, J. Meyer, M. Benalia, *Liquid Crystals* **1987**, *2*, 651–664.

[255] H. Kapitza, R. Zentel, *Macromol. Chem.* **1988**, *189*, 1793.

[256] Z. Pei, Y. Yang, Q. Chen, E. M. Terentjev, Y. Wei, Y. Ji, *Nature Materials* **2014**, *13*, 36–41.

[257] Z. Wang, H. Tian, Q. He, S. Cai, *ACS Applied Materials and Interfaces* **2017**, *9*, 33119–33128.

[258] M. Chambers, H. Finkelmann, M. Remškar, A. Sánchez-Ferrer, B. Zalar, S. Žumer, *J. Mater. Chem.* **2009**, *19*, 1524–1531.

[259] T. Ikeda, J. I. Mamiya, Y. Yu, *Angewandte Chemie - International Edition* **2007**, *46*, 506–528.

[260] M. Vennes, S. Martin, T. Gisler, R. Zentel, *Macromolecules* **2006**, *39*, 8326–8333.

[261] M. Seo, Z. Nie, S. Xu, P. C. Lewis, E. Kumacheva, *Langmuir* **2005**, *21*, 4773–4775.

[262] K. K. Kim, D. W. Pack in *BioMEMS and Biomedical Nanotechnology, Volume I - Biological and Biomedical Nanotechnology*, (Eds.: M. Ferrari, A. Lee, L. Lee), Springer US, **2006**, pp. 19–50.

[263] C. Serra, N. Berton, M. Bouquey, L. Prat, G. Hadziioannou, *Langmuir* **2007**, *23*, 7745–7750.

LIST OF FIGURES

LIST OF TABLES

ACRONYMS

AM	acrylamide monomer
AR	aspect ratio
ARGET	activator regeneration by electron transfer
ATRP	atom transfer radical polymerization
$B_{LC/A}$	surface area of the LCE/polyacrylamide interface
C_a	capillary number
co-flow	continuous flow
CP	continuous phase
CV	coefficient of variation
d	diameter
D	capillary dimension
DMF	dimethylformamide
DP	dispersed phase
DSC	differential scanning calorimetry
EDT	1,2-ethanedithiol
FEP	fluorinated ethylene propylene
FFD	flow-focusing device
HM	hydrophilic monomer mixture
HPLC	high performance liquid chromatography
I	intensity
IBA	isobornyl acrylate
ID	inner diameter
L	length
L_{Am}	LCE length in the amorphous state
L_{Iso}	LCE length in the isotropic state
LC	liquid crystalline

LCD	liquid crystalline display
LCE	liquid crystalline elastomer
LCM	liquid crystalline monomer
LCN	liquid crystalline network
LCST	lower critical solution temperature
MEMS	microelectromechanical systems
N	nematic phase
NIPAAm	*N*-isopropylacrylamide
n_e	extraordinary refractive index
n_o	ordinary refractive index
OD	outer diameter
P2MVP	poly(*N*-methyl-2-vinylpyridinium iodide)
P2VN	poly(2-vinyl naphthalene)
PAA	poly(acrylic acid)
PAAm	poly(acrylamide)
pAM	high viscous acrylamide monomer
PB	poly(butadiene)
PDEA	poly(*N*,*N*-diethylamino-2-ethylmethacrylate)
PDMAEMA	poly(2-(dimethylamino)ethyl methacrylate)
PDMS	poly(dimethylsiloxane)
PDMS-PEG	poly(dimethylsiloxane)-poly(ethyleneglycole)
PEEK	poly(etheretherketone)
PEO	poly(ethylene oxide)
PFS	poly(pentafluorostyrene)
PI	poly(isoprene)
PMAA	poly(methacrylic acid)
PMMA	poly(methyl methacrylate)
PnBuA	poly(*n*-butylacrylate)
PNIPAAm	poly(*N*-isopropylacrylamide)

POM	polarized optical microscopy
PS	poly(styrene)
PTFE	poly(tetrafluoroethylene)
PVA	poly(vinylalcohol)
q	flow velocity
R_e	Reynolds number
RT	room temperature
$R_\perp$	radius of gyration perpendicular to $\vec{n}$
$R_\parallel$	radius of gyration parallel to $\vec{n}$
SDBS	sodium dodecylbenzene sulfonate
SDS	sodium dodecyl sulfate
SEM	scanning electron microscopy
SmA	smectic A phase
T	temperature
T_{cr}	crystallization temperature
TEM	transmission electron microscopy
T_I	clearing temperature
T_{NI}	nematic-isotropip phase transition temperature
TPGDA	tripropylene glycol diacrylate
UV	ultraviolet
UV-VIS	ultraviolet-visible
$V/B_{LC/A}$	LCE volume divided by the surface area of the LCE/polyacrylamide interface
V_A	polyacrylamide volume
V_{LC}	LCE volume
WAXS	wide-angle X-ray scattering
χ	scattering angle
μ	fluid viscosity
θ	azimuthal angle
ρ	fluid density
Υ	interfacial tension DP/CP

DANKSAGUNG

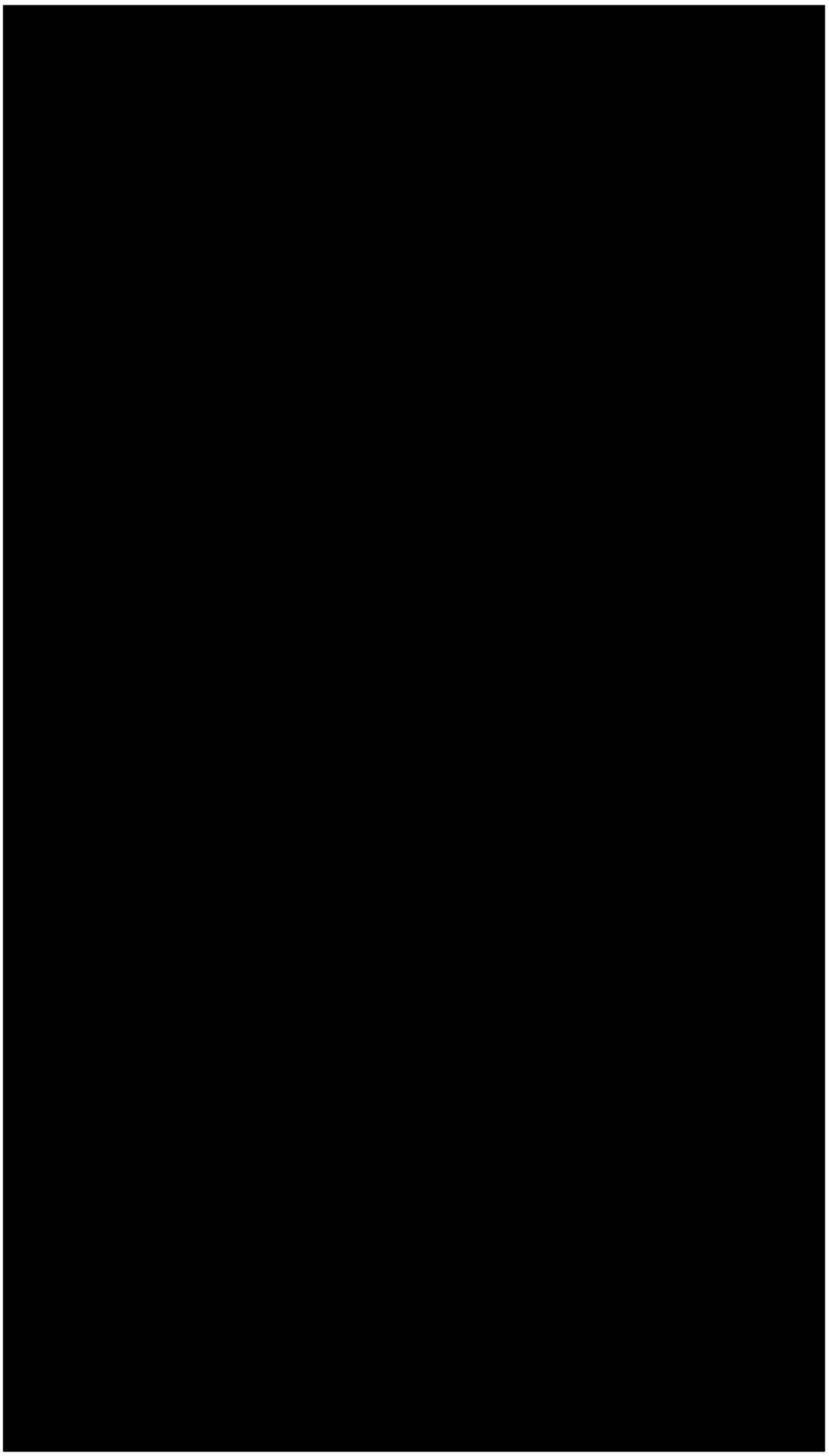

DECLARATION

I hereby declare that I wrote the dissertation submitted without any unauthorized external assistance and used only sources acknowledged in the work. All textual passages, which are appropriated verbatim or paraphrased from published and unpublished texts as well as all information obtained from oral sources are duly indicated and listed in accordance with bibliographical rules. In carrying out this research, I complied with the rules of standard scientific practice as formulated in the statutes of the Johannes Gutenberg University Mainz to insure standard scientific practice.

Mainz, 2018

Tristan Hessberger

COLOPHON

This document was typeset using the typographical look-and-feel `classicthesis` developed by André Miede. The style was inspired by Robert Bringhurst's seminal book on typography "*The Elements of Typographic Style*". `classicthesis` is available for both LaTeX and LyX:

`https://bitbucket.org/amiede/classicthesis/`

Happy users of `classicthesis` usually send a real postcard to the author, a collection of postcards received so far is featured here:

`http://postcards.miede.de/`

Final Version as of May 22, 2018 (`classicthesis`).